ORNL/TM-2016/660

ORNL Interim Progress Report on Hydride Reorientation CIRFT Tests

Approved for public release.
Distribution is unlimited.

Jy-An John Wang
Hong Wang
Yong Yan

October 28, 2016

DOCUMENT AVAILABILITY

Reports produced after January 1, 1996, are generally available free via the U.S. Department of Energy (DOE) Information Bridge.

Web site http://www.osti.gov/bridge

Reports produced before January 1, 1996, may be purchased by members of the public from the following source.

National Technical Information Service
5285 Port Royal Road
Springfield, VA 22161
Telephone 703-605-6000 (1-800-553-6847)
TDD 703-487-4639
Fax 703-605-6900
E-mail info@ntis.gov
Web site http://www.ntis.gov/support/ordernowabout.htm

Reports are available to DOE employees, DOE contractors, Energy Technology Data Exchange (ETDE) representatives, and International Nuclear Information System (INIS) representatives from the following source.

Office of Scientific and Technical Information
P.O. Box 62
Oak Ridge, TN 37831
Telephone 865-576-8401
Fax 865-576-5728
E-mail reports@osti.gov
Web site http://www.osti.gov/contact.html

This report was prepared as an account of work sponsored by an agency of the United States Government. Neither the United States Government nor any agency thereof, nor any of their employees, makes any warranty, express or implied, or assumes any legal liability or responsibility for the accuracy, completeness, or usefulness of any information, apparatus, product, or process disclosed, or represents that its use would not infringe privately owned rights. Reference herein to any specific commercial product, process, or service by trade name, trademark, manufacturer, or otherwise, does not necessarily constitute or imply its endorsement, recommendation, or favoring by the United States Government or any agency thereof. The views and opinions of authors expressed herein do not necessarily state or reflect those of the United States Government or any agency thereof.

ORNL/TM-2016/660

Materials Science and Technology Division
Oak Ridge National Laboratory

ORNL Interim Progress Report on Hydride Reorientation CIRFT Tests

Jy-An Wang, Hong Wang, and Yong Yan

NRC Program Manager: Michelle Bales
ORNL Program Manager: Bruce Bevard

Date Published: October 28, 2016

Prepared by
OAK RIDGE NATIONAL LABORATORY
Oak Ridge, Tennessee 37831-6283
managed by
UT-BATTELLE, LLC
for the
US DEPARTMENT OF ENERGY
under contract DE-AC05-00OR22725

This page intentionally left blank.

CONTENTS

LIST OF FIGURES v

LIST OF TABLES vii

SUMMARY ix

1. INTRODUCTION 1

2. MATERIALS, EQUIPMENT, AND TEST METHODS 2
   - 2.1 Description of Cladding Material and High-Burnup Fuel Segments 2
   - 2.2 Equipment for Sample Preparation 4
   - 2.3 Hydride Reorientation System 6

3. MATERIALS HYDRIDING AND CHARACTERIZATION 8

4. OUT-OF-CELL HYDRIDE REORIENTATION TESTING 9
   - 4.1 HR-HBR#1, 145 MPa at 400°C, one cycle 9
   - 4.2 HR-HBR#2, 145–150 MPa at 400°C, five cycles 12
   - 4.3 HR-HBR#3, 100 MPa at 400°C, five cycles 15
   - 4.4 HR-HBR#4, 120 MPa at 400°C, five cycles 18

5. DISCUSSION 21

6. CIRFT EVALUATIONS OF HBR FUEL FOR HYDRIDE REORIENTATION STUDY 22
   - 6.1 Overview of CIRFT Evaluations and Results for HBR Fuel Rods 22
   - 6.2 FY 2016 PHASE II CIRFT HR Test Results (Appendix A) 23
     - 6.2.1 Hydride Reorientation Test Samples Preparation 23
     - 6.2.2 Measurements and Monitoring Data 24
     - 6.2.3 Fatigue Life 25

7. CONCLUSION 31

General observations from Phase II CIRFT test data evaluations are: 31

9. ACKNOWLEDGMENTS 32

10. REFERENCES 33

APPENDIX A: CIRFT TESTING RESULTS OF HBR SNF– Phase II……...…A-1

This page intentionally left blank.

LIST OF FIGURES

Fig. 1. High-burnup H. B. Robinson fuel morphology for Sample 607D4A. 4

Fig. 2. Hydrogen charging apparatus. 5

Fig. 3. A typical pressure and temperature profile of the hydrogen charging process. 5

Fig. 4. An Astro Arc Polysoude tubing welder. 6

Fig. 5 The hydride reorientation system (a) before and (b) after installed into the hot cell. 7

Fig. 6. Micrographs showing typical, uniform circumferential hydride distributions in hydrogen charged Zircaloy-4. 8

Fig. 7. Pressure and sample temperature as a function of time for Test HR-HBR#1. 9

Fig. 8. High magnification micrograph showing radial hydrides of Sample HR-HBR#1 with hydrogen content H ≈ 274 wppm. 10

Fig. 9. Radial hydride distribution shown in eight areas in different circumferential directions of Sample HR-HBR#1. 11

Fig. 10. Pressure and sample temperature as a function of time for Test HR-HBR#2. 12

Fig. 11. High magnification micrograph showing radial hydrides of Sample HR-HBR#2 with hydrogen content H ≈ 286 ppm. 13

Fig. 12. Radial hydride distribution shown in eight areas in different circumferential directions of Sample HR-HBR#2. 14

Fig. 13. Pressure and sample temperature as a function of time for Test HR-HBR#3. 15

Fig. 14. High magnification micrograph showing radial hydrides of Sample HR-HBR#3 with hydrogen content H ≈ 310 ppm. 16

Fig. 15. Radial hydride distribution shown in eight areas in different circumferential directions of Sample HR-HBR#3. 17

Fig. 16. Pressure and sample temperature as a function of time for Test HR-HBR#4. 18

Fig. 17. High magnification micrograph showing radial hydrides of Sample HR-HBR#4 with hydrogen content H ≈ 312 ppm. 19

Fig. 18. Radial hydride distribution shown in eight areas in different circumferential directions of Sample HR-HBR#4. 20

Fig. 20. Terminal solid solubility for dissolution (TSSd) of hydrogen in Zircaloy. 21

Fig. 21. Sample temperature as a function of time for in-cell HR test HR-1. 23

Fig. 22. (a) High magnification micrograph showing radial hydrides of Sample HR-1 (H ≈ 360–400 ppm). The HBU HBR specimen was pressurized to 145 MPa at 400°C with five thermal cycles. (b) High magnification micrograph showing radial hydrides of Sample HR-HBR#2 (H ≈ 286 ppm). The specimen was sectioned at the midplane of a 6 in.-long sample. 24

Fig. 23. (a) Moment amplitude, (b) stress amplitude, (c) curvature amplitude, and (d) strain amplitude rigidity as a function of cycles or cycles to failure. 27

Fig. 24. Images showing the failure modes for (a) (b) (c) (d) HR1, (e) (f) (g) (h) HR2, (i) (j) HR3, and (k) (l) (m) (n) HR4. 30

LIST OF TABLES

Table 1. Dimensions and chemistry of H. B. Robinson (HBR) type Zircaloy-4 used in the Oak Ridge National Laboratory test program (--- = below the detection limit) 2

Table 2. Characteristics of high-burnup H. B. Robinson fuel rods for the Oak Ridge National Laboratory hydride reorientation test[a] 3

Table 3. Specimen labels used for HBR SNF 22

Table 4a. Dynamic test results for HBR SNF rods, FY 2016 25

This page intentionally left blank.

SUMMARY

A systematic study of H. B. Robinson (HBR) high burnup spent nuclear fuel (SNF) vibration integrity was performed in Phase I project under simulated transportation environments, using the Cyclic Integrated Reversible-Bending Fatigue Tester (CIRFT) hot cell testing technology developed at Oak Ridge National Laboratory in 2013–14. The data analysis on the as-irradiated HBR SNF rods demonstrated that the load amplitude is the dominant factor that controls the fatigue life of bending rods. However, previous studies have shown that the hydrogen content and hydride morphology has an important effect on zirconium alloy mechanical properties. To address the effect of radial hydrides in SNF rods, in Phase II a test procedure was developed to simulate the effects of elevated temperatures, pressures, and stresses during transfer-drying operations. Pressurized and sealed fuel segments were heated to the target temperature for a preset hold time and slow-cooled at a controlled rate. The procedure was applied to both non-irradiated/prehydrided and high-burnup Zircaloy-4 fueled cladding segments using the Nuclear Regulatory Commission-recommended 400°C maximum temperature limit at various cooling rates.

Before testing high-burnup cladding, four out-of-cell tests were conducted to optimize the hydride reorientation (R) test condition with pre-hydride Zircaloy-4 cladding, which has the same geometry as the high burnup fuel samples. Test HR-HBR#1 was conducted at the maximum hoop stress of 145 MPa, at a 400°C maximum temperature and a 5°C/h cooling rate. On the other hand, thermal cycling was performed for tests HR-HBR#2, HR-HBR#3, and HR-HBR#4 to generate more radial hydrides. It is clear that thermal cycling increases the ratio of the radial hydride to circumferential hydrides. The internal pressure also has a significant effect on the radial hydride morphology. This report describes a procedure and experimental results of the four out-of-cell hydride reorientation tests of hydrided Zircaloy-4 cladding, which served as a guideline to prepare in-cell hydride reorientation samples with high burnup HBR fuel segments.

This report also provides the Phase II CIRFT test data for the hydride reorientation irradiated samples. The variations in fatigue life are provided in terms of moment, equivalent stress, curvature, and equivalent strain for the tested SNFs. The CIRFT results appear to indicate that hydride reoriented treatment (HRT) have a negative effect on fatigue life, in addition to hydride reorientation effect. For HR4 specimen that had no pressurization procedure applied, the thermal annealing treatment alone showed a negative impact on the fatigue life compared to the HBR rod.

This page intentionally left blank.

1. INTRODUCTION

Hydrogen embrittlement of zirconium alloys is a growing concern in the United States because of the lack of a long-term solution for disposal of spent nuclear fuel (SNF). Normal operation of nuclear fuel in a reactor results in the formation of a waterside corrosion layer (oxide) and the introduction of hydrogen into the zirconium cladding via the reaction $2H_2O + Zr \rightarrow ZrO_2 + 4H$. With increasing corrosion, the hydrogen concentration in the cladding will exceed its terminal solid solubility, and brittle zirconium hydrides ($Zr + 2H \rightarrow ZrH_2$) may precipitate as the cladding cools. The formation of these hydride precipitates causes cladding ductility and failure energy to decrease [1, 2] and increases the likelihood of failure during very long-term storage and/or transportation of SNF. However, failure because of embrittlement is highly dependent upon the microstructural condition, especially the orientation of the zirconium hydride precipitates.

Under pool-storage conditions after fuel is discharged from reactors, the precipitated hydride platelets are oriented in a circumferential direction. Circumferential hydrides—in combination with hardening caused by irradiation effects—will decrease cladding ductility in response to axial and hoop loads; however, even with circumferential hydrides, the cladding still retains some ductility. At elevated temperatures during drying-transfer operations, some of the hydrogen may go into solution (up to 200 wppm at 400°C). The pressure-induced cladding tensile hoop stress during drying-transfer operations is high relative to in-reactor and pool-storage conditions. During cooling under tensile hoop stress, some of the dissolved hydrogen will precipitate in the radial direction across the cladding wall when the hoop stress is sufficient. Further cooling during storage may result in radial-hydride-induced embrittlement. This was confirmed by some recent research [3–7] that featured hydrided Zircaloy-4 cladding and high burnup zirconium alloy samples that were exposed to a tensile hoop stress from the internally pressurized cladding at ≈ 400°C—conditions similar to drying operations of the SNF.

The objective of the program is to collect experimental data on hydride reorientation testing of HBR Zircaloy-4 high burnup fuels under simulated drying operation conditions of the SNF. This report describes a procedure and test results of out-of-cell hydride reoriented tests of hydrided HBR cladding; that procedure will be used as a guideline for preparing in-cell hydride reorientation samples with high burnup fuel segments. This report also provides the Phase II CIRFT test data for the hydride reorientation samples.

2. MATERIALS, EQUIPMENT, AND TEST METHODS

2.1 Description of Cladding Material and High-Burnup Fuel Segments

The out-of-cell experiments were conducted with unirradiated, 15 × 15 pressurized water reactor (PWR) Zircaloy-4 cladding material provided by AREVA; the material has dimensions, oxygen content, and mechanical properties similar to those of the HBR cladding. After the cladding was received by Oak Ridge National Laboratory (ORNL), measurements were performed to determine the outer diameter (OD) and wall thickness. Table 1 summarizes the dimensions and chemical compositions of the unirradiated AREVA-provided clad (similar to HBR clad) compared with the nominal commercial Zircaloy-4 cladding alloys.

Table 1. Dimensions and chemistry of H. B. Robinson (HBR) type Zircaloy-4 used in the Oak Ridge National Laboratory test program (--- = below the detection limit)

Parameter	15 × 15 Zircaloy-4 HBR-type cladding[a]	Nominal composition of commercial Zircaloy-4[b,c] cladding alloys
Outer diameter, mm	10.76	10.72
Wall thickness, mm	0.76	0.617
Tin, wt %	---	1.29 ± 0.1
Niobium, wt %	---	---
Oxygen, wt %	≈0.13	0.120
Iron, wt %	---	---
Chromium, wt %	---	---
Nickel, wppm	---	---
Sulfur, wppm	---	---
Carbon, wppm	---	---
Hafnium, wppm	---	---
Silicon, wppm	---	---
Nitrogen, wppm	---	---
Hydrogen, wppm	≈20	5

[a]ORNL data based on AREVA lots received in 2014.
[b]ASTM B811. *Source:* M. C. Billone, T. Burtseva, and Y. Yan. "Overview of Spent Nuclear Fuel Program: Test Plan and High Burnup Cladding at ANL," *NRC Program Review Meeting*, Argonne National Laboratory, Argonne, IL, July 7, 2010.

[c]ORNL/TM-9591/V1&R1, "Physical and Dccay Characteristics of Commerical LWR Spent Fuel, January 1986.

Irradiated materials used in the ORNL test program are high-burnup HBR PWR fuel rods received by ORNL in 2008. They were from a 15 × 15 assembly of the HBR plant Unit 2 [8] that was operated for seven cycles and reached a rod-average burnup of 67 GWd/MTU (73 GWd/MTU peak pellet). The fuel enrichment is 2.90%. The nominal fuel pellet dimensions are 9.06 mm diameter × 9.93 mm height, and the active fuel height is 3.66 m. The cladding is cold-worked/stress-relieved Zircaloy-4, measuring 10.77 mm OD and 9.25 mm inner diameter (ID), with a nominal tin content of 1.42%. The rods were pressurized with helium to 2.0 MPa during initial fabrication. A detailed description of the as-fabricated cladding, the irradiation history, and the nondestructive testing results (eddy current, profilometry, fission-gas release, etc.) is provided in a 2001 Electric Power Research Institute report [8].

Irradiated HBR fuel used in the ORNL test program is summarized in Table 2. Detailed characterization was performed to determine the fuel morphology, fuel-cladding bond, corrosion layer, and hydride morphology. Figure 1 shows a low magnification image of the fuel morphology, which reveals the typical reactor start-up and shut-down cracks.

Table 2. Characteristics of high-burnup H. B. Robinson fuel rods for the Oak Ridge National Laboratory hydride reorientation test[a]

Parameter	**H. B. Robinson**
Reactor	Pressurized water reactor
Enrichment, wt %	2.90
Rod average burnup, GWd/MTU	63–67
Discharge date	1995
Fast fluence, 10^{25} n/m^2	14
Cladding	15 × 15 Zircaloy-4
Initial wall thickness, mm	0.76
Outer diameter oxide, μm	≤ 100
Hydrogen pickup, wppm	≤ 800
Fueled	Yes

Fig. 1. High-burnup H. B. Robinson fuel morphology for Sample 607D4A.

2.2 Equipment for Sample Preparation

Hydride reorientation tests were conducted with 152-mm-long Zircaloy-4 cladding samples (see Table 1 for cladding geometry), which were hydrogen charged for a target hydrogen concentration of 300 wppm. After hydrogen charging, the hydrided samples were subject to hydride reorientation to simulate dry cask storage drying conditions, which consists of a high pressure piping system and test chamber within a programmable crucible furnace. The hydrided sample was sealed (end-cap welded) at one end and connected to the high pressure piping system within the test chamber at the other end. The piping system was used to internally pressurize the sample to cause a hoop stress ranging up to 150 MPa.

The hydriding apparatus consists of a closed stainless steel tube that contains zirconium alloy specimens and hydrogen gas, as shown in Fig. 2. The tube is heated to facilitate hydrogen absorption by the metal. By controlling the initial hydrogen gas pressure in the vessel and the temperature profile, hydrogen concentration can be processed selectively. A typical pressure and temperature profile is shown in Fig. 3.

Fig. 2. Hydrogen charging apparatus.

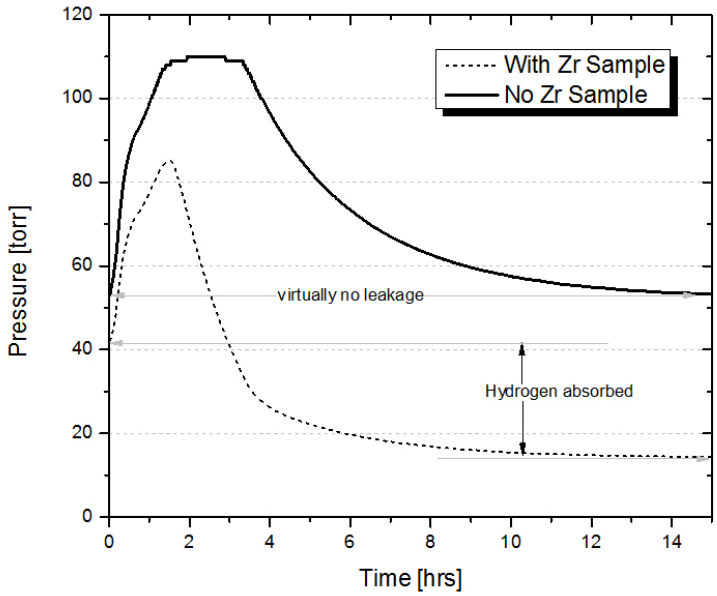

Fig. 3. A typical pressure and temperature profile of the hydrogen charging process.

An Astro Arc Polysoude welder (see Fig. 4) was used for automatic orbital welding of the cladding. A circular movement of the welding torch/electrode around fuel cladding, controlled by the welder power source, creates an orbital weld. This welder can be operated remotely with manipulators in a hot cell.

Fig. 4. An Astro Arc Polysoude tubing welder.

2.3 Hydride Reorientation System

The reorientation system consists of a high pressure piping system and test chamber within a programmable crucible furnace (see Fig. 5). The system was installed into the hot cell in FY16. Calibrations and benchmark tests were performed with unirradiated materials. For each experiment, a 6-in.-long specimen was welded with two end plugs, with one end sealed and the other end connected to the high-pressure piping system within the test chamber. The test chamber was purged with pure argon gas in order to remove air and moisture contents, and then the sample was internally pressurized to cause a hoop stress ranging from 0 to 150 MPa [5]. Pressurized samples were subjected to a preprogrammed temperature profile for up to five cycles, with each cycle being heated to 400°C, held for 2 hours, and slow-cooled/heated (1°C/min) to 170°C; the final cycle cooled from 170°C to room temperature (RT). Hoop stress was calculated using values r = 4.62 mm for inner radius and t = 0.76 mm for the wall thickness of the HBR Zircaloy-4 cladding.

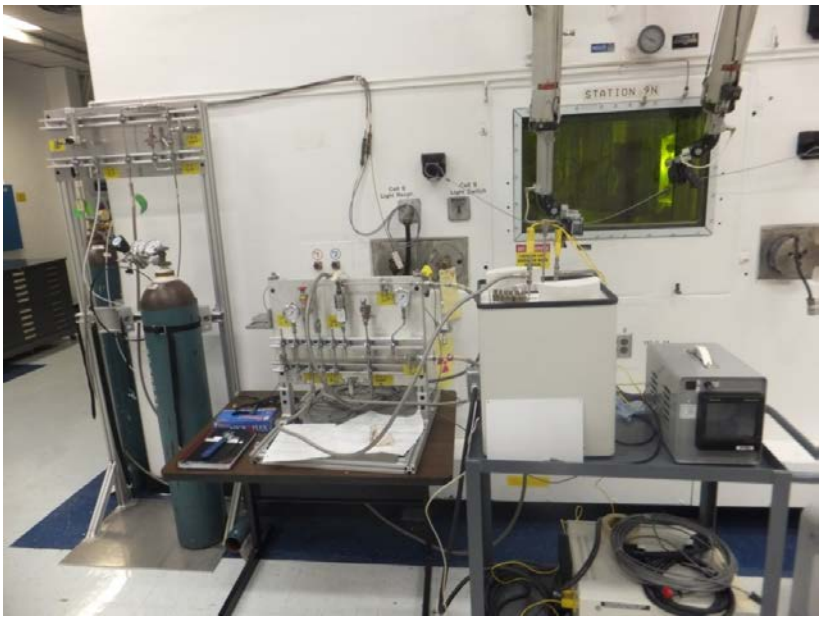

(a)

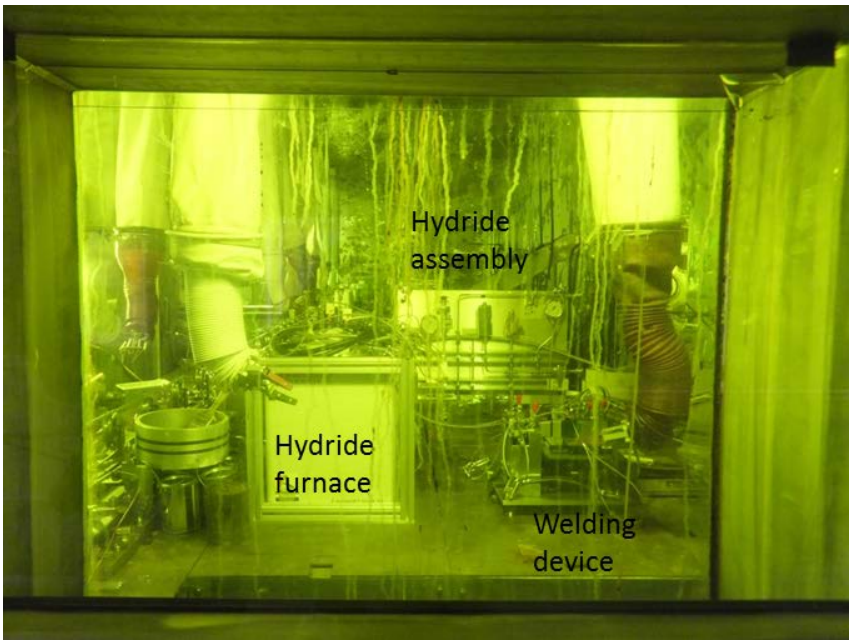

(b)

Fig. 5 The hydride reorientation system (a) before and (b) after installed into the hot cell.

3. MATERIALS HYDRIDING AND CHARACTERIZATION

The Zircaloy-4 cladding samples were hydrogen charged by the gaseous method, as described in Sect. 2. Gas charging was conducted under stress-free conditions. The target hydrogen concentrations can range from tens to a few thousand weight parts per million. The most important ranges for licensing and modeling real reactor fuel are usually less than 1,000 wppm. For this work, the Zircaloy-4 was hydrided to a target concentration of 300–400 wppm, which is similar to hydrogen content of HBR high burnup cladding to be tested in a hot cell.

Metallographic examinations were performed on hydrided Zircaloy-4 samples. As shown in Fig. 6, the hydride density increases as the hydrogen concentration in the sample increases. Hydrogen measurements indicated the hydrogen content of the specimens shown in Fig. 6 range from 70 to 320 wppm.

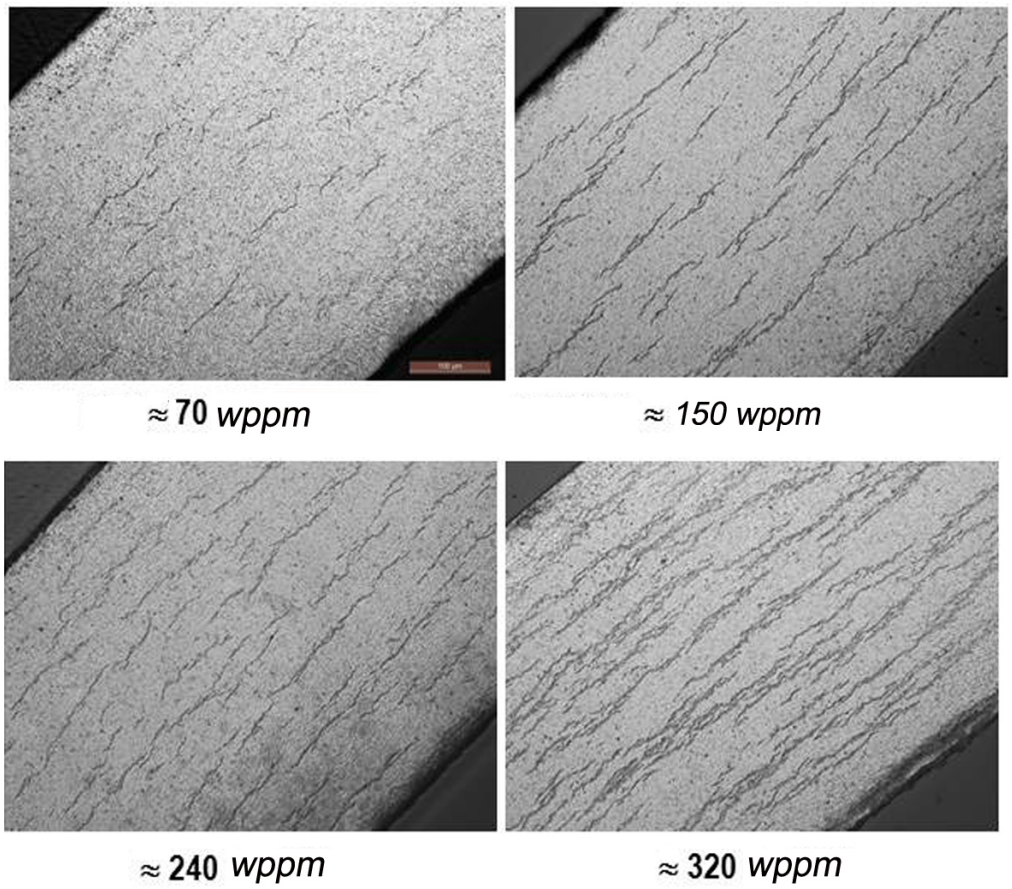

Fig. 6. Micrographs showing typical, uniform circumferential hydride distributions in hydrogen charged Zircaloy-4.

4. OUT-OF-CELL HYDRIDE REORIENTATION TESTING

To optimize the in-cell test condition, four out-of-cell hydride reorientation tests with hydrided HBR cladding were performed. The out-of-cell test results have provided a guideline to in-cell hydride reorientation procedures with high burnup HBR fuel segments.

4.1 HR-HBR#1, 145 MPa at 400°C, one cycle

A hydride reorientation (HR) test HR-HBR#1 on a hydrided 15 × 15 Zircaloy-4 was conducted at the maximum hoop stress of 145 MPa and the hold temperature T = 400°C. Total test time was over 72 hours. After fabrication, the specimen was assembled into a holder within the furnace for heating to 400°C, held at 400°C for 2 hours, cooled at 5°C/h to 170°C, then cooled at a faster rate from 170°C to RT. The internal pressure was dynamically monitored with a digital pressure transducer.

Figure 7 shows the temperature and pressure history for a drying-storage simulation experiment conducted with a 2 h hold time and one-cycle cooling. The plotted temperature is a thermocouple reading near the specimen surface. The drying simulation also is referred to as radial hydride treatment in this work.

Figure 8 shows the hydride morphology of Sample HR-HBR#1 with hydrogen content H ≈ 274 wppm. The specimen was sectioned at the midplane of a 6-in.-long sample. The radial hydrides can be observed clearly. The maximum length of radial hydrides is about 50–60 μm, as they often are terminated when intersecting with circumferential hydrides. Figure 9 includes micrographs taken in eight areas in different circumferential directions of Sample HR-HBR#1, which shows that hydrides are uniformly distributed in circumferential directions.

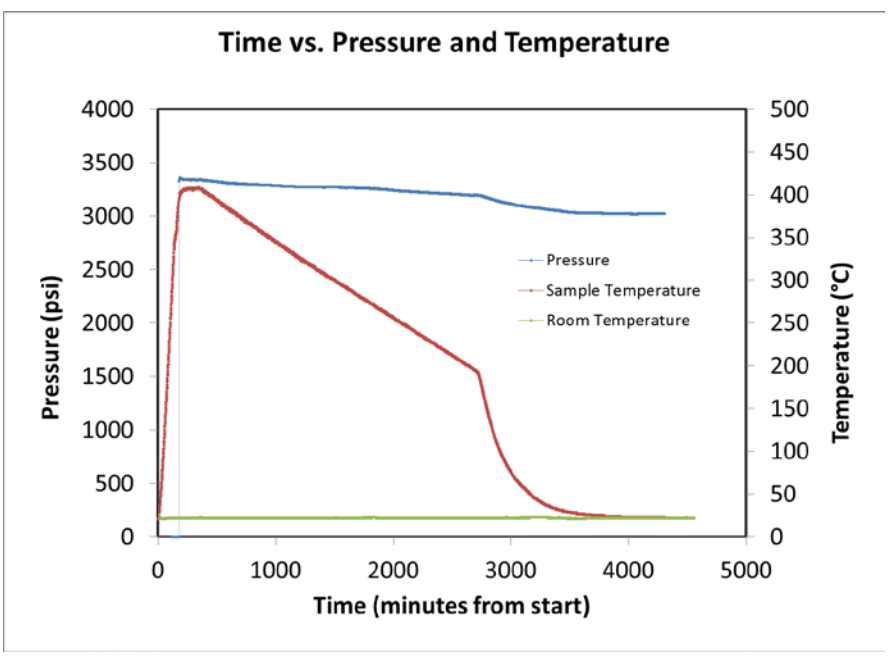

Fig. 7. Pressure and sample temperature as a function of time for Test HR-HBR#1.

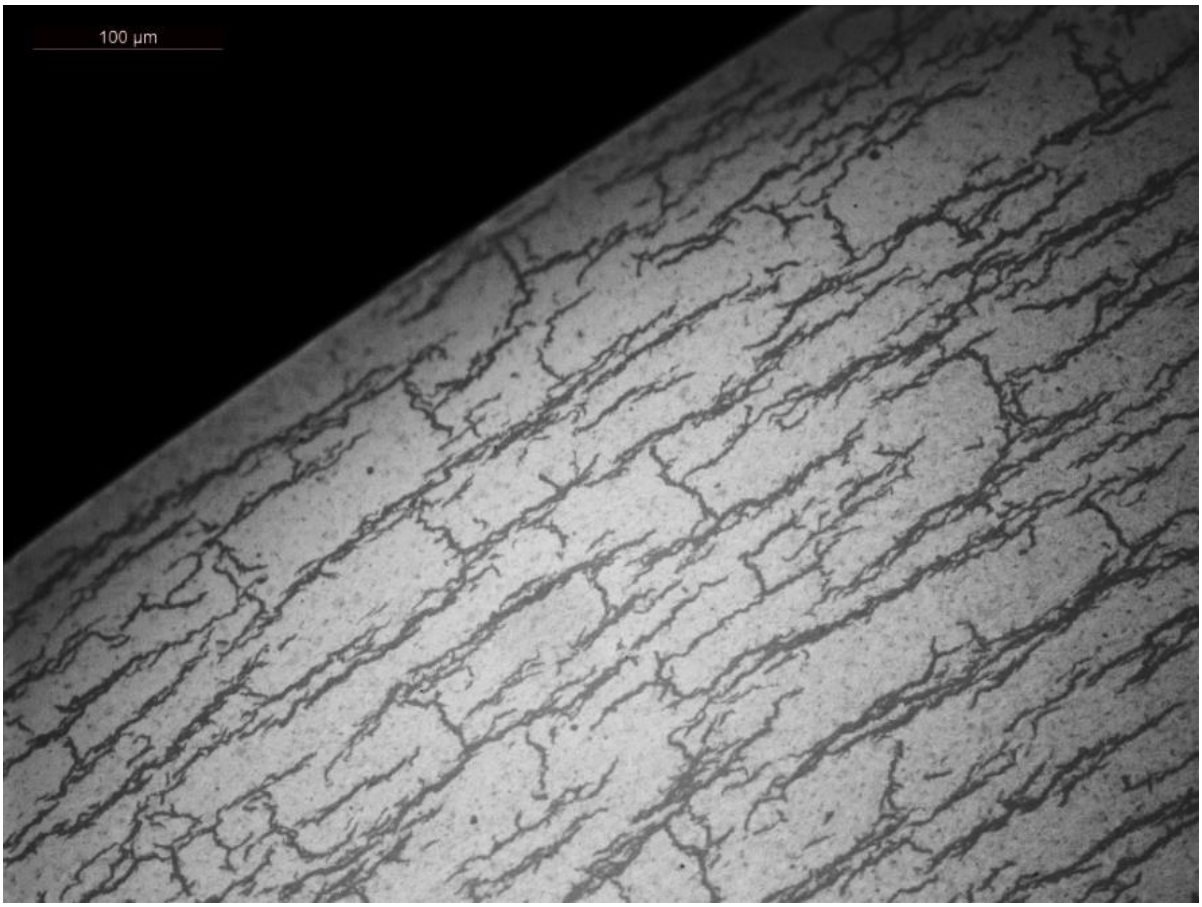

Fig. 8. High magnification micrograph showing radial hydrides of Sample HR-HBR#1 with hydrogen content H ≈ 274 wppm.
The specimen was sectioned at the midplane of a 6-in.-long sample.

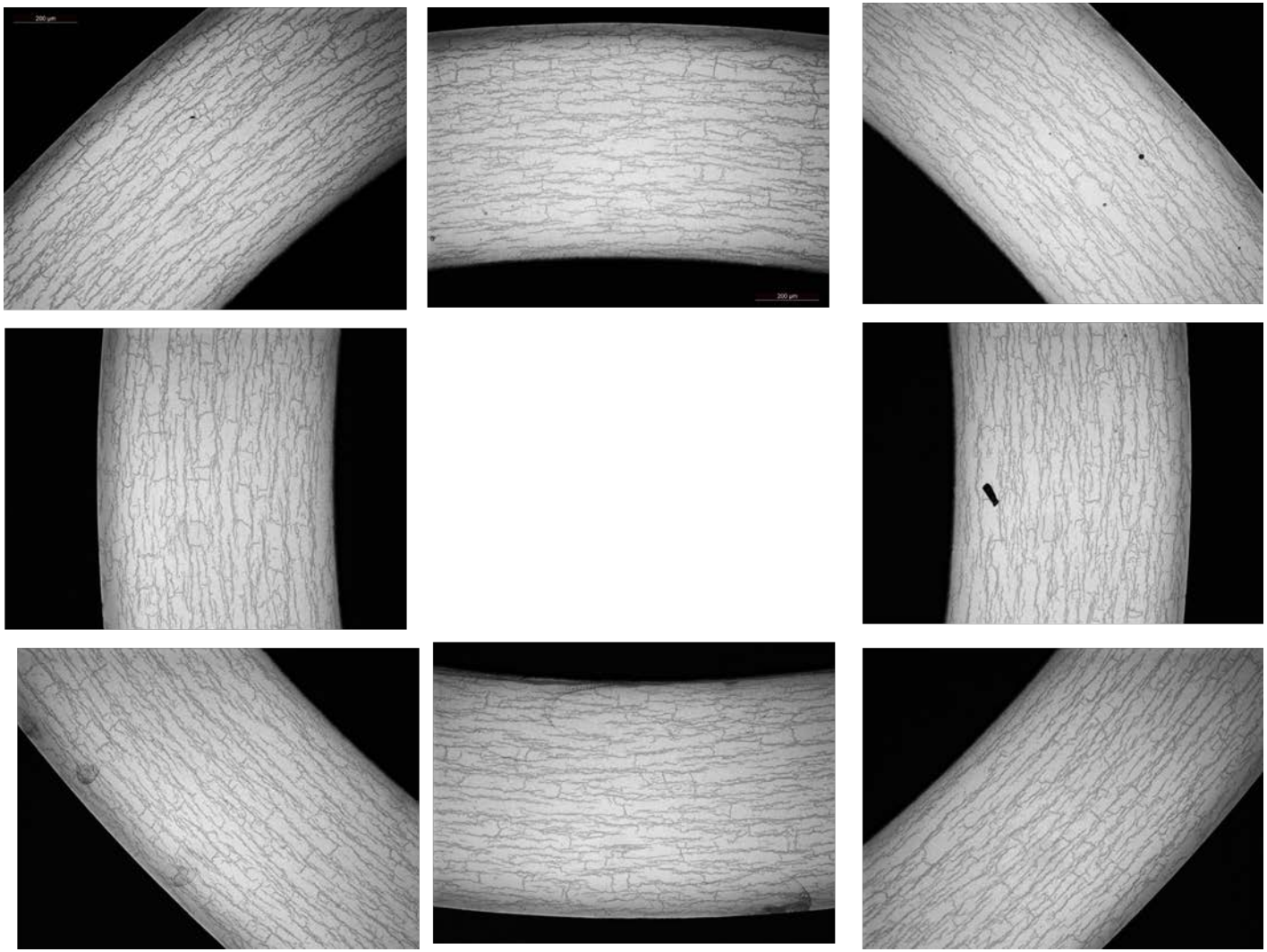

Fig. 9. Radial hydride distribution shown in eight areas in different circumferential directions of Sample HR-HBR#1.
The specimen was sectioned at the midplane of a 6-in.-long sample.

4.2 HR-HBR#2, 145–150 MPa at 400°C, five cycles

Test HR-HBR#2 was conducted on a hydrided 15 × 15 Zircaloy-4 at the maximum hoop stress of 145 MPa and the target hold temperature T = 400°C. However, thermal cycling was performed to increase the radial hydrides. After fabrication, the specimen was assembled into a holder within the furnace for heating to target temperature 400°C, held for 2 hours, cooled at 1°C/min to 170°C, and then heated at 1°C/min to target hold temperature 400°C again for five cycles. The sample was furnace cooled from 170°C to RT for the last cycle. Figure 10 shows the temperature and pressure history for HR-HBR#2. The plotted temperature is a thermocouple reading near the specimen surface.

Figure 11 shows the hydride morphology of Sample HR-HBR#2 with hydrogen content H ≈ 286 wppm. The specimen was sectioned at the midplane of a 6-in.-long sample. The radial hydride can be observed clearly. The maximum length of the radial hydride is about 50–60 μm, similar to HR-HBR#1. However, the density of radial hydrides in HR-HBR#2 is much higher than the density in HR-HBR#1, mainly because of multithermal cycles. Figure 12 shows radial hydride distribution in eight areas in different circumferential directions of Sample HR-HBR#2.

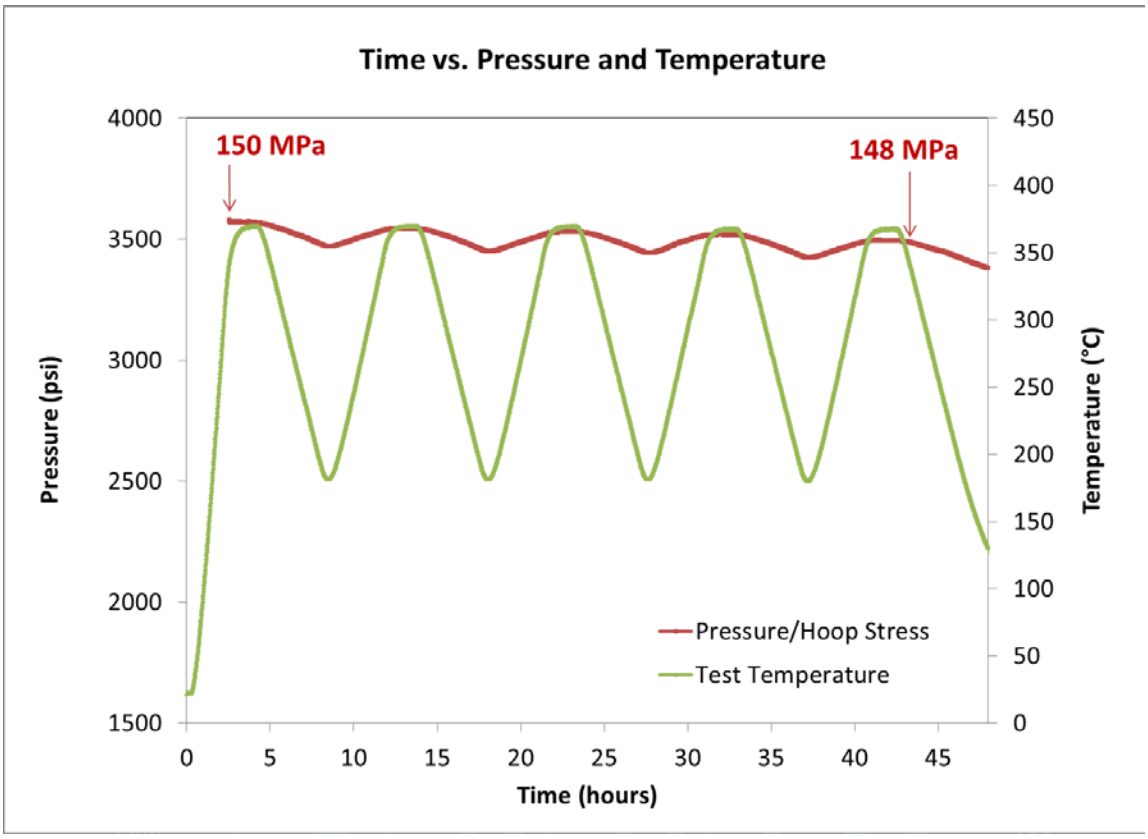

Fig. 10. Pressure and sample temperature as a function of time for Test HR-HBR#2.

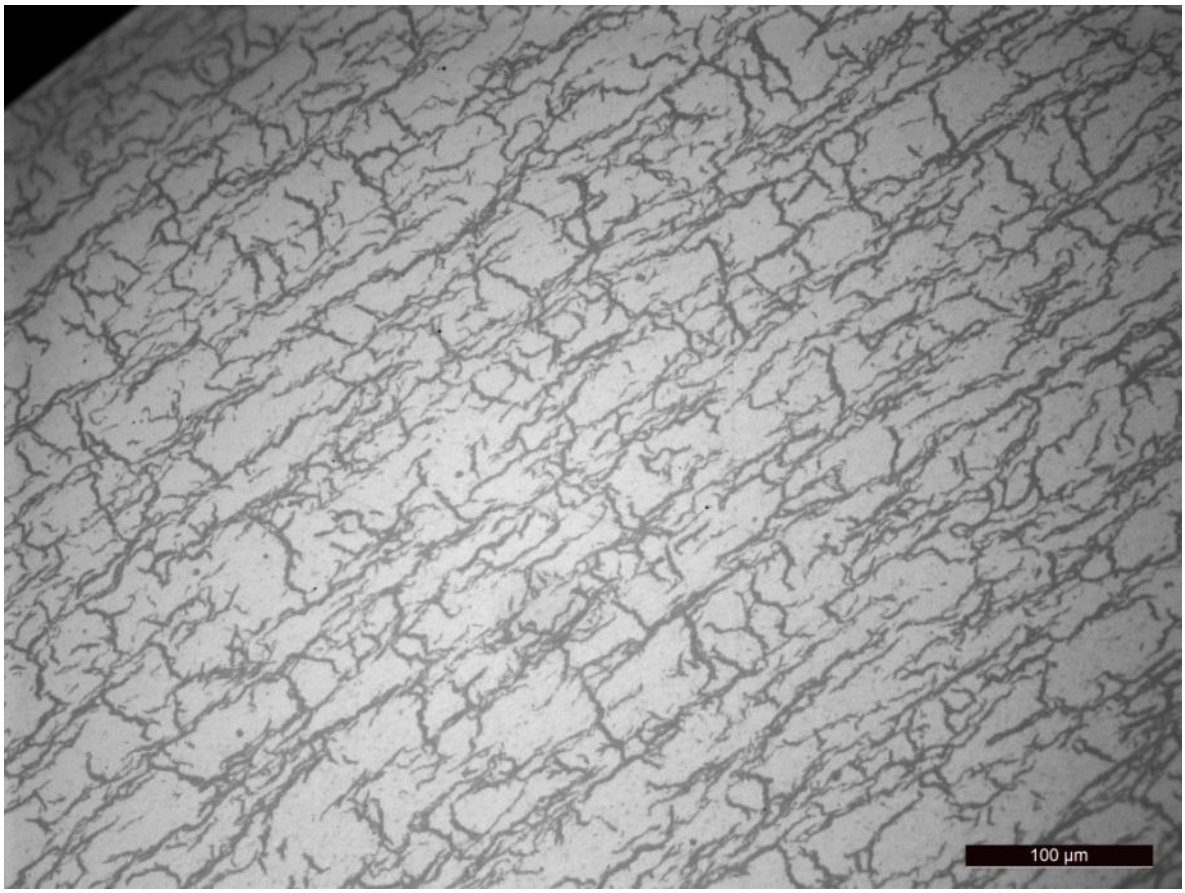

Fig. 11. High magnification micrograph showing radial hydrides of Sample HR-HBR#2 with hydrogen content H ≈ 286 ppm. The specimen was sectioned at the midplane of a 6-in.-long sample.

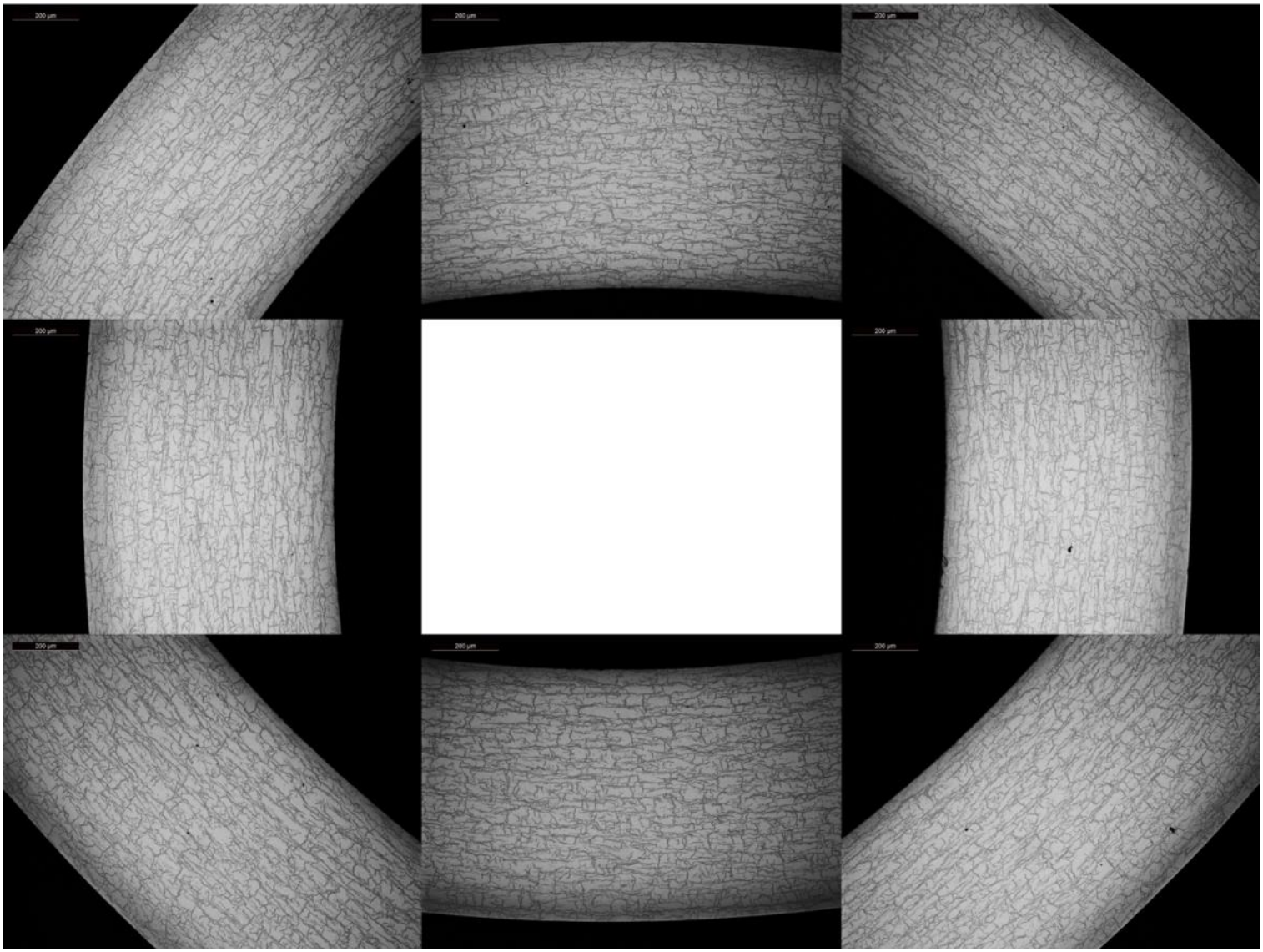

Fig. 12. Radial hydride distribution shown in eight areas in different circumferential directions of Sample HR-HBR#2.
The specimen was sectioned at the midplane of a 6-in.-long sample.

4.3 HR-HBR#3, 100 MPa at 400°C, five cycles

Test HR-HBR#3 was conducted on a hydrided 15 × 15 Zircaloy-4 at the maximum hoop stress of 100 MPa and the hold temperature T = 400°C. After fabrication, the specimen was assembled into a holder within the furnace for heating to 400°C, held at 400°C for 2 hours, cooled at 1°C/min to 170°C, and then heated at 1°C/min to 400°C again for five cycles. The sample was furnace cooled from 170°C to RT for the last cycle. Figure 13 shows the temperature and pressure history for HR-HBR#3. The plotted temperature is a thermocouple reading near the specimen surface.

Figure 14 shows the hydride morphology of Sample HR-HBR#3 with hydrogen content H ≈ 310 wppm. The specimen was sectioned at the midplane of a 6-in.-long sample. The radial hydrides can be observed clearly in Figure 14. The maximum length of the radial hydride is < 30 μm. The radial hydride ratio of HR-HBR#3 also is lower than HR-HBR#2. Figure 15 shows radial hydride distribution in eight areas in different circumferential directions of Sample HR-HBR#3.

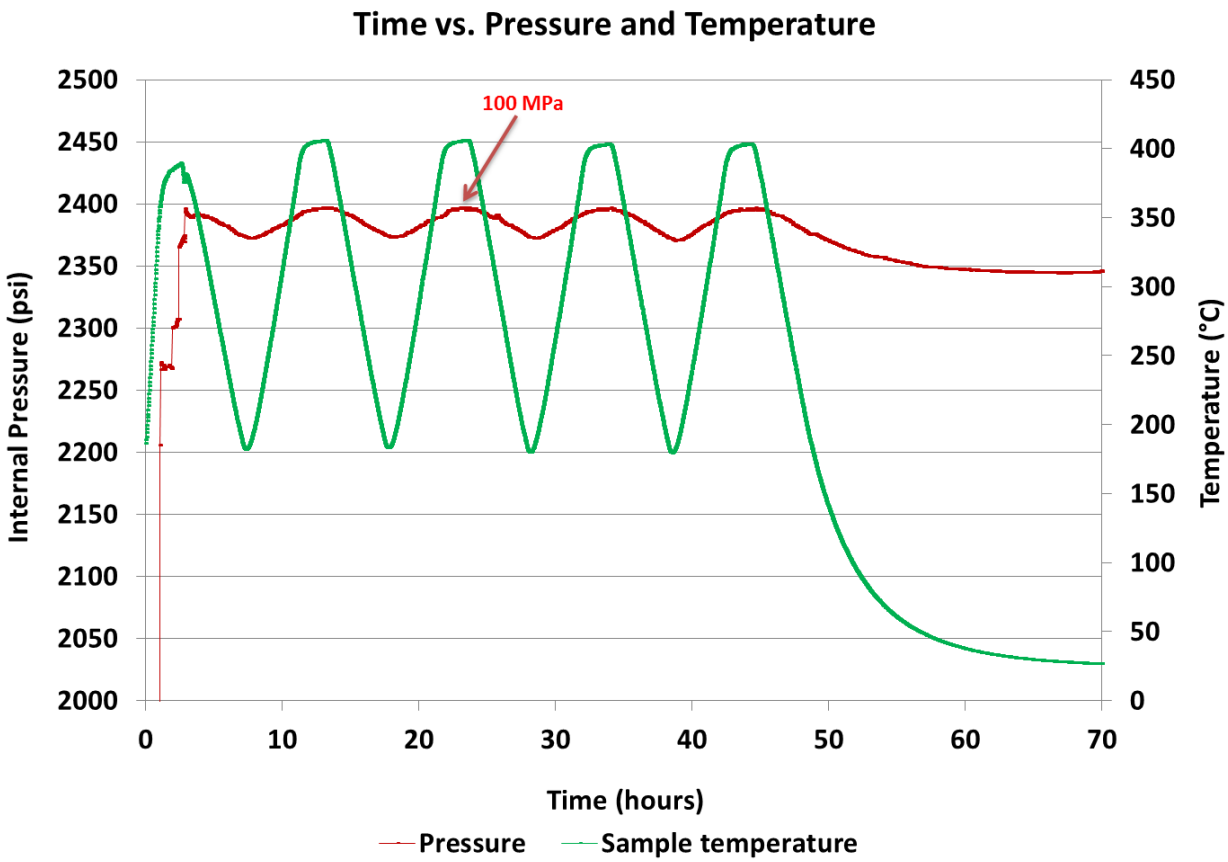

Fig. 13. Pressure and sample temperature as a function of time for Test HR-HBR#3.

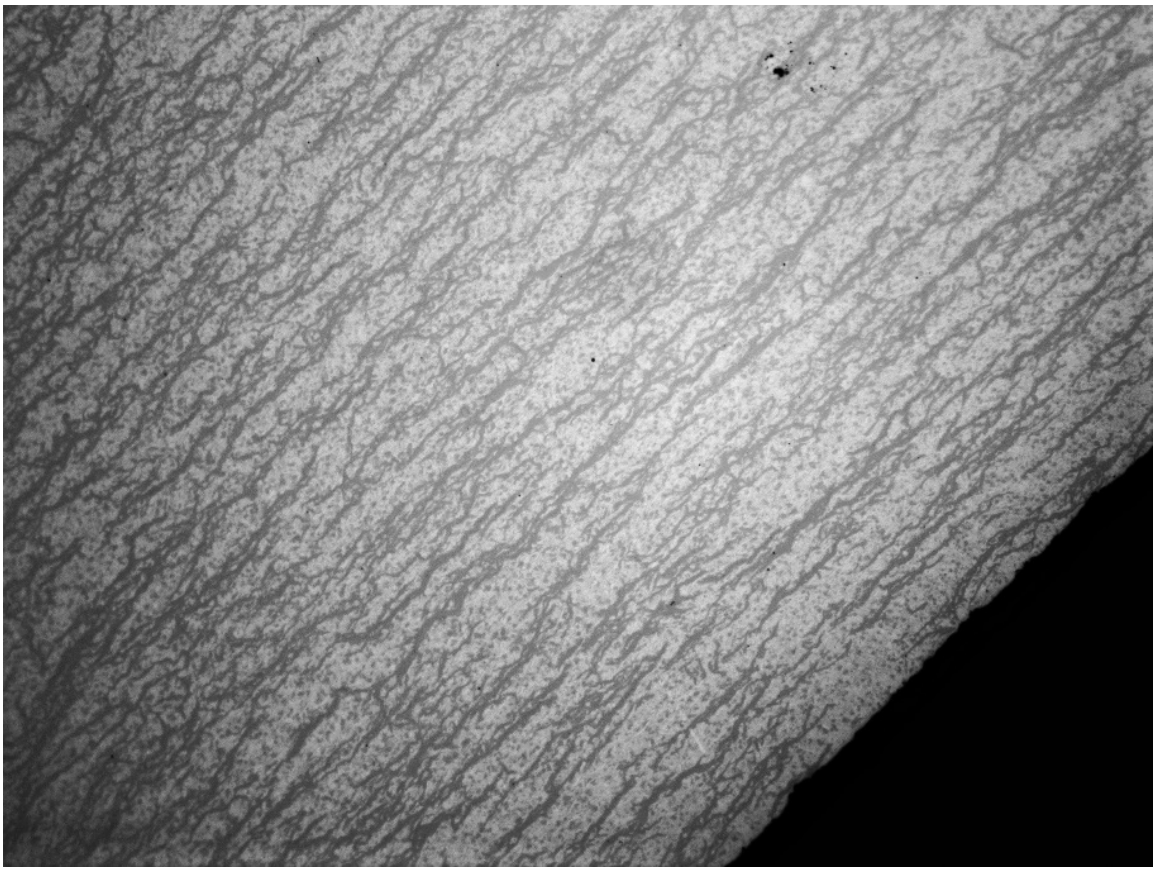

Fig. 14. High magnification micrograph showing radial hydrides of Sample HR-HBR#3 with hydrogen content H ≈ 310 ppm.
The specimen was sectioned at the midplane of a 6-in.-long sample.

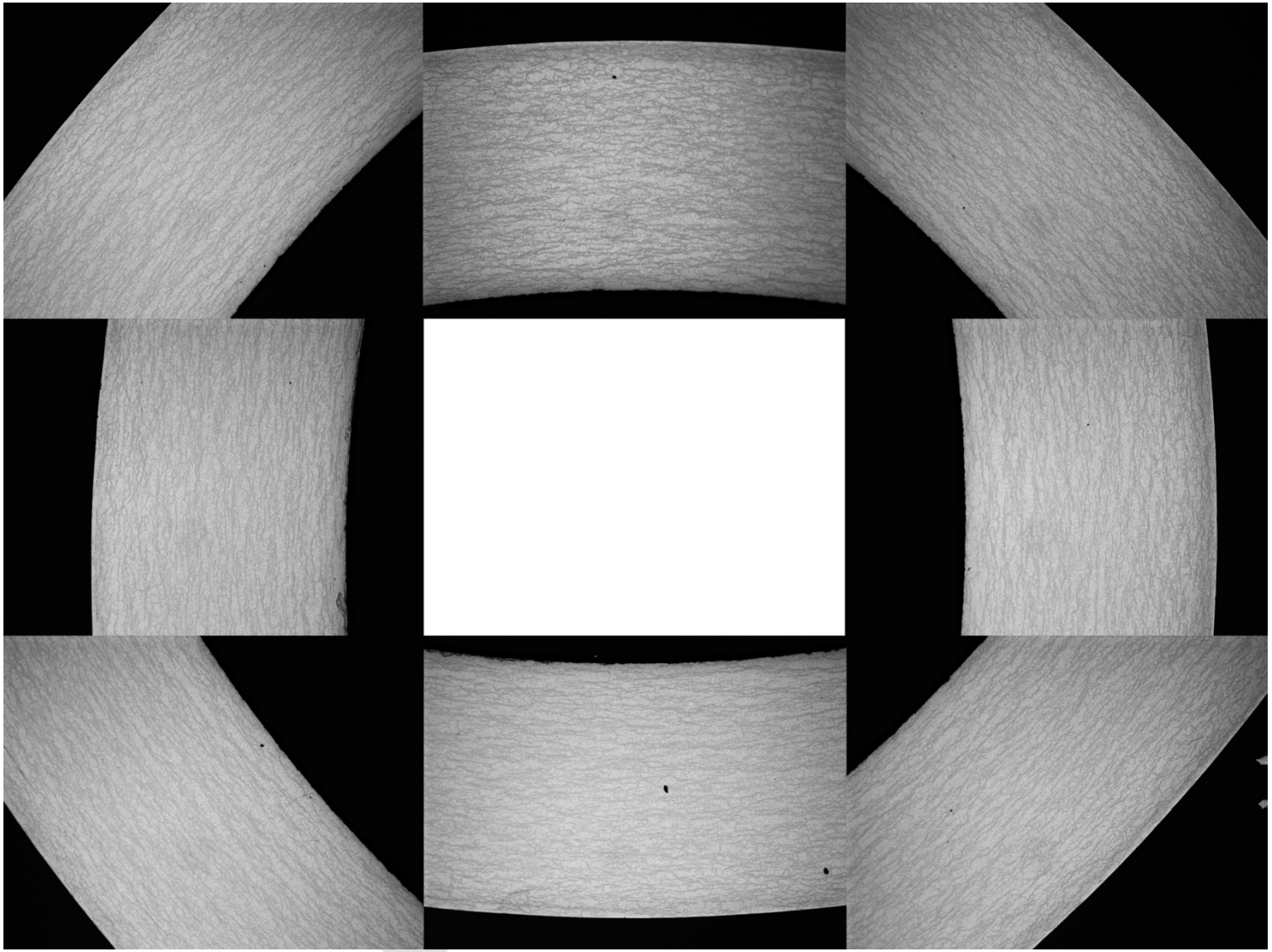

Fig. 15. Radial hydride distribution shown in eight areas in different circumferential directions of Sample HR-HBR#3.
The specimen was sectioned at the midplane of a 6-in.-long sample.

4.4 HR-HBR#4, 120 MPa at 400°C, five cycles

Test HR-HBR#4 was conducted on a hydrided 15 × 15 Zircaloy-4 at the maximum hoop stress of 120 MPa and the hold temperature T = 400°C. After fabrication, the specimen was assembled into a holder within the furnace for heating to 400°C, held at 400°C for 2 hours, cooled at 1°C/min to 170°C, and then heated at 1°C/min to 400°C again for five cycles. The sample was furnace cooled from 170°C to RT for the last cycle. Figure 16 shows the temperature and pressure history for HR-HBR#4. The plotted temperature is a thermocouple reading near the specimen surface.

Figure 17 shows the hydride morphology of Sample HR-HBR#4 with hydrogen content H ≈ 312 wppm. The specimen was sectioned at the midplane of a 6-in.-long sample. The radial hydride can be observed. The maximum length of the radial hydride is < 30 μm. The radial hydride ratio of HR-HBR#4 also is lower than the ratio of HR-HBR#2. However, the radial hydride ratio of HR-HRB#4 is higher than that of HR-HRB#3 because of the higher pressure. Figure 18 shows radial hydride distribution in eight areas in different circumferential directions of Sample HR-HBR#4.

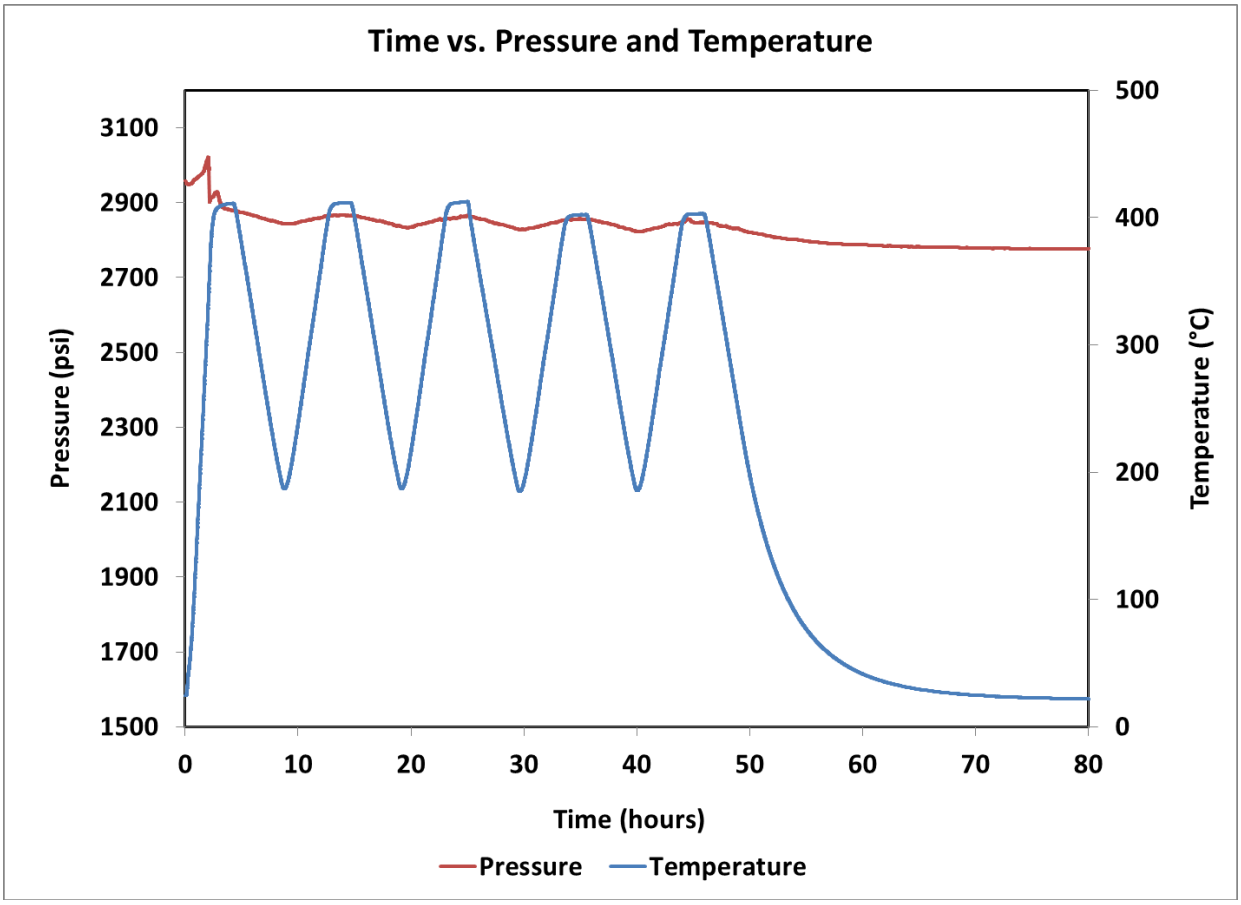

Fig. 16. Pressure and sample temperature as a function of time for Test HR-HBR#4.

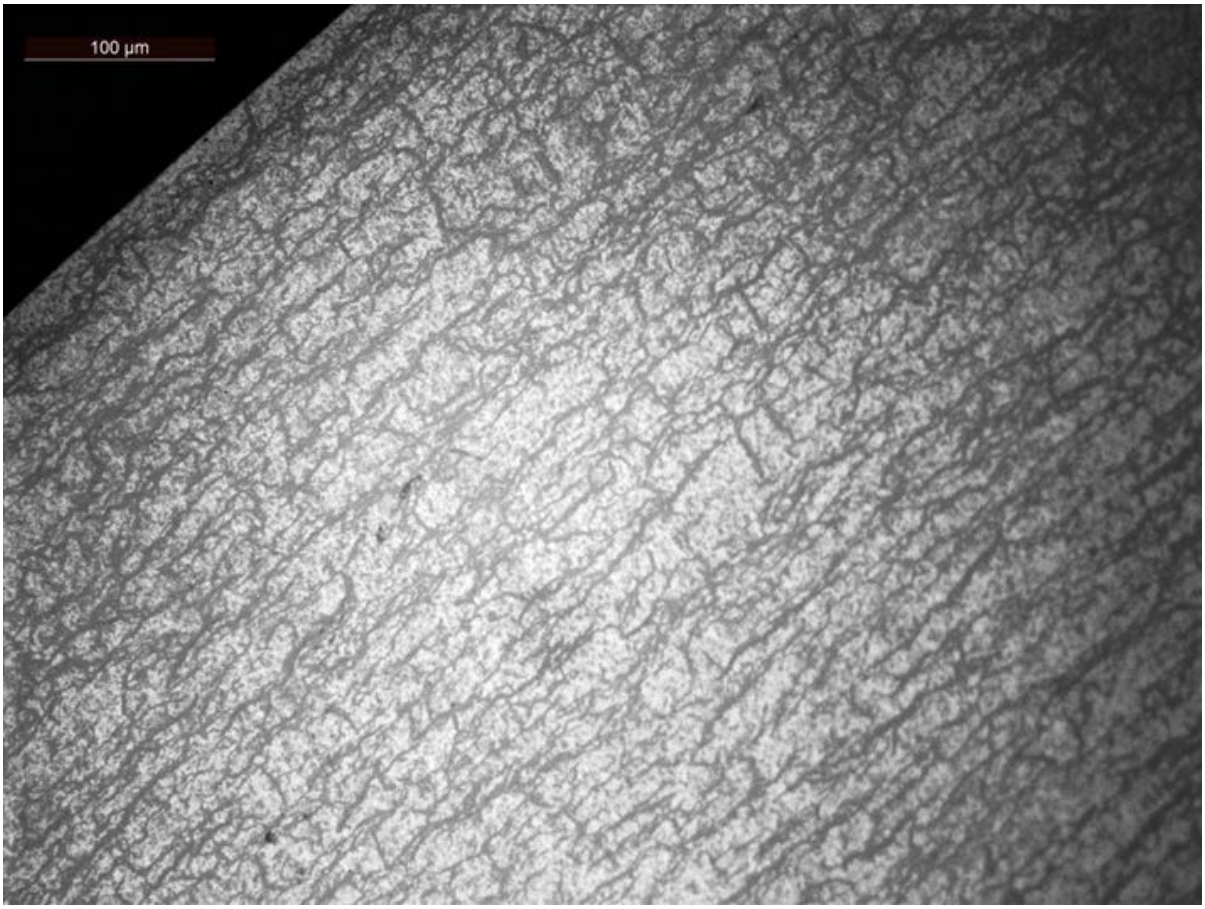

Fig. 17. High magnification micrograph showing radial hydrides of Sample HR-HBR#4 with hydrogen content H ≈ 312 ppm. The specimen was sectioned at the midplane of a 6-in.-long sample.

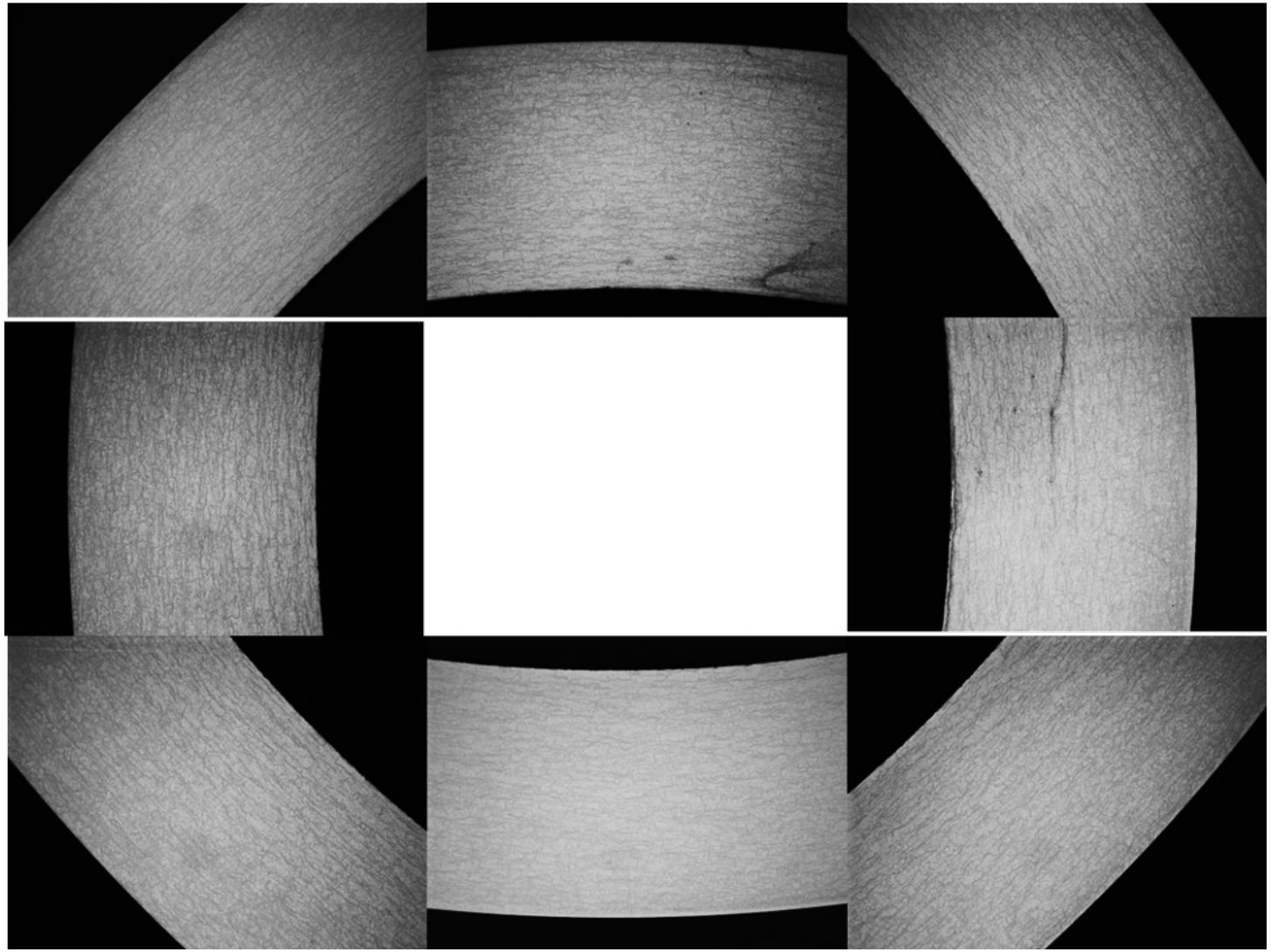

Fig. 18. Radial hydride distribution shown in eight areas in different circumferential directions of Sample HR-HBR#4.
The specimen was sectioned at the midplane of a 6-in.-long sample

5. DISCUSSION

The terminal solid solubility (TSSd) of hydrogen in Zircaloy is shown in Fig. 19 [9- 11]. The solubility limit is very low at room temperature (< 10 wppm is soluble), and ≈ 200 wppm is soluble at 400°C according to the phase diagram for the zirconium–hydrogen binary system [12, 13]. Therefore, when the furnace is cooled from an elevated temperature to RT, the hydrogen precipitates as a hydride in hydrided cladding samples. In fact, the hydrided Zircaloy-4 is a composite material that consists of a ductile matrix, α-Zr, and brittle second-phase hydrides. It was found that radial hydrides can be formed under a hoop tensile stress when the cladding sample is pressurized internally [3–6].

In this work, the hydrided tubing samples have been pressurized internally to produce a hoop stress up to 150 MPa to form radial hydrides using the hydride reorientation system (see Sect. 4). Tests HR-HBR#1 and HR-HBR#2 indicate that multithermal cycling will increase the ratio of radial hydrides under the same maximum temperature and maximum internal pressure. In addition, our test results of Tests HR-HBR#2 through HR-HBR#4 reveal that the ratio of radial hydrides decreases as the internal pressure decreases when the temperature and pressure profiles remain the same.

Our goal is to investigate the impact of radial hydrides on high burnup fuel cladding ductility, for which we need to produce a reasonably high percentage of radial hydrides within the cladding by the hydride reorientation tests. The out-of-cell tests are very important to support planning of the in-cell hydride reorientation tests, as it establishes a test procedure and provides a guideline for in-cell test conditions. Based on the four out-of-cell tests, we decided to start our in-cell hydride reorientation test under the same test conditions of Test HR-HBR#2 to maximize the radial hydride condition.

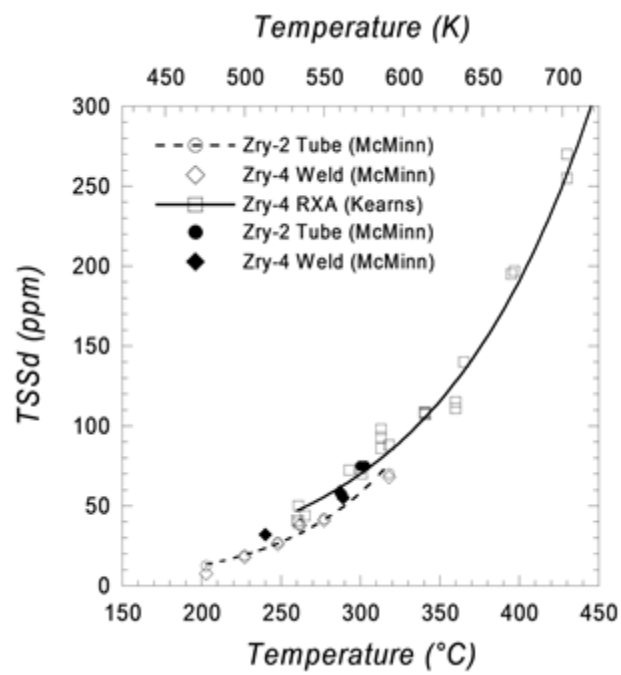

Fig. 19. Terminal solid solubility for dissolution (TSSd) of hydrogen in Zircaloy. (*Sources:* [1] J. J. Kearns, "Terminal Solubility and Partitioning of Hydrogen in the Alpha Phase of Zirconium, Zircaloy-2 and Zircaloy-4," *Journal of Nuclear Materials* 22 [1967]: 292. [2] A. McMinn, E. C. Darby, and J. S. Schofield, "The Terminal Solid Solubility of Hydrogen in Zirconium Alloys," *Zirconium in the Nuclear Industry: 12th International Symposium,* ASTM STP 1354, p. 173–195 [2000].)

6. CIRFT EVALUATIONS OF HBR FUEL FOR HYDRIDE REORIENTATION STUDY

6.1 Overview of CIRFT Evaluations and Results for HBR Fuel Rods

Rod segments, measuring 6 in. long, for CIRFT evaluations were prepared from five HBU HBR SNF rods. Specimen labels and corresponding segment IDs are given in Table 3.

ORNL completed 24 tests in FY 2013 and FY 2014. Fifteen tests were dedicated to dynamic testing conditions with amplitudes ranging between 5.08 and 35.56 Nm. Several tests were run at amplitudes below 8.89 Nm over tens of millions of cycles, and the specimens did not show any sign of failure, so these tests were stopped.

Table 3. Specimen labels used for HBR SNF

Spec ID	ORNL ID	Endcap A	Endcap B	Seg. ID	Note
S1	S1	S1-A	S1-B	606C3C	
S2	S2	S2-A	S2-B	605D1E	
S3	Dcal	Dcal-A	Dcal-B	609C5	
S4	Scal	Scal-A	Scal-B	609C6	
D1	DL1	DL1-A	DL1-B	607C4B	
D2	DL2	DL2-A	DL2-B	608C4B	
D3	DL3	DL3-A	DL3-B	605C10A	
D5	DM2	DM2-A	DM2-B	605D1B	
D4	DM1	DM1-A	DM1-B	605D1C	
D6	DH1	DH1-A	DH1-B	609C4	
D7	DH2	DH2-A	DH2-B	609C3	
D8	DM3	DM3-A	DM3-B	606C3E	
D9	DH3	DH3-A	DH3-B	609C7	
D10	S5	S5-A	S5-B	606C3A	
D11	R1	R1-A	R1-B	607C4A	
D12	R2	R2-A	R2-B	608C4A	
D13	R3	R3-A	R3-B	606B3E	
D14	R4	R4-A	R4-B	606B3D	
D15	R5	R5-A	R5-B	606B3C	
D16	S3	S3-A	S3-B	605D1F	
Demo1	Demo1	Demo1-A	Demo1-B	606B2	
HR1	HR1	HR1-A	HR1-B	607D4C	FY 2016
HR2	HR2	HR2-A	HR2-B	607D4A	FY 2016
HR3	HR3	HR3-A	HR3-B	608D4A	FY 2016
HR4	HR4	HR4-A	HR4-B	608D4C	FY 2016

6.2 FY 2016 PHASE II CIRFT HR Test Results (Appendix A)

6.2.1 Hydride Reorientation Test Samples Preparation

Four CIRFT evaluations were completed on the HBR specimens with hydride reoriented treatment (HRT), 145 MPa hoop stress, 170 to 400°C, five cycles in FY 2016. Bending amplitudes ranging from 10.16 and 16.26 Nm were tested. One of the HBR HRT specimens (HR2) was tested under static conditions, however the specimen survived the static loading without failure and was then tested under dynamic loading, as will be discussed. Due to a welded endcap leak, only thermal heat treatment was applied to the HR4 sample.

The sample preparation for the hydride reorientation (HR) project is detailed below.

- The HBU HBR fuels under simulated drying operation conditions of the SNF were used for the HR testing study. Based on out-of-cell benchmark HR tests with hydrided HBR Zircaloy-4 cladding, four in-cell tests were conducted with HBU HBR fuel samples subjected to hydride reorientation at approximately 145 MPa at 400°C.
- The HBR fuel samples for HR tests were prepared in the irradiation fuel examination laboratory. After the samples were sectioned into 6 in.-long pieces, the surface oxide layer and fuel material were removed from both ends to a depth of approximately 0.5 in. Endcaps were welded at both ends, and the HBR fuel specimens were then pressurized with argon gas at a maximum hoop stress level of 145 MPa and a target hold temperature (T = 400°C). Thermal cycling was performed to increase the radial hydrides. All in-cell tests had the same temperature profiles. Fig. 20 shows the temperature history of the first in-cell HR test, HR1, with a HBU HBR sample.

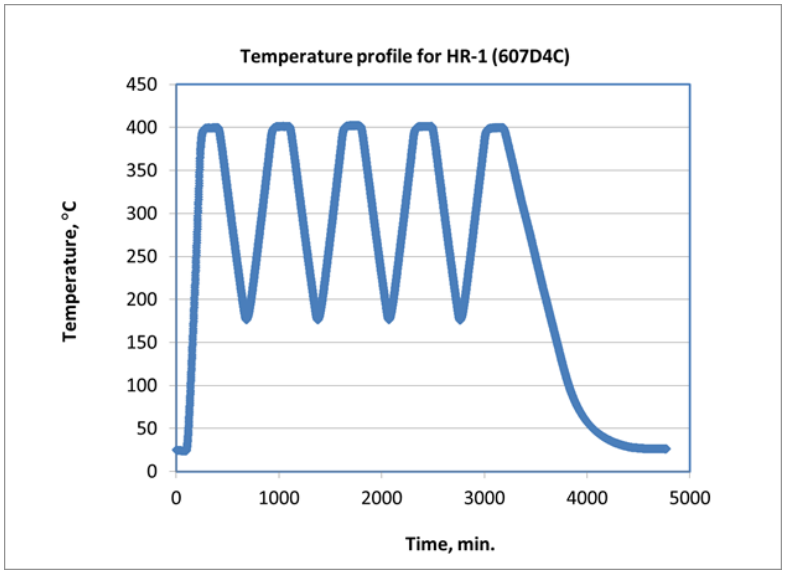

Fig. 20. Sample temperature as a function of time for in-cell HR test HR-1.

- The hydride-reoriented samples were subjected to CIRFT testing at room temperature to evaluate the materials performance after hydride reorientation. After the tests were completed in the CIRFT, the specimens were examined to verify the radial hydrides had been generated. Fig. 21 shows the hydride morphology of hydride-reoriented sample HR1. The hydrogen concentration of this sample was about 360–400 wppm. The MET mount specimen was sectioned at the midplane of a 6 in.-long sample. Although the in-cell HR test conditions were the same as the out-of-cell test HR-HBR#2 and the hydrogen concentration of these two samples were compatible, the morphology of HBU sample HR1 was different from hydrided sample HR-HBR#2. For the

unirradiated sample, the circumferential hydrides were uniformly distributed across the wall, and the maximum length of its radial hydrides was about 50–60 μm. For HBU samples, the radial hydrides were mainly distributed near the inner surface, and the circumferential hydrides are mostly seen near the outer surface. The length of the radial hydride of the HBU sample, Fig. 21(a), was also much longer than the unirradiated sample, Fig. 21(b).

(a)

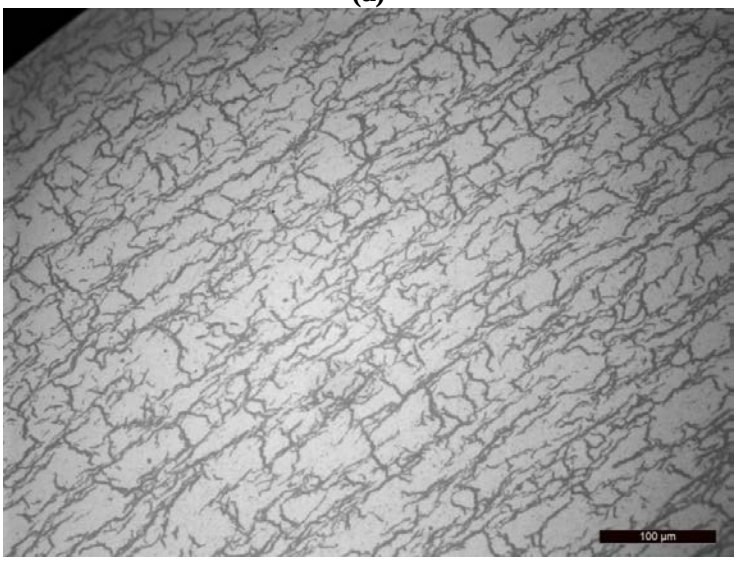

(b)

Fig. 21. (a) High magnification micrograph showing radial hydrides of Sample HR-1 (H ≈ 360–400 ppm). The HBU HBR specimen was pressurized to 145 MPa at 400°C with five thermal cycles. (b) High magnification micrograph showing radial hydrides of Sample HR-HBR#2 (H ≈ 286 ppm). The specimen was sectioned at the midplane of a 6 in.-long sample.

6.2.2 Measurements and Monitoring Data

The results for each test are given in Appendix A.

The flexural rigidity of the rod specimens treated by hydride reorientation was shown to be much lower than as-received specimens under equivalent amplitude. For example, under the same amplitude of 100 N,

the rigidity of the HRT specimen (HR3) was only about 57% of the as-received specimen (DL3). The variation of rigidity during a cyclic test was continuous. In HR3, a sudden drop was observed before failure.

6.2.3 Fatigue Life

The results for the dynamic tests of HBR fuel in FY 2016 are summarized in Table 4. Again, definitions of the column heads are same as those for LMK fuels in Table 10.

The plots based on the mean values of quantities are given in Fig. 22(a)–(d), where HBR1 represents the as-received specimen, and HBR2 represents the specimen after radial hydride treatment (RHT). Note the data of as-received HBR specimens were based on the original analysis method; (i.e., no correction was applied). It has been shown that the HRT reduces the fatigue life of SNF rods, which can be seen from the tests around 15 Nm. It was further observed for HR2, as indicated by the arrow, there was an additional fatigue life reduction. Such reduction obviously resulted from the large-deformation static loading before the dynamic cyclic loading.

Several images of the failed specimens that were subjected to the reorientation procedure are provided in Fig. 23. The failures of these specimens were in the gauge section, and in two of them, the failure was taking place at a pellet-to-pellet interface.

Table 4a. Dynamic test results for HBR SNF rods, FY 2016

TN	Spec	Load in.	N cycles	Fail	ma Nm	ma_std Nm	ka m^1	ka_std m^−1	km m^−1	km_std m^−1
25	HR1	150	4.19E + 04	1	15.152	0.549	0.517	0.016	0.527	0.019
26	HR2	160	9.47E + 03	1	14.702	0.806	0.478	0.121	0.511	0.205
27	HR3	100	2.44E + 05	1	8.982	0.066	0.267	0.005	0.291	0.009
28	HR4	160	5.47E + 04	1	14.759	0.089	0.394	0.008	0.421	0.009

Table 4b. Dynamic test results for HBR SNF rods, FY 2016

TN	Spec	R Nm^2	R_std Nm^2	Sa MPa	sa_std MPa	ea %	ea_std %	em %	em_std %	Lg2 mm	Lg2_std mm	dh mm	dh_std mm
25	HR1	29.329	0.775	128.788	4.666	0.278	0.009	0.284	0.010	44.733	0.565	1.329	0.197
26	HR2	31.567	3.256	124.964	6.848	0.257	0.065	0.275	0.110	50.657	1.593	-0.174	0.372
27	HR3	33.659	0.602	76.342	0.560	0.144	0.003	0.157	0.005	43.368	0.643	-1.649	0.252
28	HR4	37.497	0.593	125.449	0.755	0.212	0.004	0.227	0.005	45.977	0.578	1.206	0.201

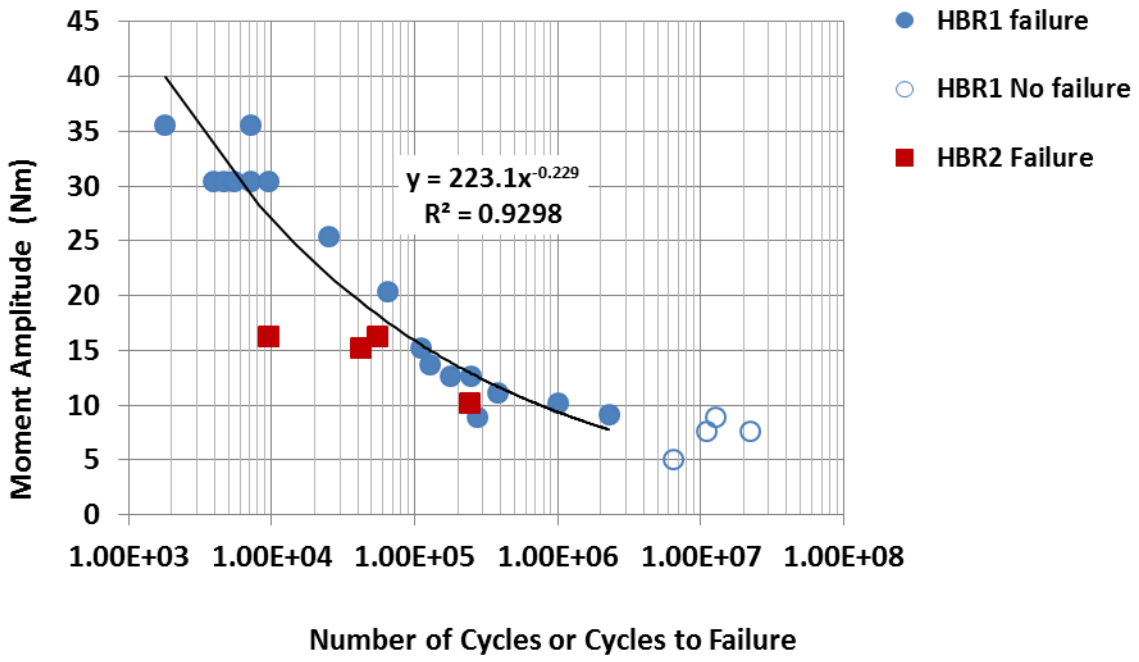
45
40
35
30
25
20
15
10
5
0
Moment Amplitude (Nm)
y = 223.1x^-0.229
R² = 0.9298
1.00E+03
1.00E+04
1.00E+05
1.00E+06
1.00E+07
1.00E+08
Number of Cycles or Cycles to Failure
HBR1 failure
HBR1 No failure
HBR2 Failure

(a)

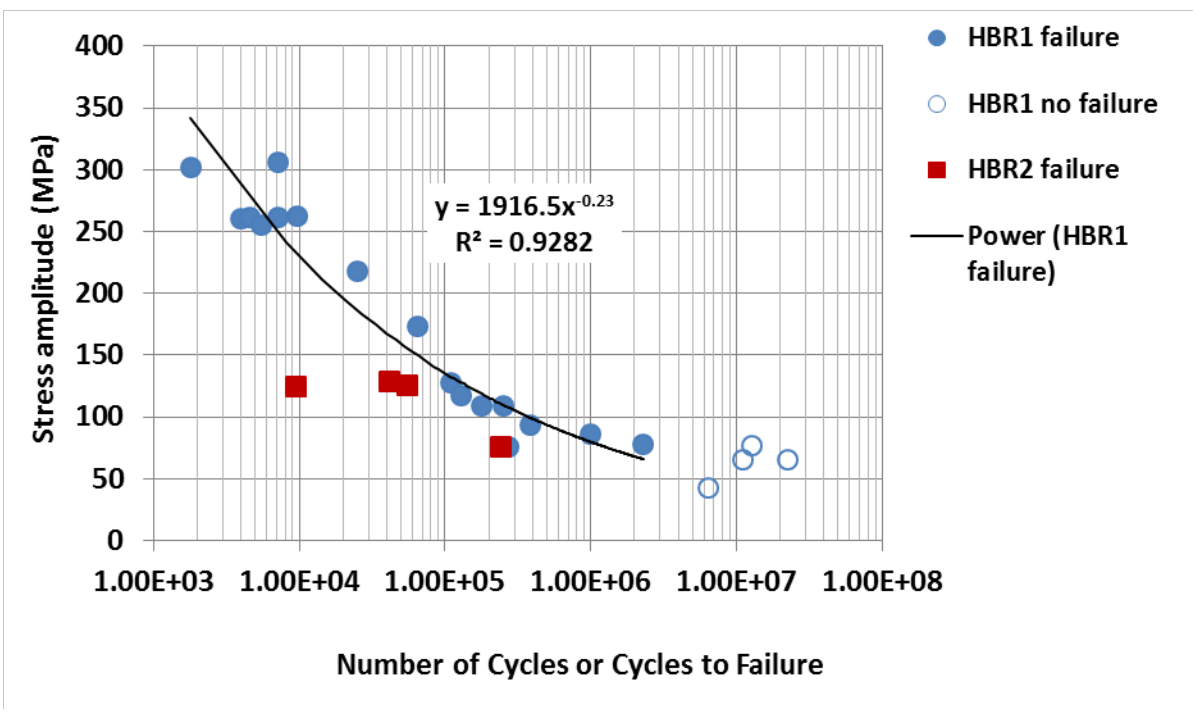
400
350
300
250
200
150
100
50
0
Stress amplitude (MPa)
y = 1916.5x^-0.23
R² = 0.9282
1.00E+03
1.00E+04
1.00E+05
1.00E+06
1.00E+07
1.00E+08
Number of Cycles or Cycles to Failure
HBR1 failure
HBR1 no failure
HBR2 failure
Power (HBR1 failure)

(b)

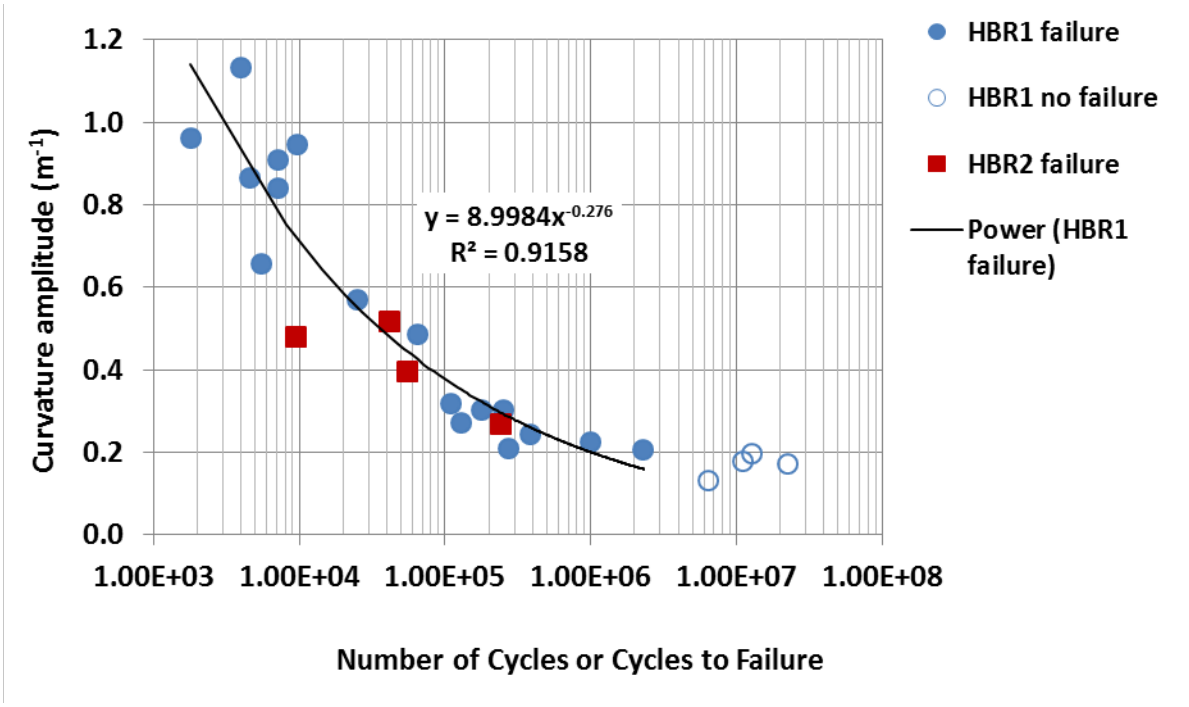

(c)

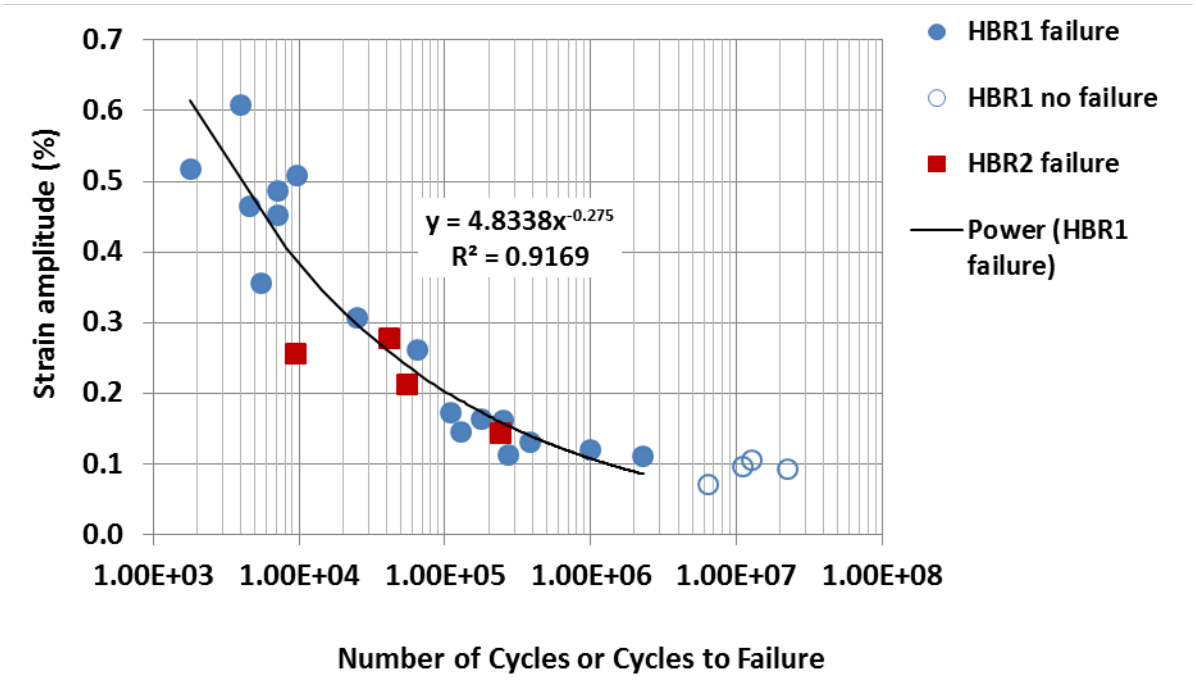

(d)

Fig. 22. (a) Moment amplitude, (b) stress amplitude, (c) curvature amplitude, and (d) strain amplitude rigidity as a function of cycles or cycles to failure.

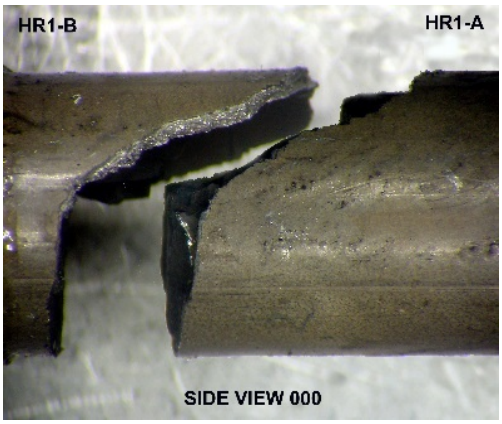
HR1-B
HR1-A
SIDE VIEW 000

(a)

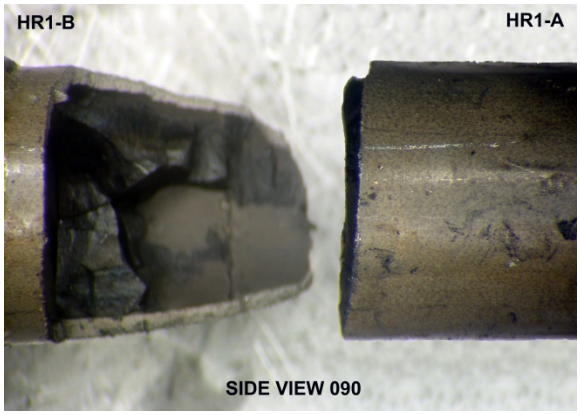
HR1-B
HR1-A
SIDE VIEW 090

(b)

HR1-A
END VIEW

(c)

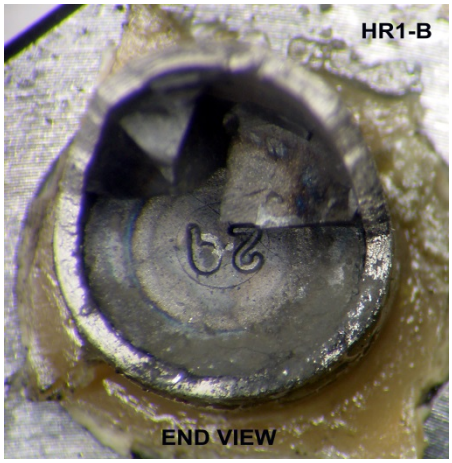
HR1-B
END VIEW

(d)

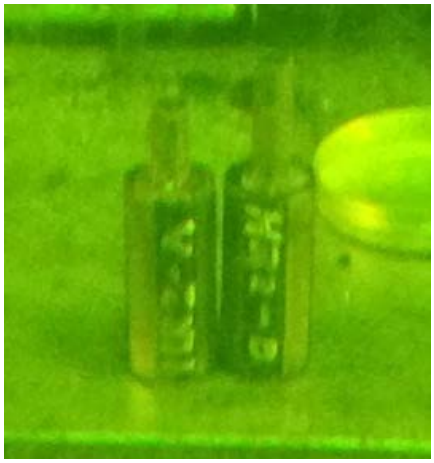

(e)

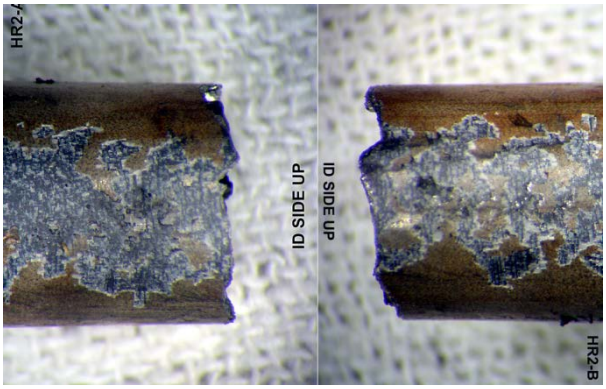
ID SIDE UP
ID SIDE UP
HR2-B

(f)

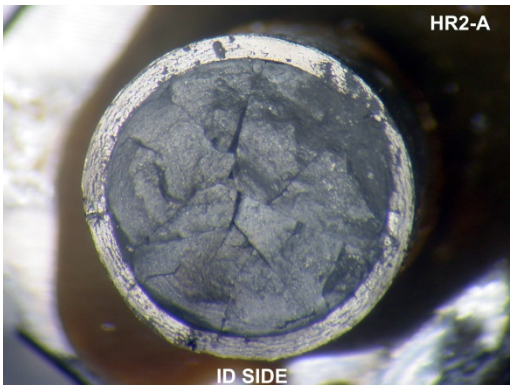
HR2-A
ID SIDE

(g)

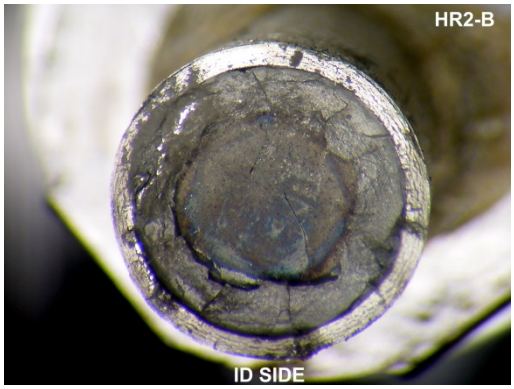
HR2-B
ID SIDE

(h)

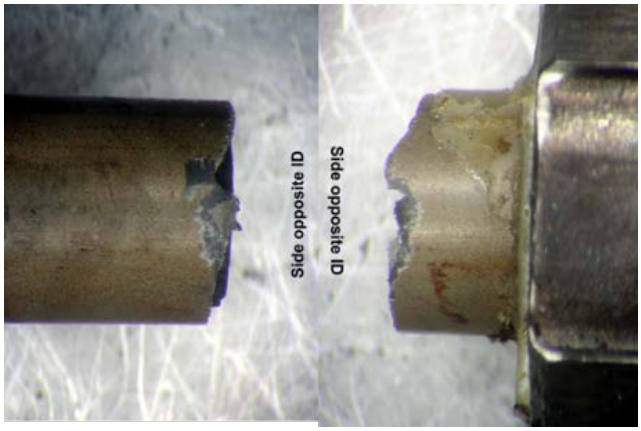
Side opposite ID
Side opposite ID

(i)

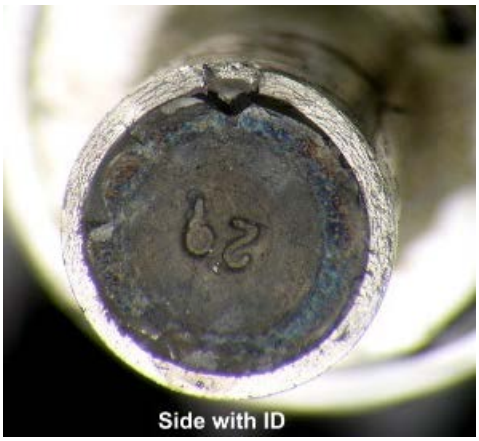
Side with ID

(j)

HR-4A
HR4-B

(k)

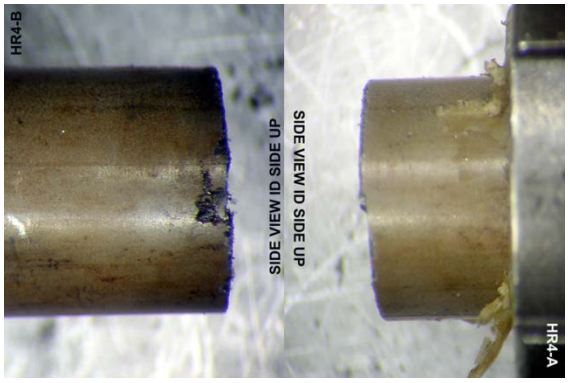
HR4-B
SIDE VIEW ID SIDE UP
SIDE VIEW ID SIDE UP
HR4-A

(l)

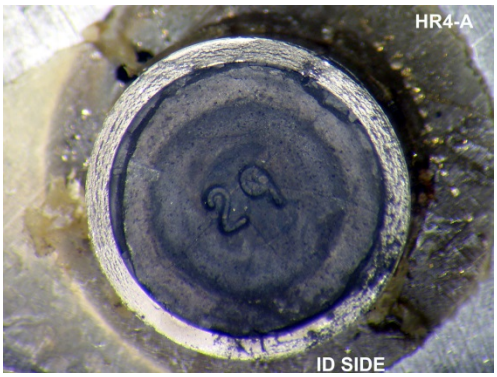

(m)

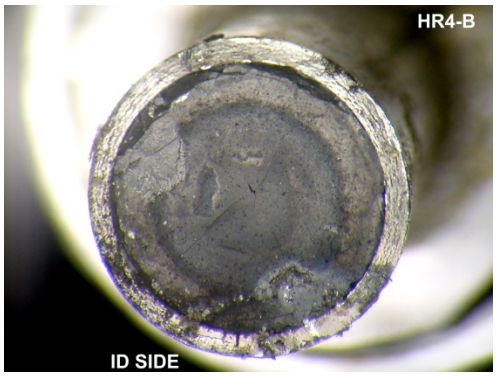

(n)

Fig. 23. Images showing the failure modes for (a) (b) (c) (d) HR1, (e) (f) (g) (h) HR2, (i) (j) HR3, and (k) (l) (m) (n) HR4.

7. CONCLUSION

Four CIRFT data evaluations were completed on the high burnup Zircaloy-4 HBR SNF rods with radial hydride treatment (145 MPa hoop stress, 170 to 400°C, five cycles) in FY 2016. Amplitudes ranging from 10.16 and 16.26 Nm were tested. One of the specimens (HR2) was tested under static loading initally. This specimen survived the static loading without failure and was then tested under dynamic loading. Due to a welded endcap leak, only thermal heat treatment was applied to the HR4 sample.

General observations from Phase II CIRFT test data evaluations are:

1) Comparing reoriented CIRFT test results to results from non-reoriented CIRFT tests on the same high burnup Zircaloy-4 material, it appears that radial hydrides and HRT could have a negative impact on the fatigue life of CIRFT specimens.
2) Comparing the CIRFT testing result on a sample subjected to temperature cycling without rod pressurization (HR4) to the baseline CIRFT test results, it appears that the thermal heating along may have a negative impact on the fatigue life of the HBR rod.

9. ACKNOWLEDGMENTS

This research was sponsored jointly by the Nuclear Regulatory Research of US Nuclear Regulatory Commission and US Department of Energy (DOE) Used Fuel Disposition Campaign under DOE contract DE-AC05-00OR22725 with UT-Battelle, LLC. The authors thank ORNL program managers Michelle Bales and Bruce Bevard for their support and guidance, Chuck Baldwin for post-irradiation examination, Dale Caquelin and Bob Morris for providing logistic hot cell support, Josh Schmidlin for fuel rod cutting and dimension measurement, Bryan Woody and Scott Thurman for hot cell operation support, Brian Sparks and Randy Parten for drawing and machining support.

10. REFERENCES

1. Y. Yan, T. A. Burtseva, and M. C. Billone, *Post-Quench Ductility Results for North Anna High Burnup 17 × 17 ZIRLO Cladding with Intermediate Hydrogen Content*, Argonne National Laboratory letter report to the Nuclear Regulatory Commission, April 17, 2009. Available online as ML091200702 at http://www.nrc.gov/reading-rm/adams.html.

2. M. C. Billone, Y. Yan, T. Burtseva, and R. Daum, *Cladding Embrittlement during Postulated Loss-of-Coolant Accidents*, NUREG/CR–6967, ANL-07/04, Argonne National Laboratory, Argonne, IL, 2008.

3. M. C. Billone, T. Burtseva, and Y. Yan. "Overview of Spent Nuclear Fuel Program: Test Plan and High Burnup Cladding at ANL," *NRC Program Review Meeting*, Argonne National Laboratory, Argonne, IL, July 7, 2010.

4. R. Daum, H. Tsai, Y. Liu, and M. Billone, "High-Burnup Cladding Mechanical Performance during Cask Storage and Post-Storage Handling and Transportation," *Nuclear Safety Research Conference*, Washington, DC, October 25–27, 2004.

5. Y. Yan, et al., "Observation and Mechanism of Hydride in Zircaloy-4 and Local Radial Hydride Induced by High Pressure at High Temperatures," *2013 International High-Level Radioactive Waste Management*, Albuquerque, NM, April 28–May 2, 2013.

6. Y. Yan, L. K. Plummer, H. Ray, T. Cool, and H. Z. Bilheux, "Ductility Evaluation of As-Hydrided and Hydride Reoriented Zircaloy-4 Cladding under Simulated Dry-Storage Condition," *2013 MRS Fall Meeting Proceeding*, Boston, MA, December 1–6, 2013.

7. M. C. Billone, T. A. Burtseva, and Y. Yan, *Ductile-to-Brittle Transition Temperature for High-Burnup Zircaloy-4 and ZIRLO™ Cladding Alloys Exposed to Simulated Drying-Storage Conditions*, Argonne National Laboratory letter report to the Nuclear Regulatory Commission, ANL-13/13, September 28, 2013. Available online as ML12181A238 at http://www.nrc.gov/reading-rm/adams.html.

8. E. J. Ruzauska and K. N. Fardell, "Design, Operation, and Performance Data for High Burnup PWR Fuel from the H. B. Robinson Plant for Use in the NRC Experimental Program at Argonne National Laboratory," Electric Power Research Institute report 1001558, May 2001.

9. M. Griffiths, J. F. Mecke, and J. E. Winegar, "Evolution of Microstructure in Zirconium Alloys During Irradiation," *Zirconium in the Nuclear Industry: 11th International Symposium*, ASTM STP 1295, pp. 580–602 (1996).

10. J. J. Kearns, "Terminal Solubility and Partitioning of Hydrogen in the Alpha Phase of Zirconium, Zircaloy-2, and Zircaloy-4," *Journal of Nuclear Materials* 22 (1967): 292.

11. A. McMinn, E. C. Darby, and J. S. Schofield, "The Terminal Solid Solubility of Hydrogen in Zirconium Alloys," *Zirconium in the Nuclear Industry: 12th International Symposium*, ASTM STP 1354, p. 173–195 (2000).

12. D. O. Northwood and U. Kosasih, "Hydrides and Delayed Hydrogen Cracking in Zirconium and its Alloys," *International Metals Review* 28, no. 2 (1983): 92.

13. S. Mishra, K. S. Sivaramakrishnan, and M. K. Asundi, "Formation of the Gamma Phase by a Peritectoid Reaction in the Zirconium–Hydrogen System," *Journal of Nuclear Materials* 45 (1972): 235.

APPENDIX A
CIRFT TESTING RESULTS OF HBR SNF– Phase II

Table of Contents

APPENDIX F CIRFT TESTING RESULTS OF HBR SNF – Phase II A-1
Measurement and monitoring rigidity curves of HBR HR data A-3

Measurement and monitoring rigidity curves of HBR HR data

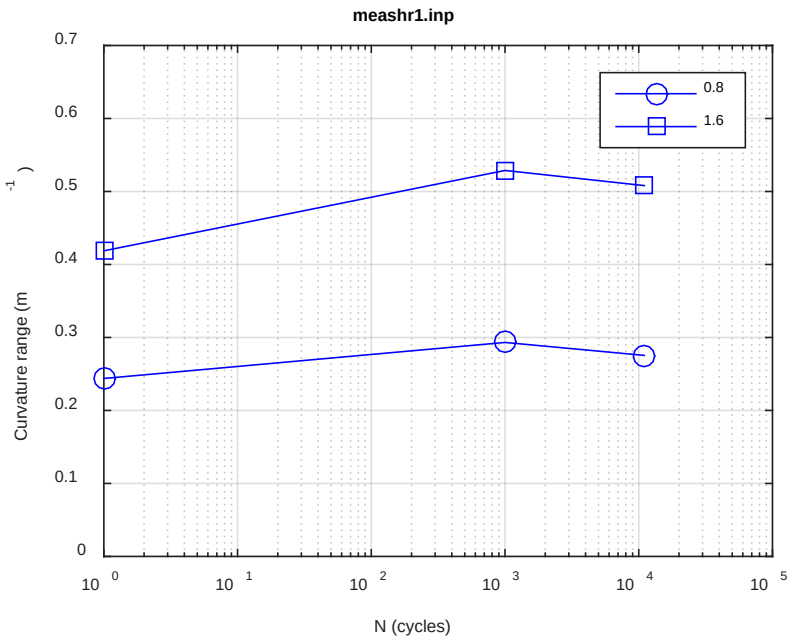
meashr1.inp
0.7
0.6
0.5
0.4
0.3
0.2
0.1
0
Curvature range (m -1)
0.8
1.6
10 0
10 1
10 2
10 3
10 4
10 5
N (cycles)

(a)

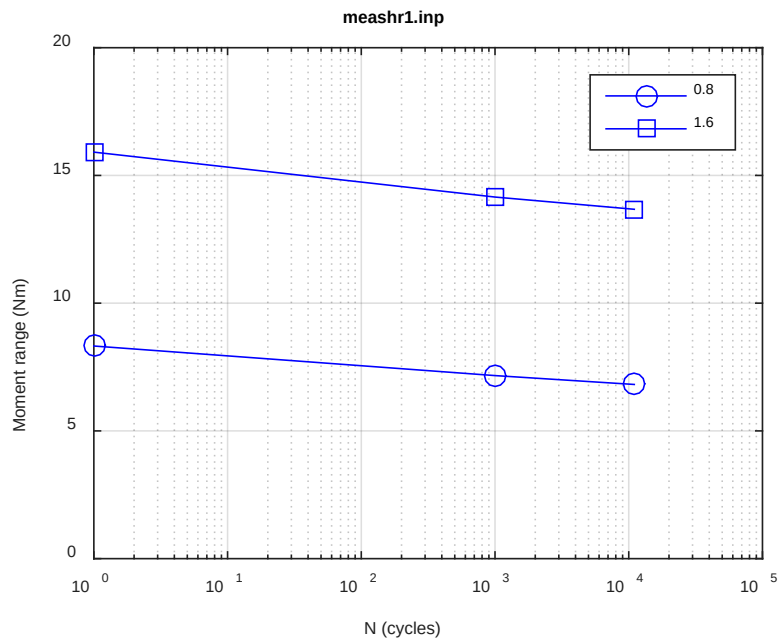
meashr1.inp
20
15
10
5
0
Moment range (Nm)
0.8
1.6
10 0
10 1
10 2
10 3
10 4
10 5
N (cycles)

(b)

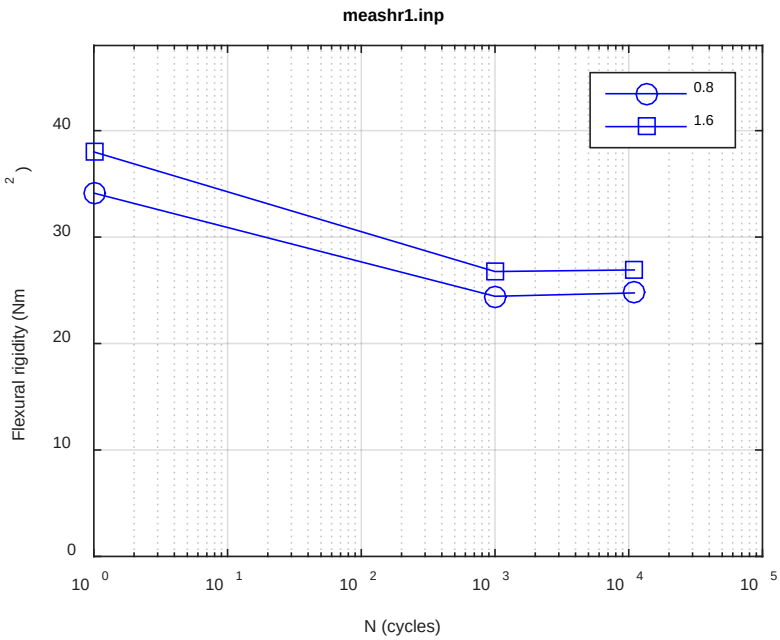
meashr1.inp
0.8
1.6
Flexural rigidity (Nm 2)
40
30
20
10
0
10 0
10 1
10 2
10 3
10 4
10 5
N (cycles)

(c)

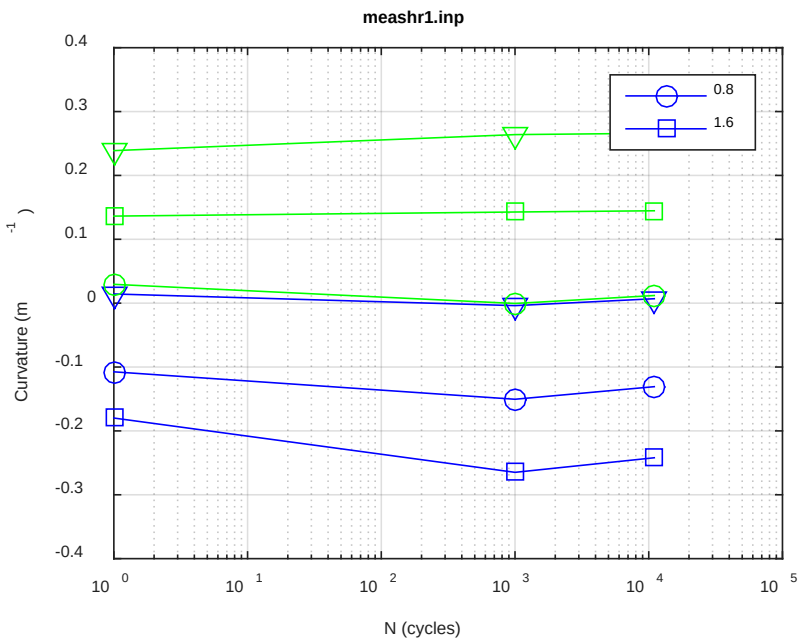
meashr1.inp
0.8
1.6
Curvature (m -1)
0.4
0.3
0.2
0.1
0
-0.1
-0.2
-0.3
-0.4
10 0
10 1
10 2
10 3
10 4
10 5
N (cycles)

(d)

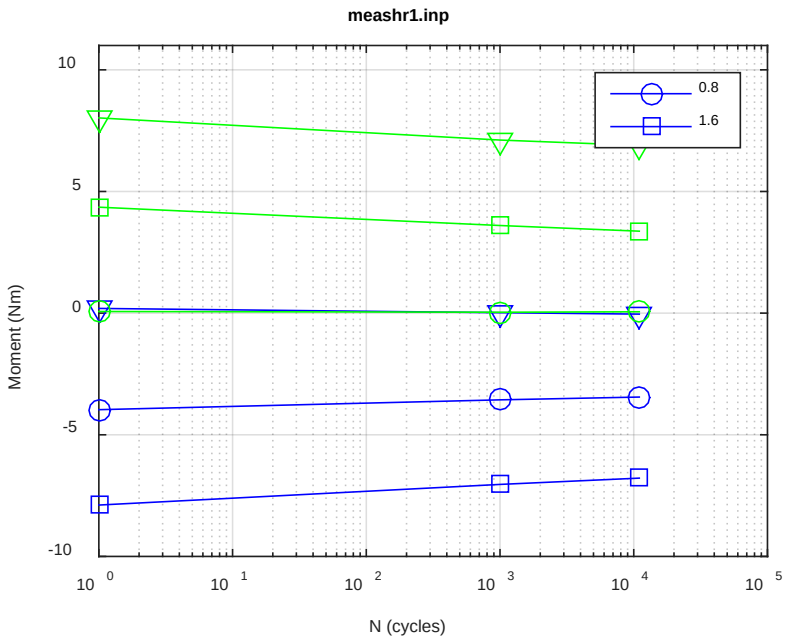

(e)

Fig. F.1 Measurement-based responses: (a) curvature range, (b) moment range, (c) rigidity, (d) curvature peak/valley, (e) moment peak/valley, HR1, 15.24 Nm.

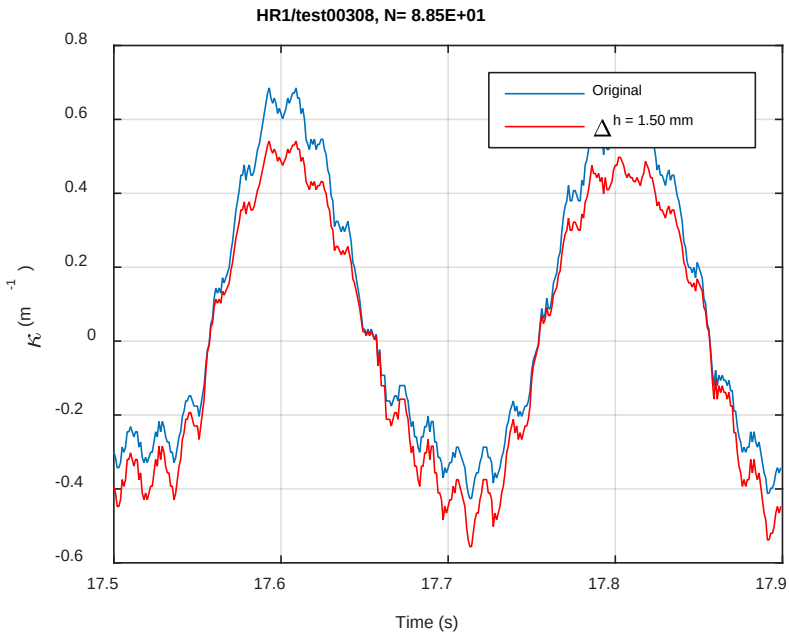
HR1/test00308, N= 8.85E+01
Original
Δh = 1.50 mm
κ (m -1)
Time (s)
0.8
0.6
0.4
0.2
0
-0.2
-0.4
-0.6
17.5
17.6
17.7
17.8
17.9

(a)

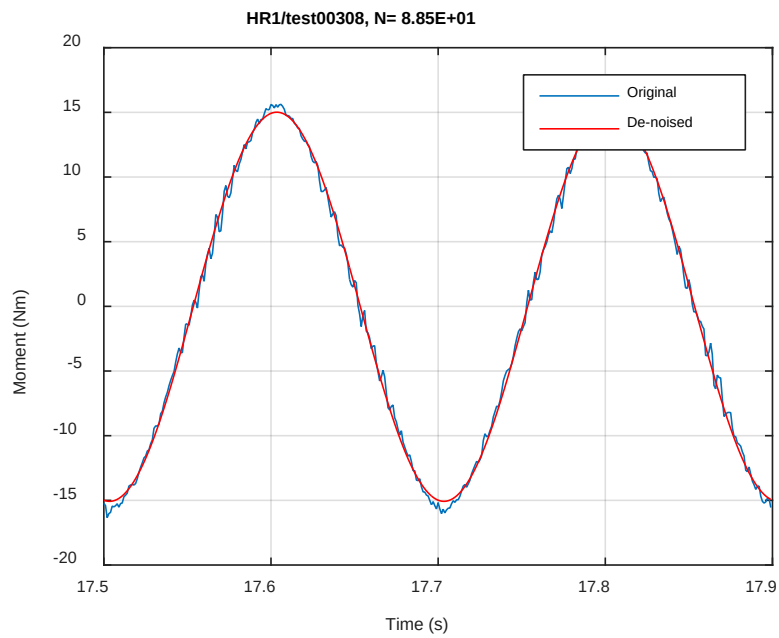
HR1/test00308, N= 8.85E+01
Original
De-noised
Moment (Nm)
Time (s)
20
15
10
5
0
-5
-10
-15
-20
17.5
17.6
17.7
17.8
17.9

(b)

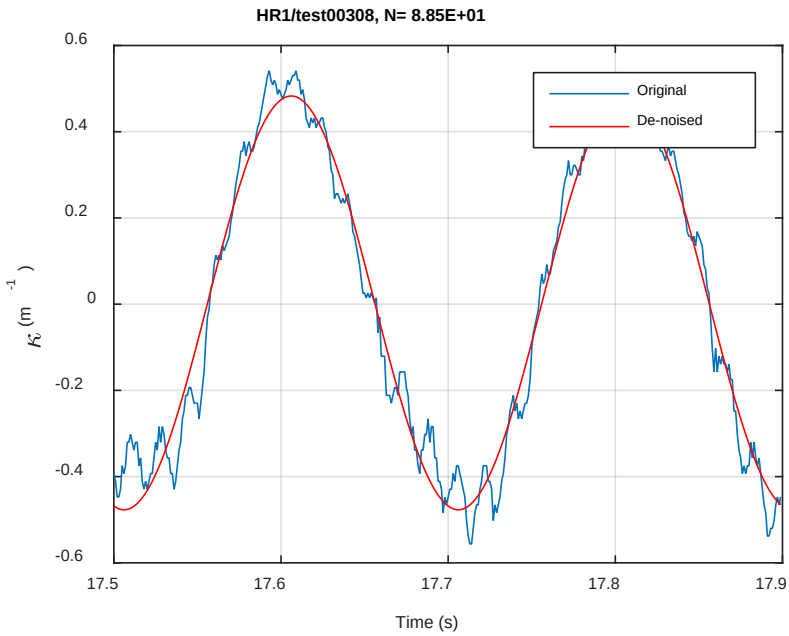

(c)

Fig. F.2 Monitoring-based responses: (a) curvature, (b) moment, (c) curvature, HR1, 15.24 Nm, Ns = 8.85E+01 cycles.

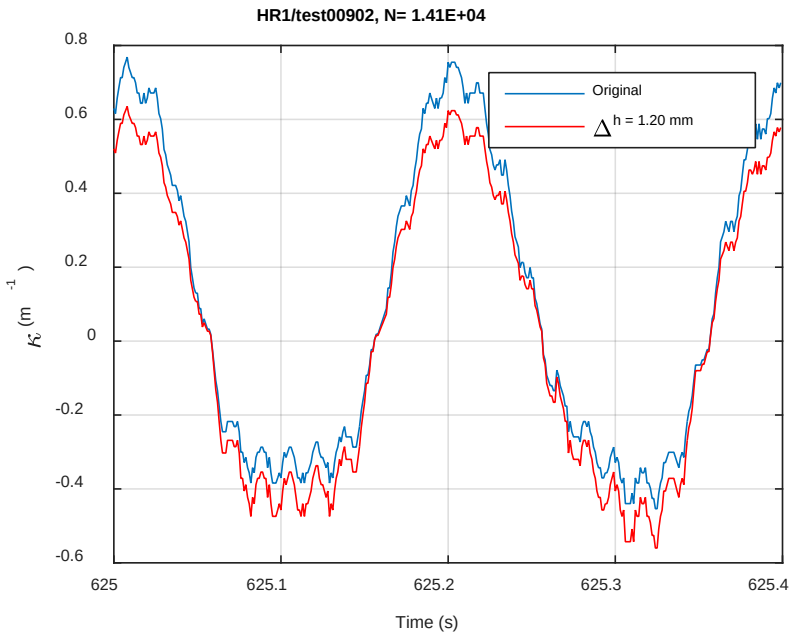
HR1/test00902, N= 1.41E+04
Original
Δh = 1.20 mm
κ (m -1)
Time (s)
0.8
0.6
0.4
0.2
0
-0.2
-0.4
-0.6
625
625.1
625.2
625.3
625.4

(a)

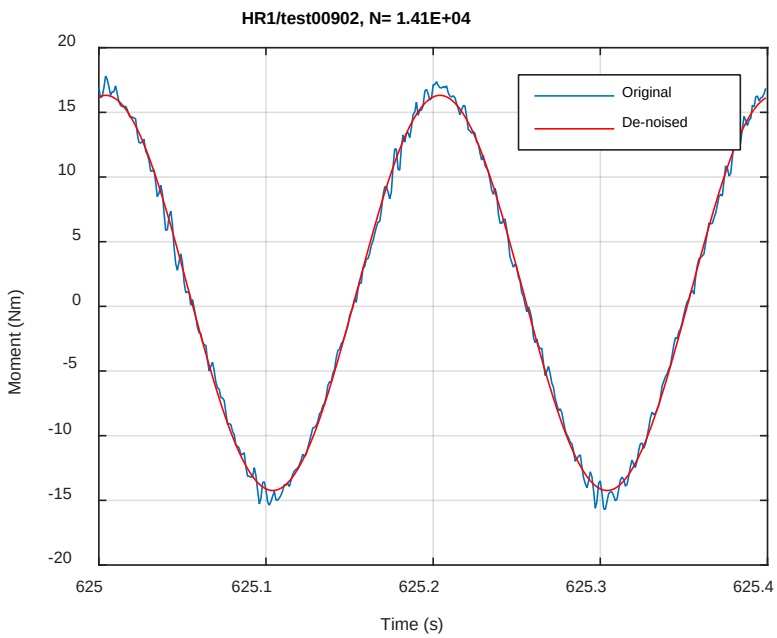
HR1/test00902, N= 1.41E+04
Original
De-noised
Moment (Nm)
Time (s)
20
15
10
5
0
-5
-10
-15
-20
625
625.1
625.2
625.3
625.4

(b)

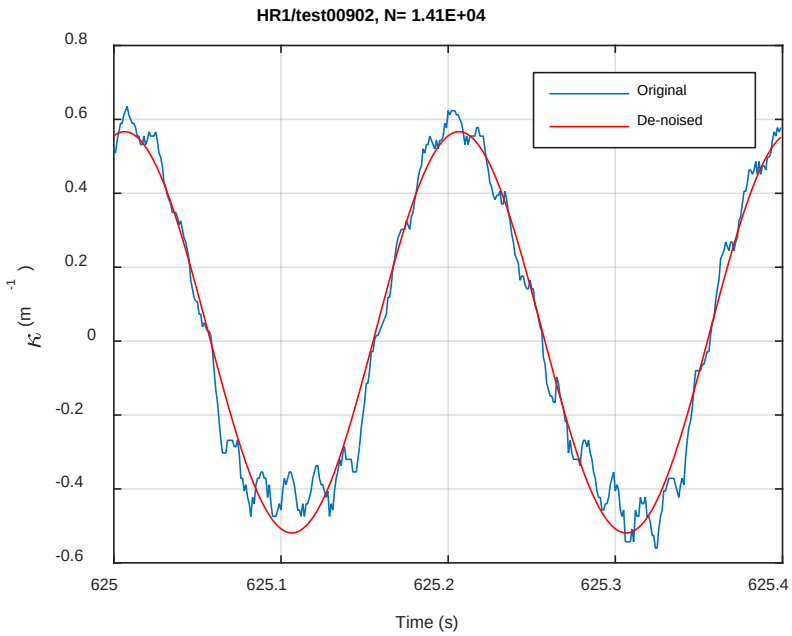

(c)

Fig. F.3 Monitoring-based responses: (a) curvature, (b) moment, (c) curvature, HR1, 15.24 Nm, Ns = 1.41E+04 cycles.

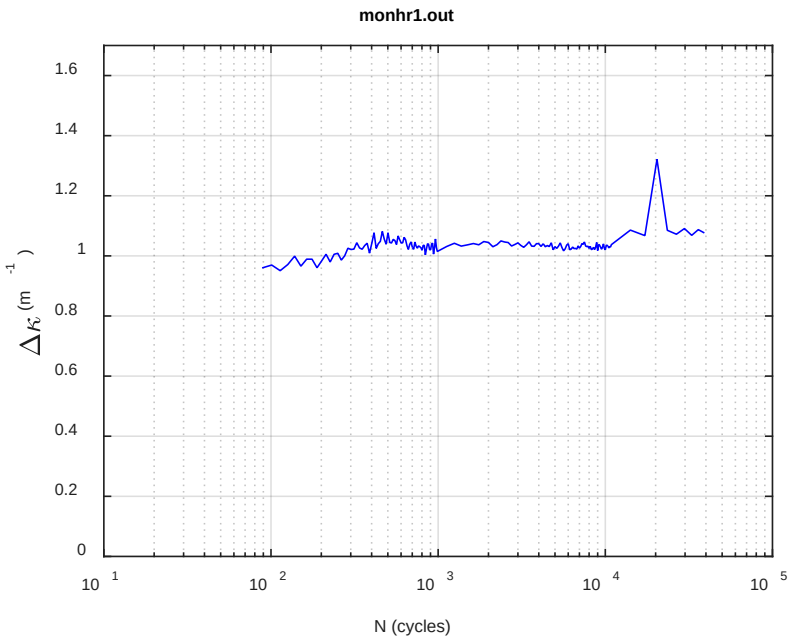
monhr1.out
1.6
1.4
1.2
1
0.8
0.6
0.4
0.2
0
Δκ (m -1)
10 1
10 2
10 3
10 4
10 5
N (cycles)

(a)

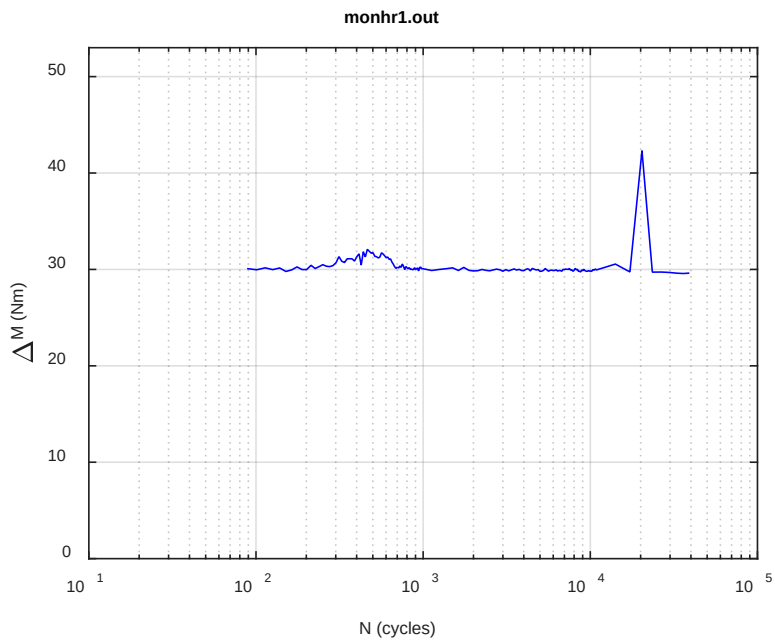
monhr1.out
50
40
30
20
10
0
Δ M (Nm)
10 1
10 2
10 3
10 4
10 5
N (cycles)

(b)

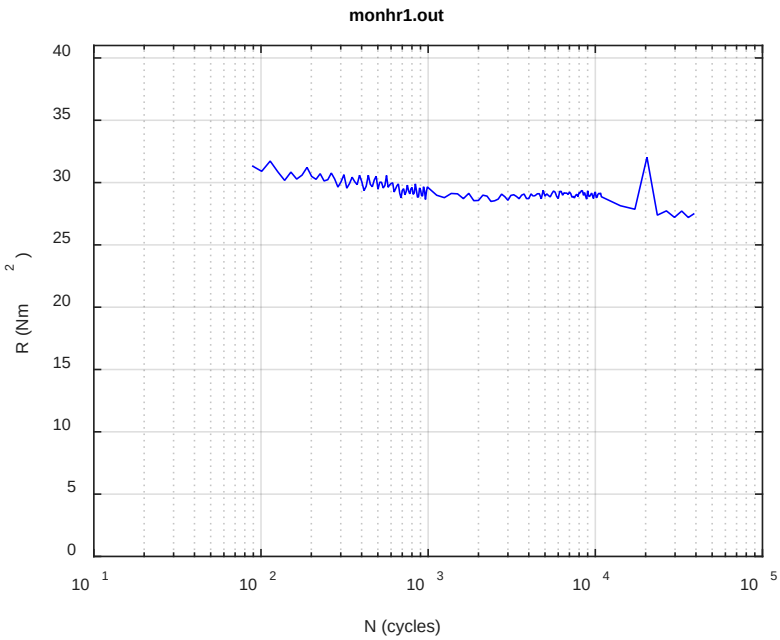

(c)

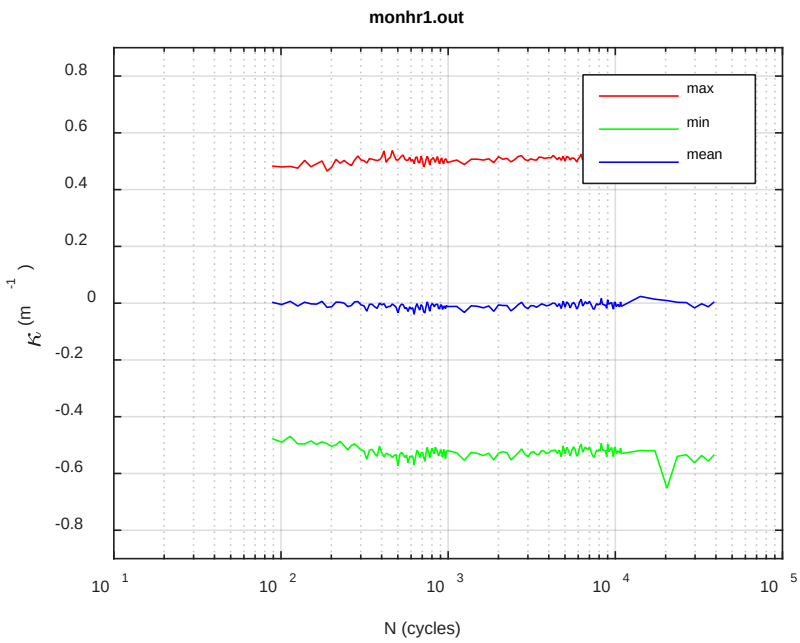

(d)

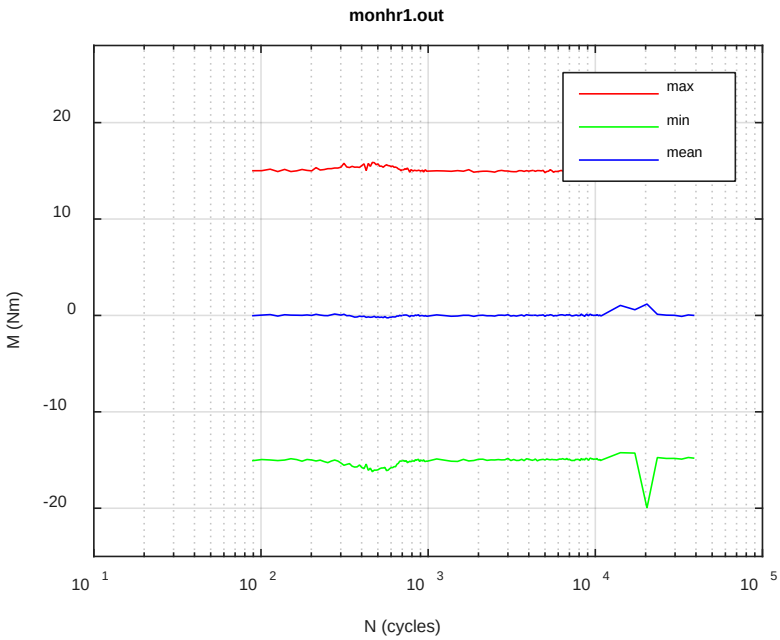

(e)

Fig. F.4 Monitoring-based responses: (a) curvature range, (b) moment range, (c) rigidity, (d) curvature peak/valley, (e) moment peak/valley, HR1, 15.24 Nm, Nf = 4.19E+04 cycles.

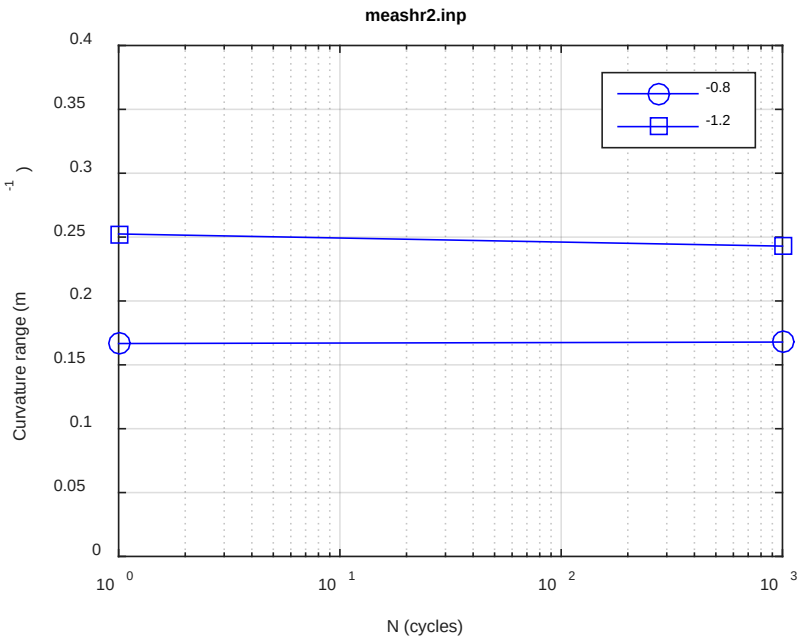
meashr2.inp
0.4
0.35
0.3
0.25
0.2
0.15
0.1
0.05
0
Curvature range (m -1)
-0.8
-1.2
10 0
10 1
10 2
10 3
N (cycles)

(a)

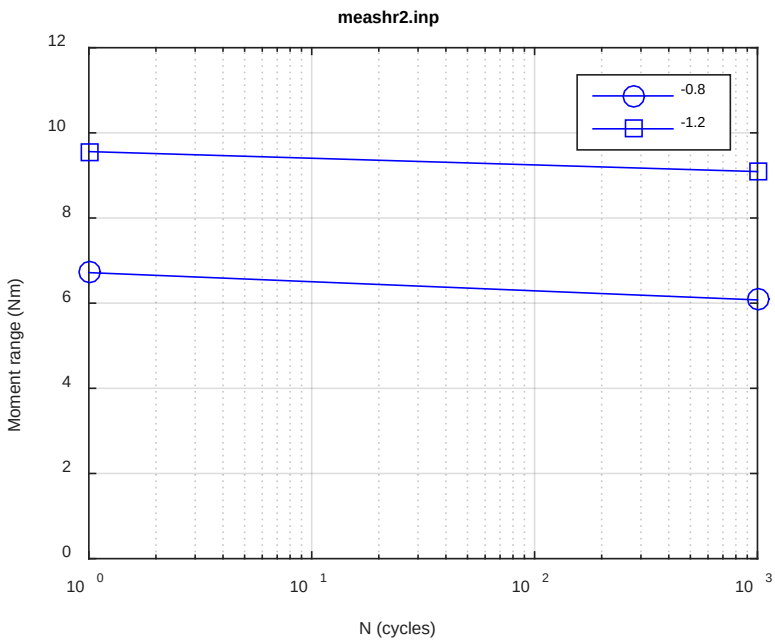
meashr2.inp
12
10
8
6
4
2
0
Moment range (Nm)
-0.8
-1.2
10 0
10 1
10 2
10 3
N (cycles)

(b)

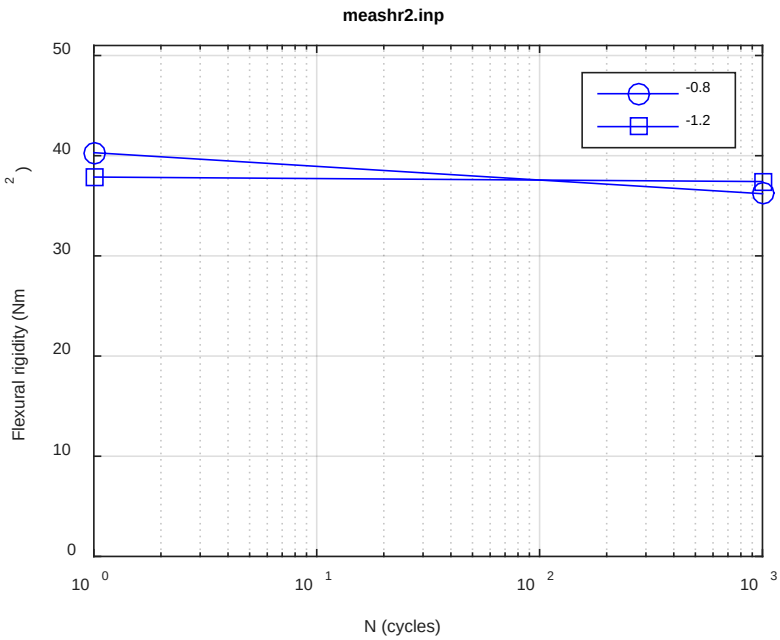
meashr2.inp
-0.8
-1.2
Flexural rigidity (Nm 2)
N (cycles)

(c)

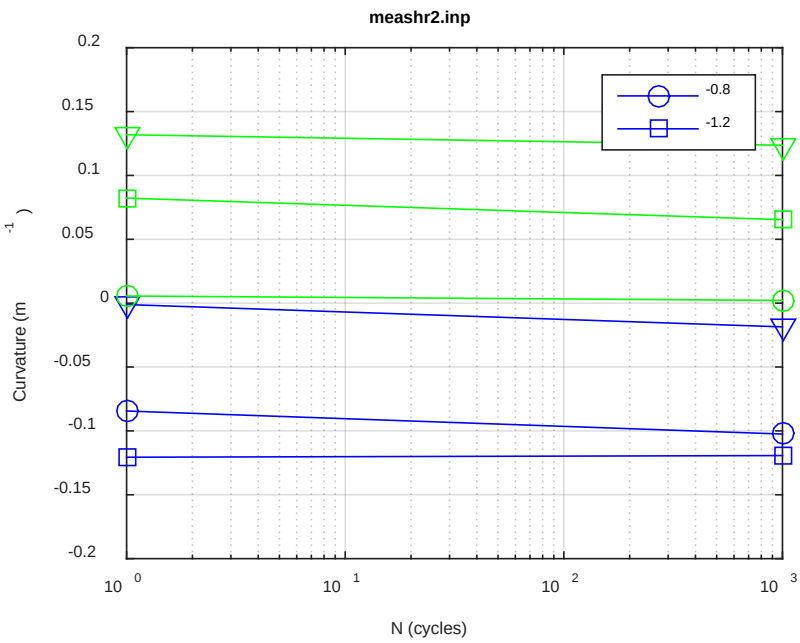
meashr2.inp
-0.8
-1.2
Curvature (m -1)
N (cycles)

(d)

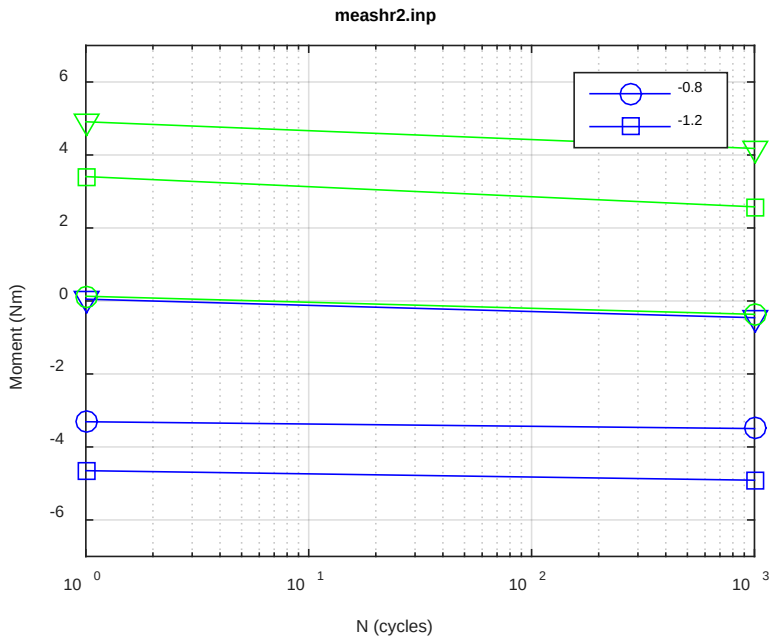

(e)

Fig. F.5 Measurement-based responses: (a) curvature range, (b) moment range, (c) rigidity, (d) curvature peak/valley, (e) moment peak/valley, HR2, 16.26 Nm.

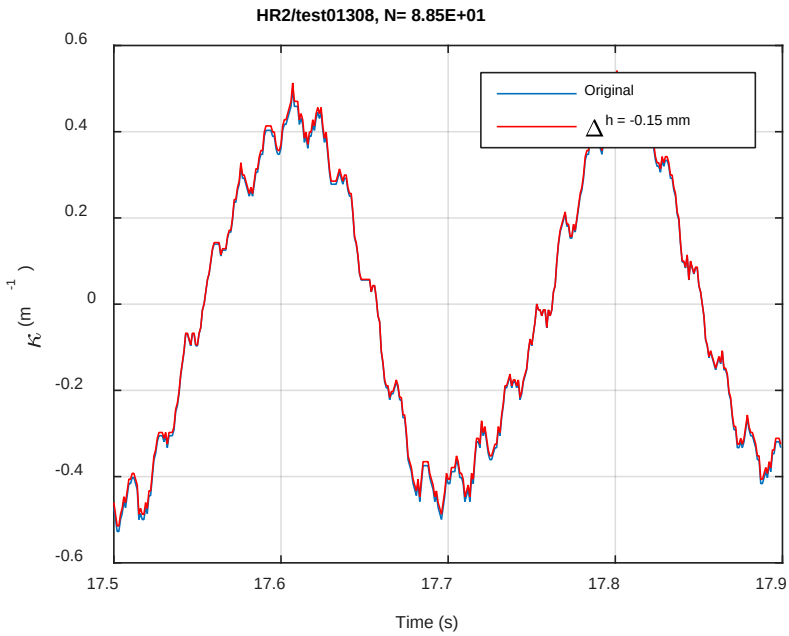
HR2/test01308, N= 8.85E+01
Original
Δh = -0.15 mm
κ (m -1)
Time (s)
0.6
0.4
0.2
0
-0.2
-0.4
-0.6
17.5
17.6
17.7
17.8
17.9

(a)

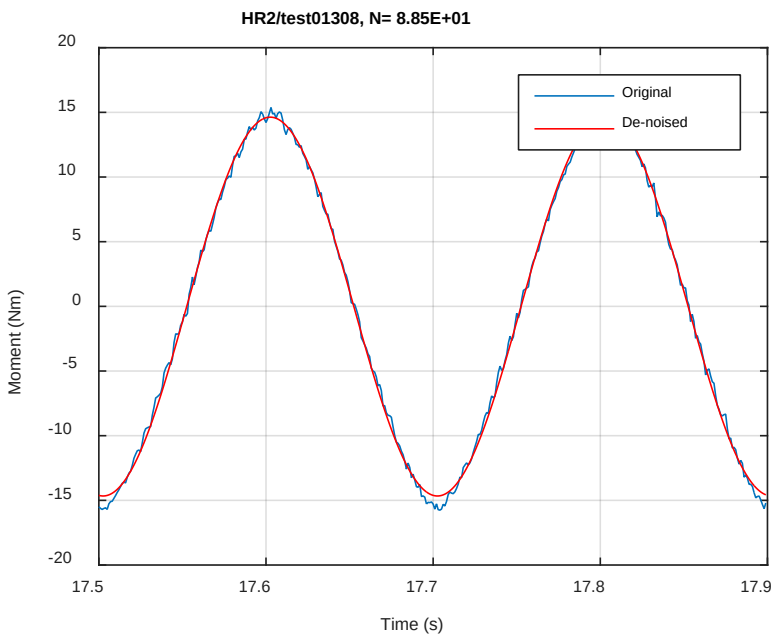
HR2/test01308, N= 8.85E+01
Original
De-noised
Moment (Nm)
Time (s)
20
15
10
5
0
-5
-10
-15
-20
17.5
17.6
17.7
17.8
17.9

(b)

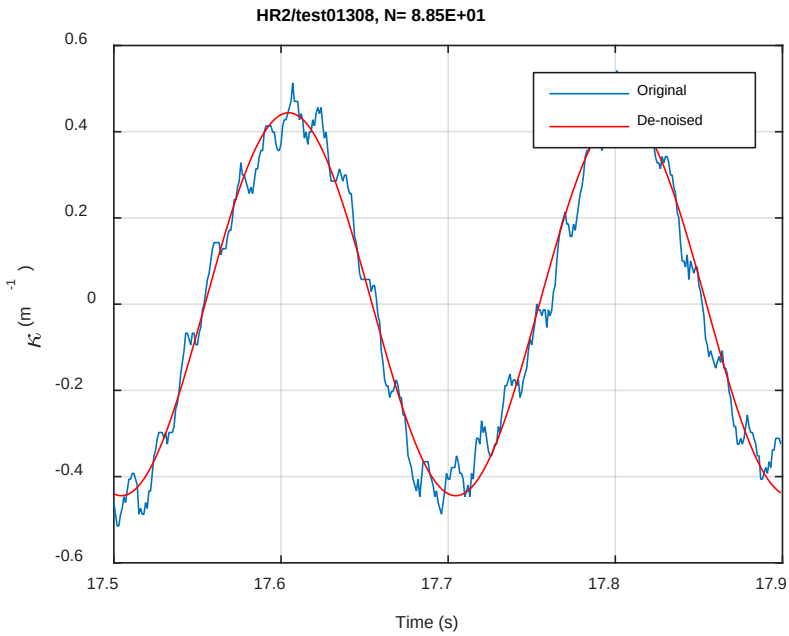

(c)

Fig. F.6 Monitoring-based responses: (a) curvature, (b) moment, (c) curvature, HR2, 16.26 Nm, Ns = 8.85E+01 cycles.

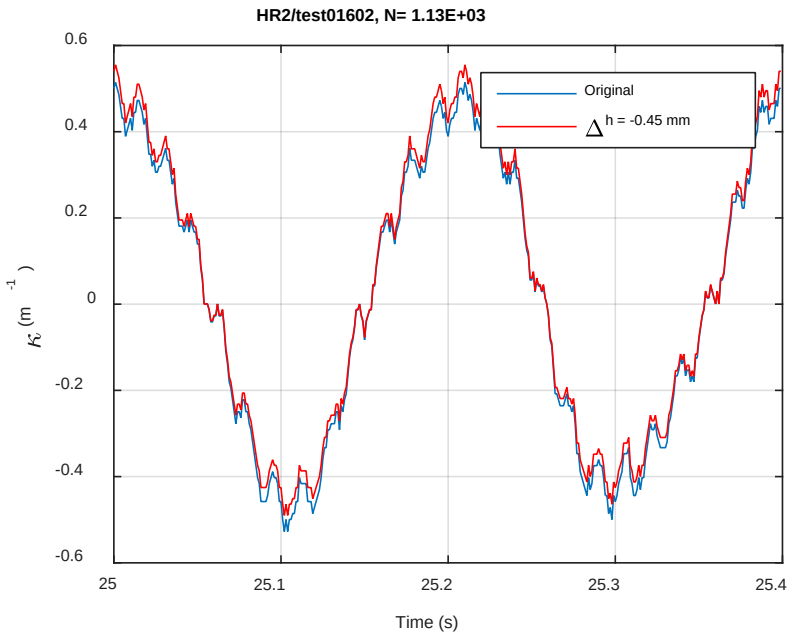
HR2/test01602, N= 1.13E+03
Original
Δh = -0.45 mm
κ (m -1)
Time (s)
0.6
0.4
0.2
0
-0.2
-0.4
-0.6
25
25.1
25.2
25.3
25.4

(a)

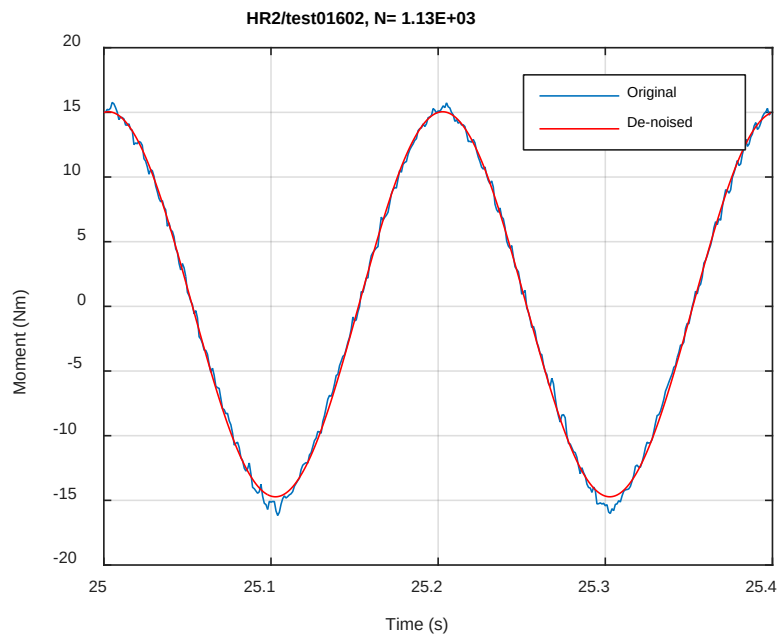
HR2/test01602, N= 1.13E+03
Original
De-noised
Moment (Nm)
Time (s)
20
15
10
5
0
-5
-10
-15
-20
25
25.1
25.2
25.3
25.4

(b)

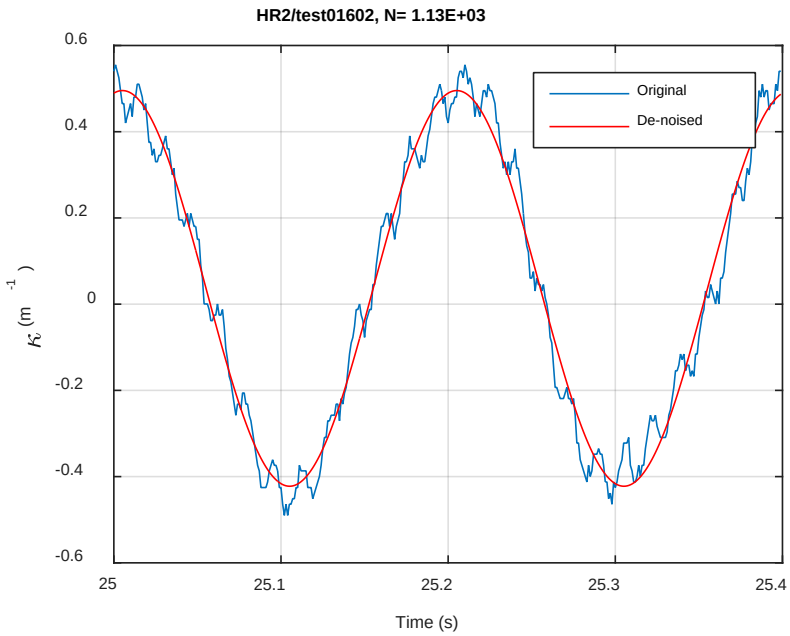

(c)

Fig. F.7 Monitoring-based responses: (a) curvature, (b) moment, (c) curvature, HR2, 16.26 Nm, Ns = 1.13E+03 cycles.

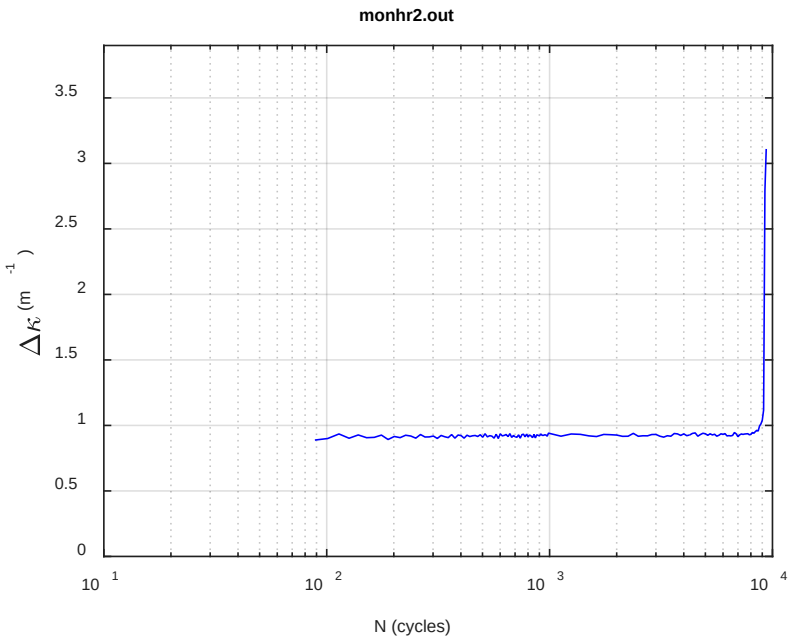
monhr2.out
3.5
3
2.5
2
1.5
1
0.5
0
Δκ (m -1)
10 1
10 2
10 3
10 4
N (cycles)

(a)

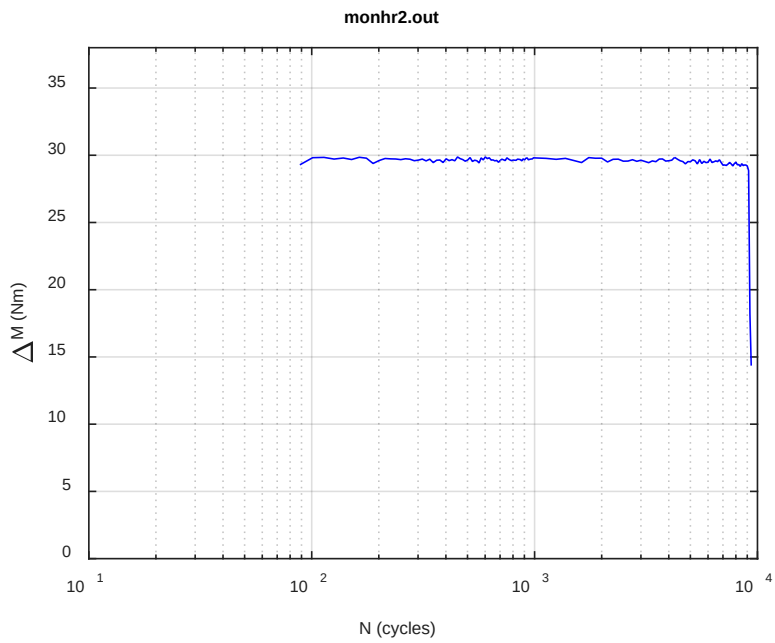
monhr2.out
35
30
25
20
15
10
5
0
Δ M (Nm)
10 1
10 2
10 3
10 4
N (cycles)

(b)

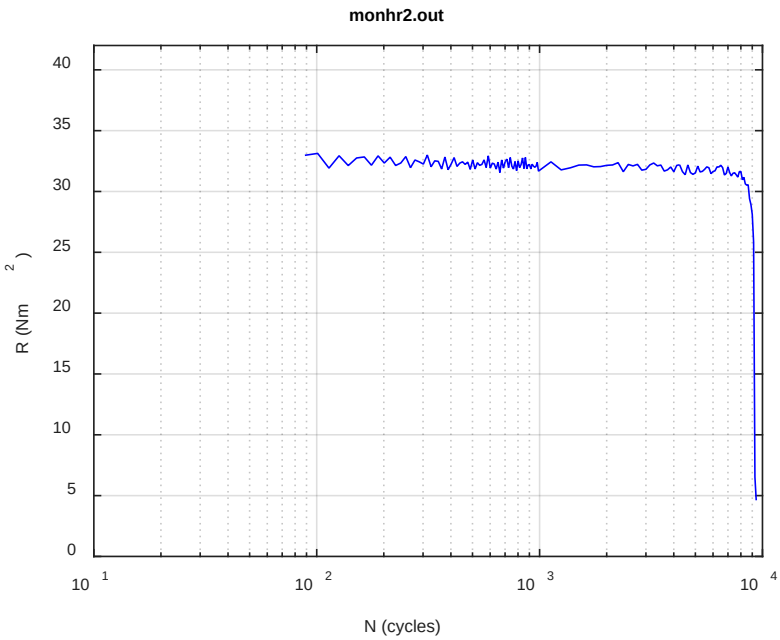

(c)

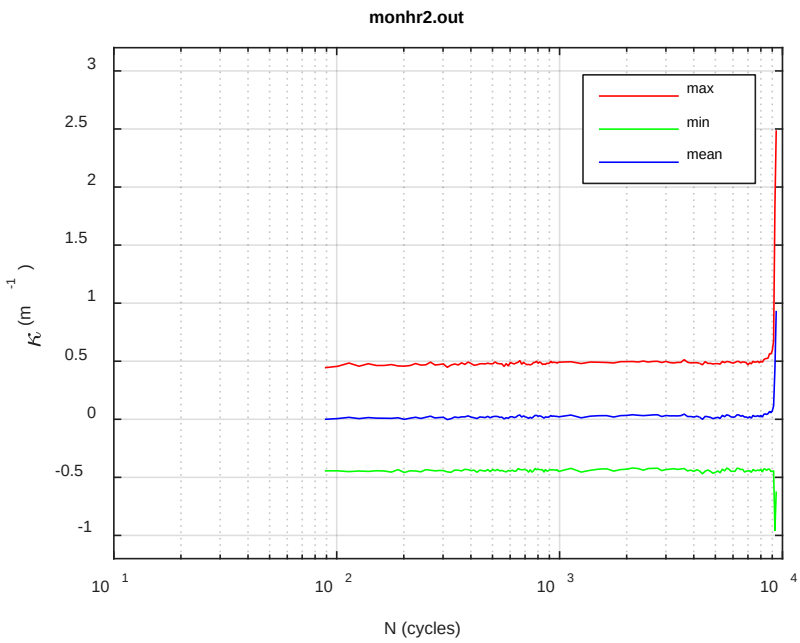

(d)

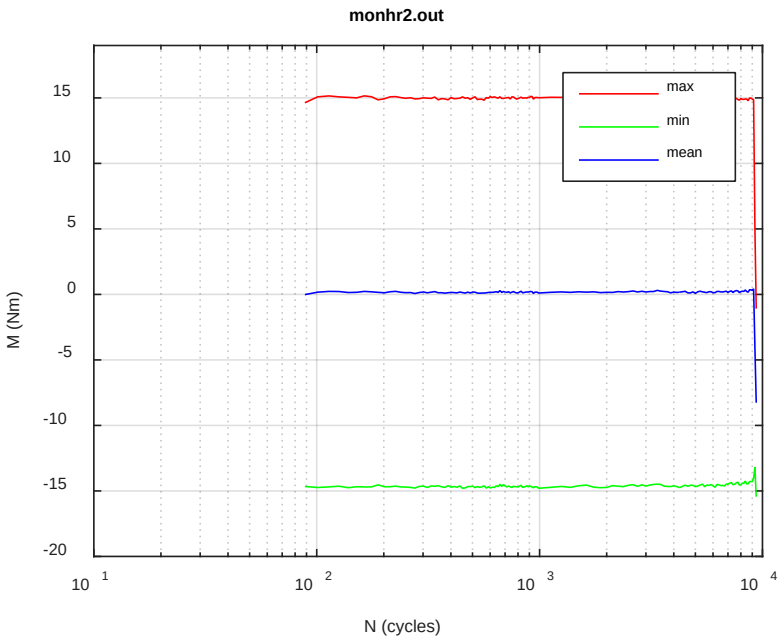

(e)

Fig. F.8 Monitoring-based responses: (a) curvature range, (b) moment range, (c) rigidity, (d) curvature peak/valley, (e) moment peak/valley, HR2, 16.26 Nm, Nf = 9.47E+03 cycles.

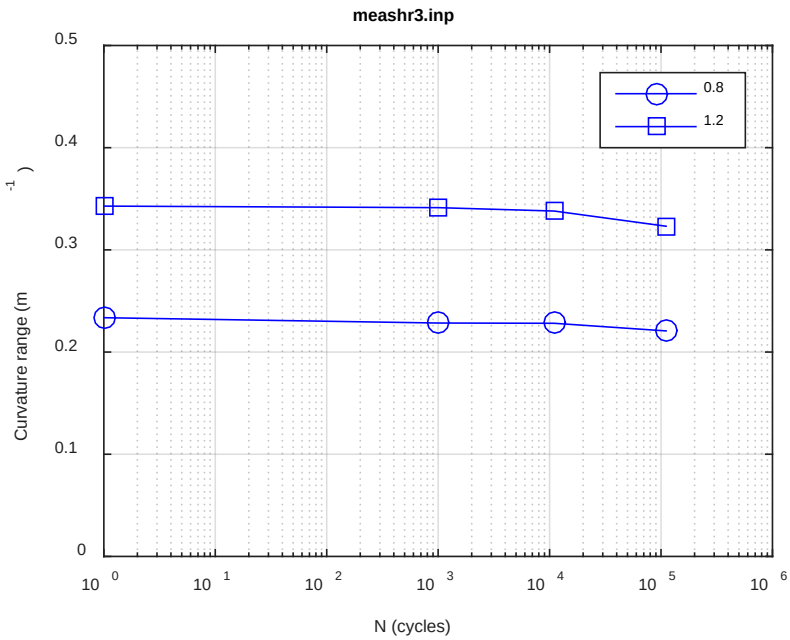
meashr3.inp
0.5
0.4
0.3
0.2
0.1
0
Curvature range (m -1)
0.8
1.2
10 0
10 1
10 2
10 3
10 4
10 5
10 6
N (cycles)

(a)

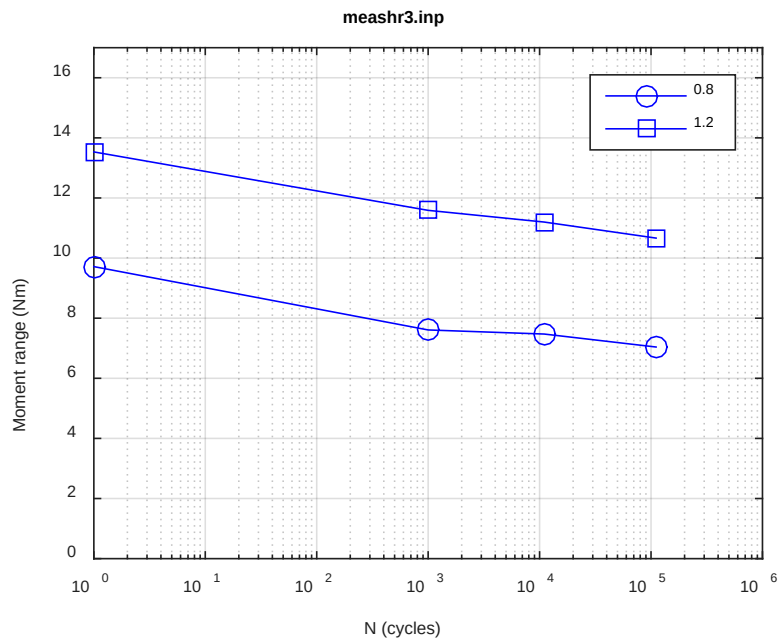
meashr3.inp
16
14
12
10
8
6
4
2
0
Moment range (Nm)
0.8
1.2
10 0
10 1
10 2
10 3
10 4
10 5
10 6
N (cycles)

(b)

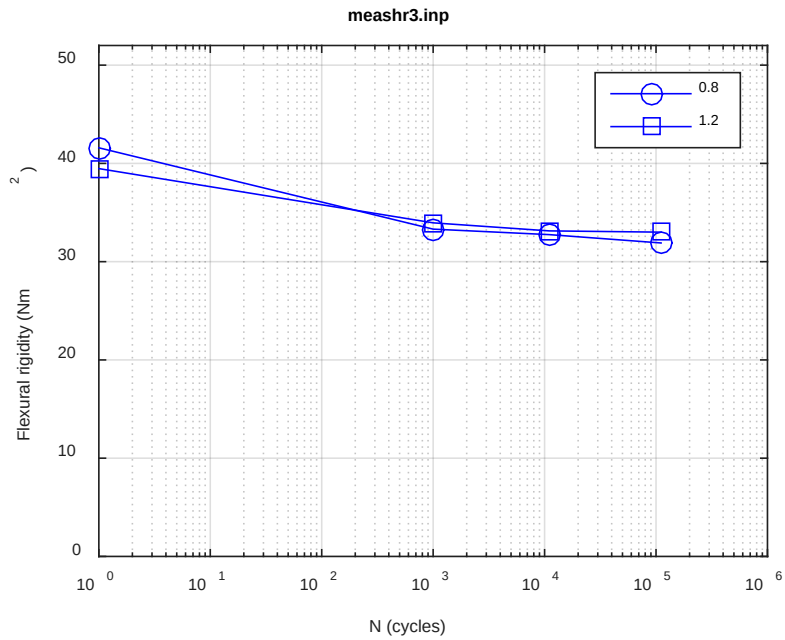
meashr3.inp
0.8
1.2
Flexural rigidity (Nm 2)
N (cycles)

(c)

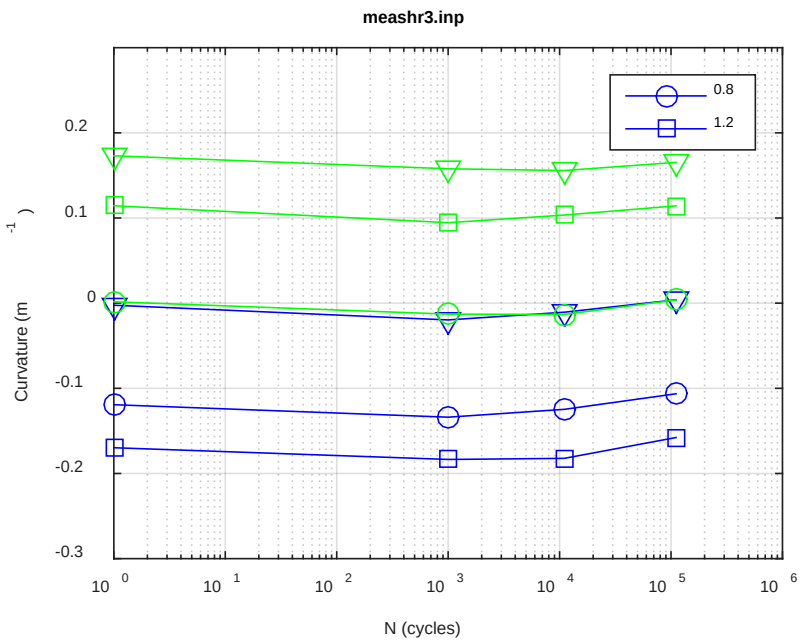
meashr3.inp
0.8
1.2
Curvature (m -1)
N (cycles)

(d)

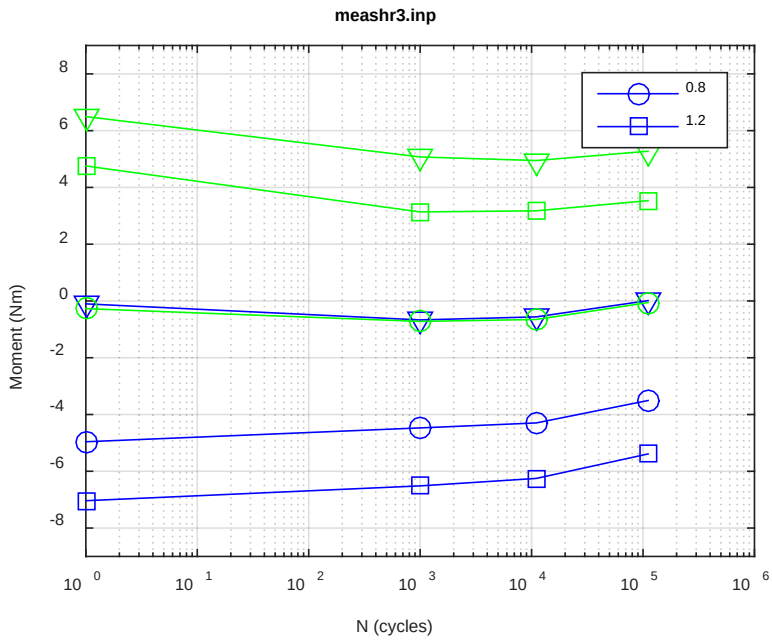

(e)

Fig. F.9 Measurement-based responses: (a) curvature range, (b) moment range, (c) rigidity, (d) curvature peak/valley, (e) moment peak/valley, HR3, 10.16 Nm.

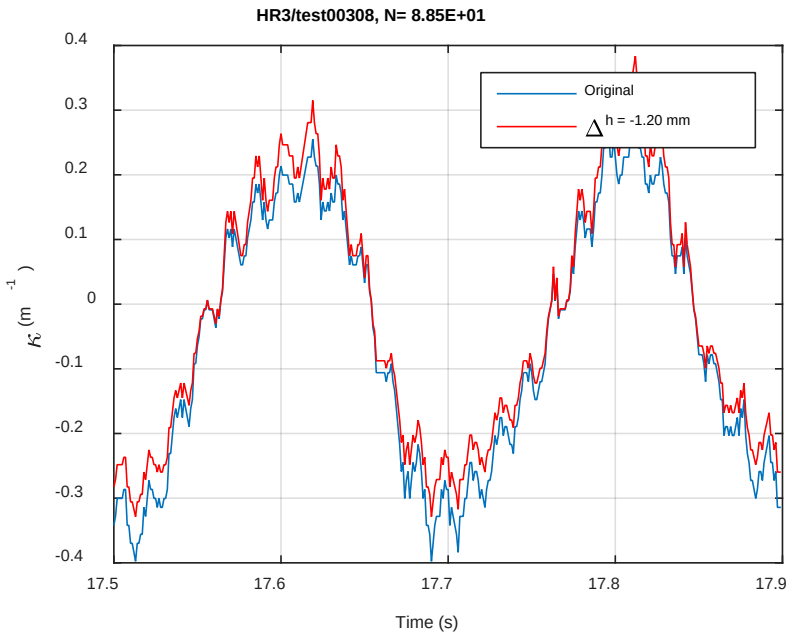
HR3/test00308, N= 8.85E+01
Original
Δh = -1.20 mm
κ (m -1)
Time (s)
0.4
0.3
0.2
0.1
0
-0.1
-0.2
-0.3
-0.4
17.5
17.6
17.7
17.8
17.9

(a)

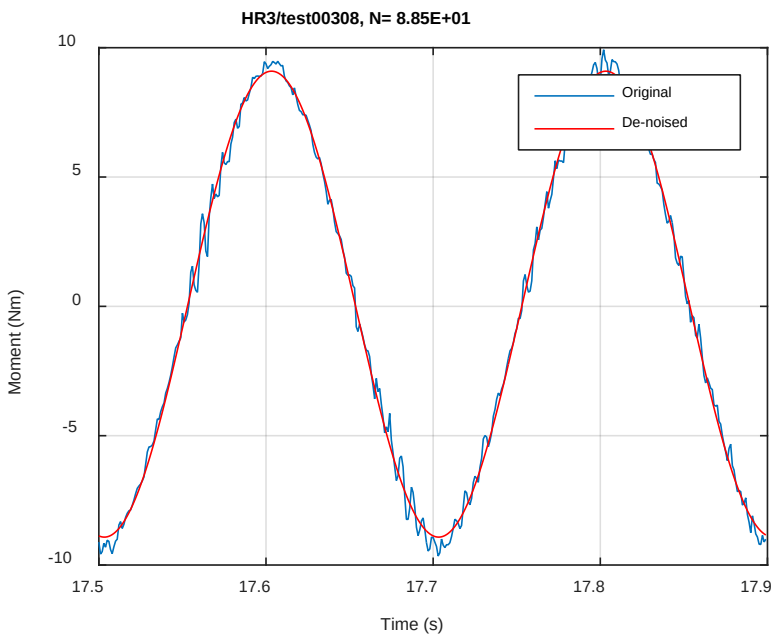
HR3/test00308, N= 8.85E+01
Original
De-noised
Moment (Nm)
Time (s)
10
5
0
-5
-10
17.5
17.6
17.7
17.8
17.9

(b)

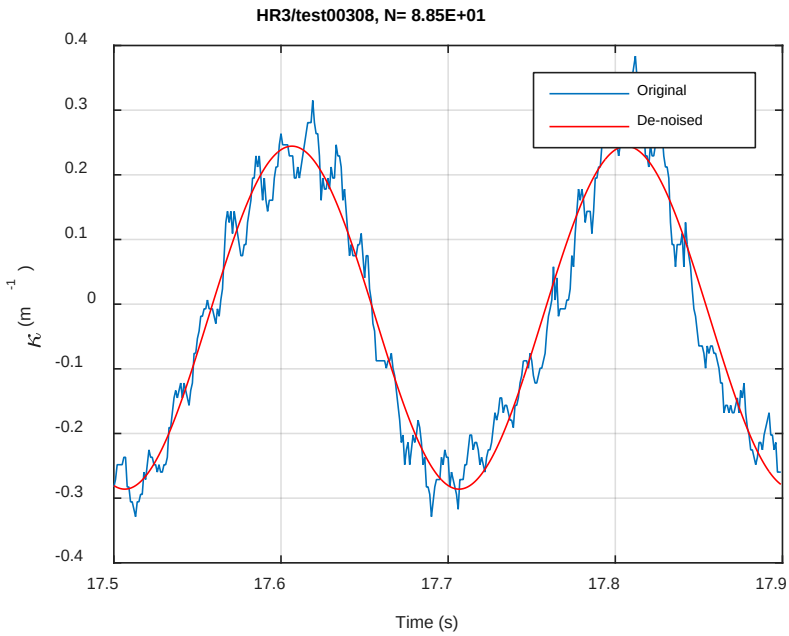

(c)

Fig. F.10 Monitoring-based responses: (a) curvature, (b) moment, (c) curvature, HR3, 10.16 Nm, Ns = 8.85E+01 cycles.

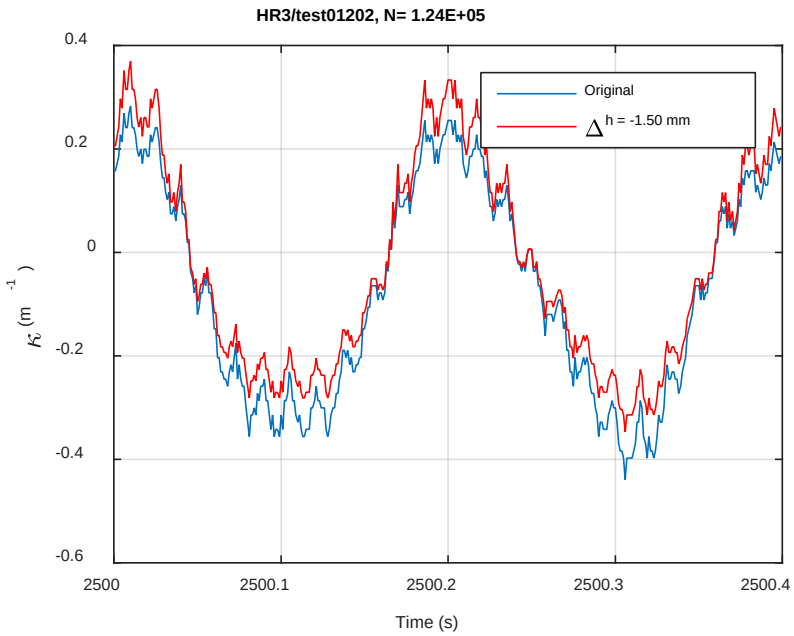
HR3/test01202, N= 1.24E+05
Original
Δh = -1.50 mm
κ (m -1)
Time (s)
0.4
0.2
0
-0.2
-0.4
-0.6
2500
2500.1
2500.2
2500.3
2500.4

(a)

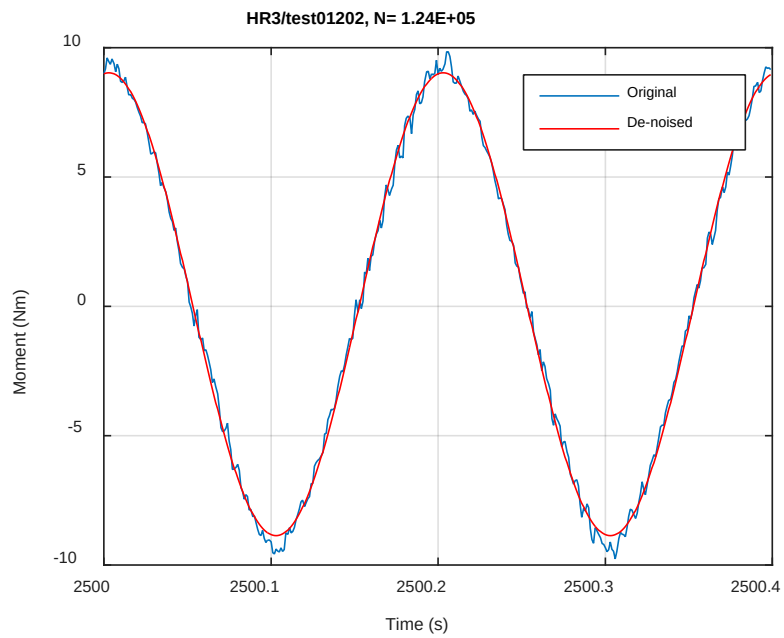
HR3/test01202, N= 1.24E+05
Original
De-noised
Moment (Nm)
Time (s)
10
5
0
-5
-10
2500
2500.1
2500.2
2500.3
2500.4

(b)

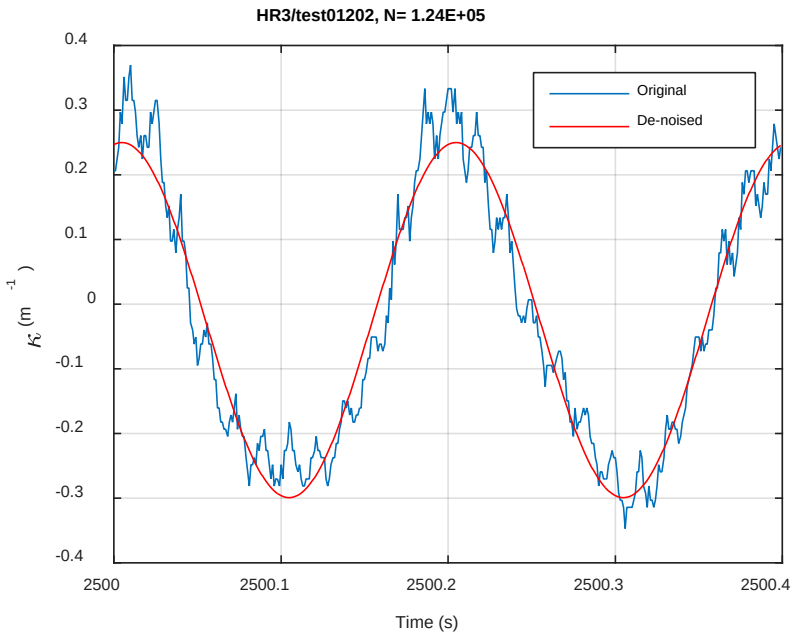

(c)

Fig. F.11 Monitoring-based responses: (a) curvature, (b) moment, (c) curvature, HR3, 10.16 Nm, Ns = 1.24E+05 cycles.

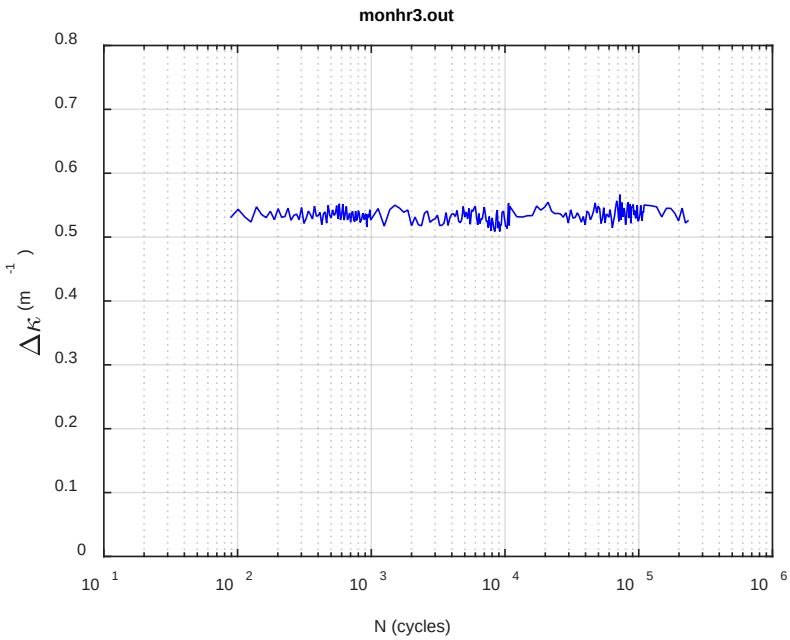
monhr3.out
0.8
0.7
0.6
0.5
0.4
0.3
0.2
0.1
0
Δκ (m -1)
10 1
10 2
10 3
10 4
10 5
10 6
N (cycles)

(a)

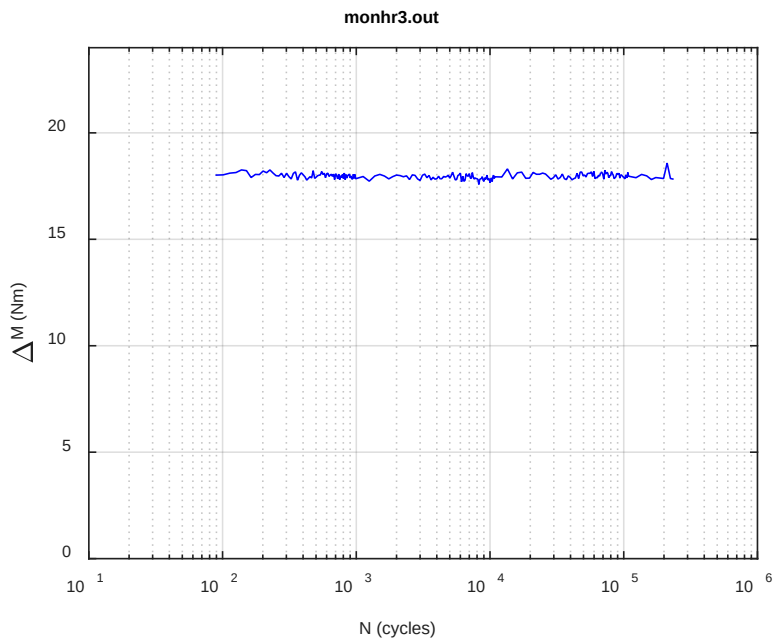
monhr3.out
20
15
10
5
0
Δ M (Nm)
10 1
10 2
10 3
10 4
10 5
10 6
N (cycles)

(b)

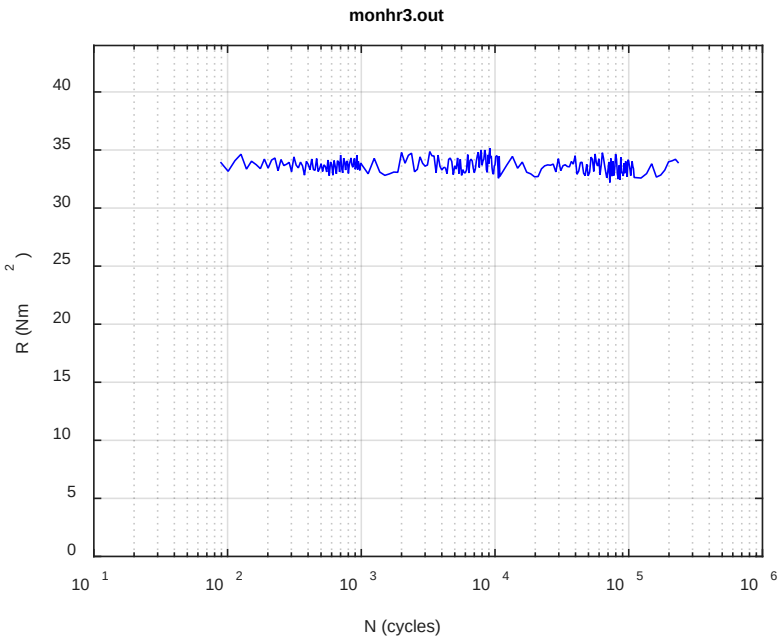

(c)

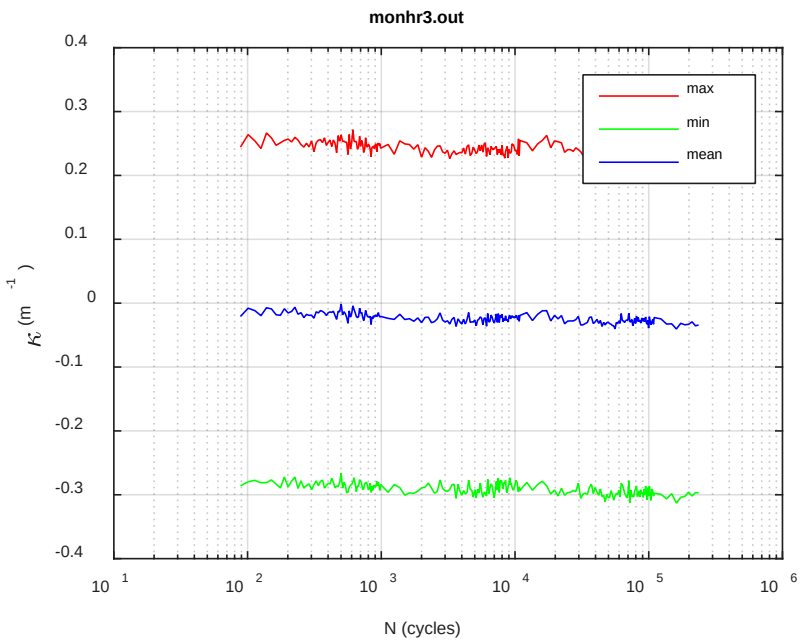

(d)

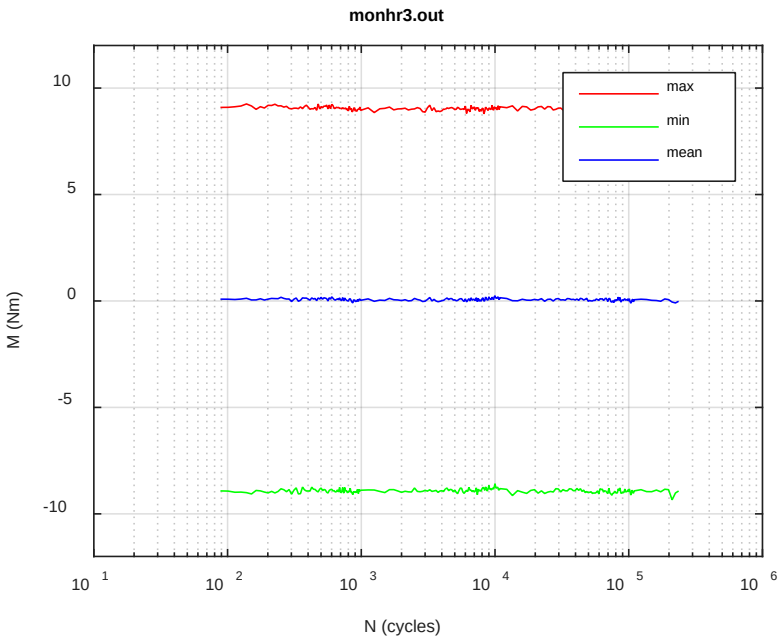

(e)

Fig. F.12 Monitoring-based responses: (a) curvature range, (b) moment range, (c) rigidity, (d) curvature peak/valley, (e) moment peak/valley, HR3, 10.16 Nm, Nf = 2.44E+05 cycles.

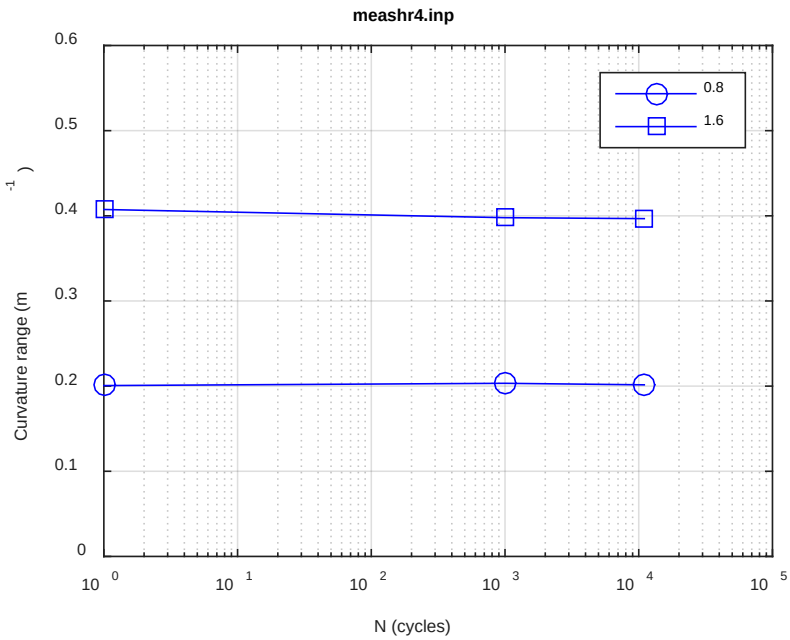
meashr4.inp
0.6
0.5
0.4
0.3
0.2
0.1
0
Curvature range (m -1)
0.8
1.6
10 0
10 1
10 2
10 3
10 4
10 5
N (cycles)

(a)

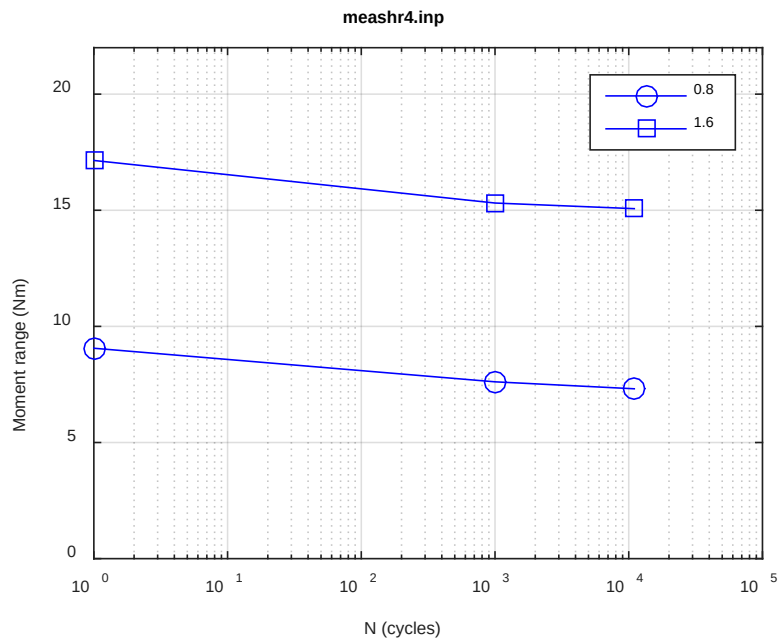
meashr4.inp
20
15
10
5
0
Moment range (Nm)
0.8
1.6
10 0
10 1
10 2
10 3
10 4
10 5
N (cycles)

(b)

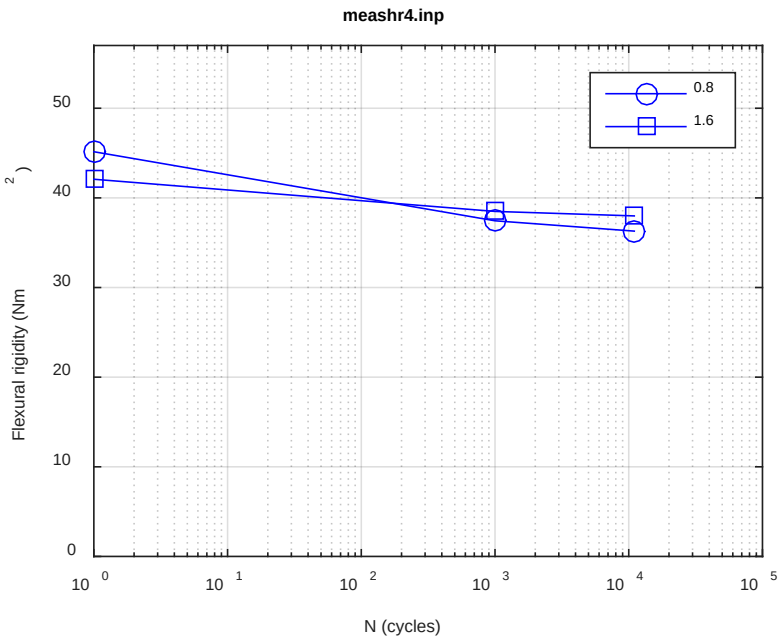
meashr4.inp
0.8
1.6
Flexural rigidity (Nm 2)
50
40
30
20
10
0
10 0
10 1
10 2
10 3
10 4
10 5
N (cycles)

(c)

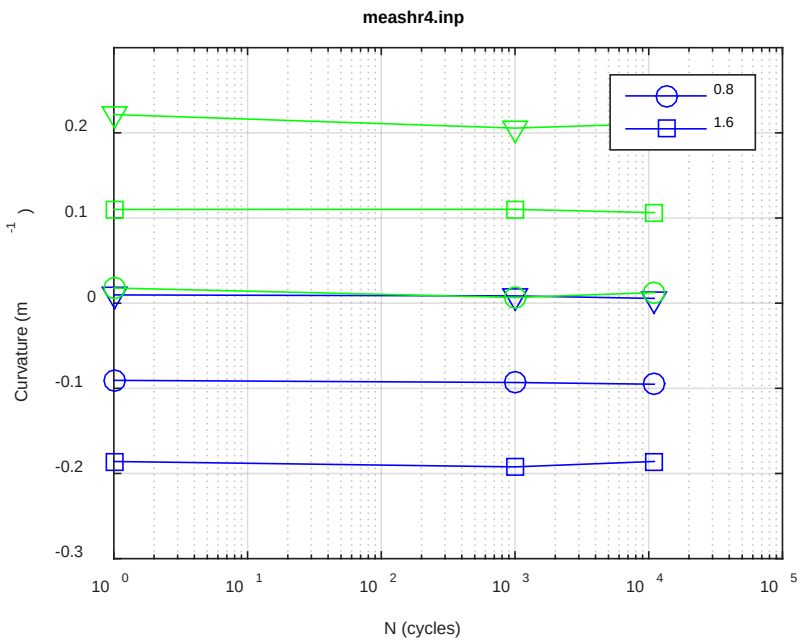
meashr4.inp
0.8
1.6
Curvature (m -1)
0.2
0.1
0
-0.1
-0.2
-0.3
10 0
10 1
10 2
10 3
10 4
10 5
N (cycles)

(d)

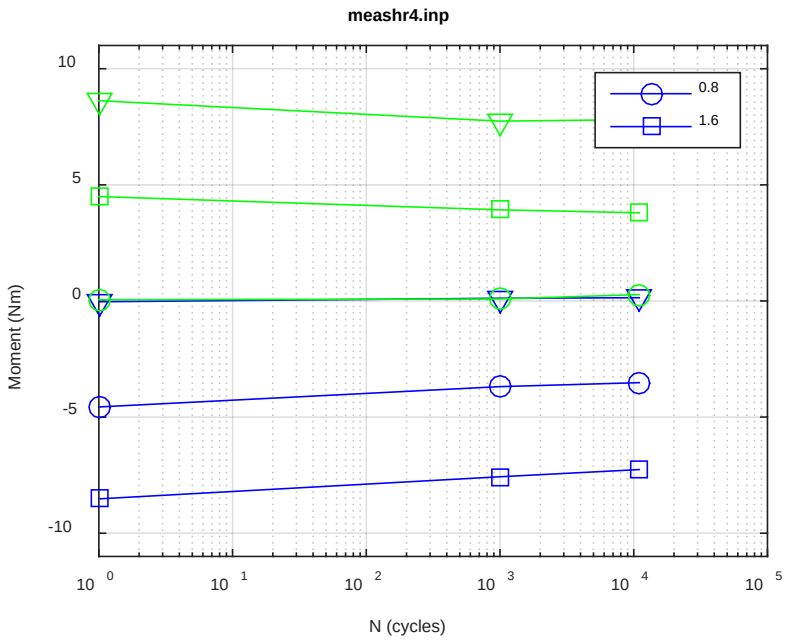

(e)

Fig. F.13 Measurement-based responses: (a) curvature range, (b) moment range, (c) rigidity, (d) curvature peak/valley, (e) moment peak/valley, HR4, 16.26 Nm.

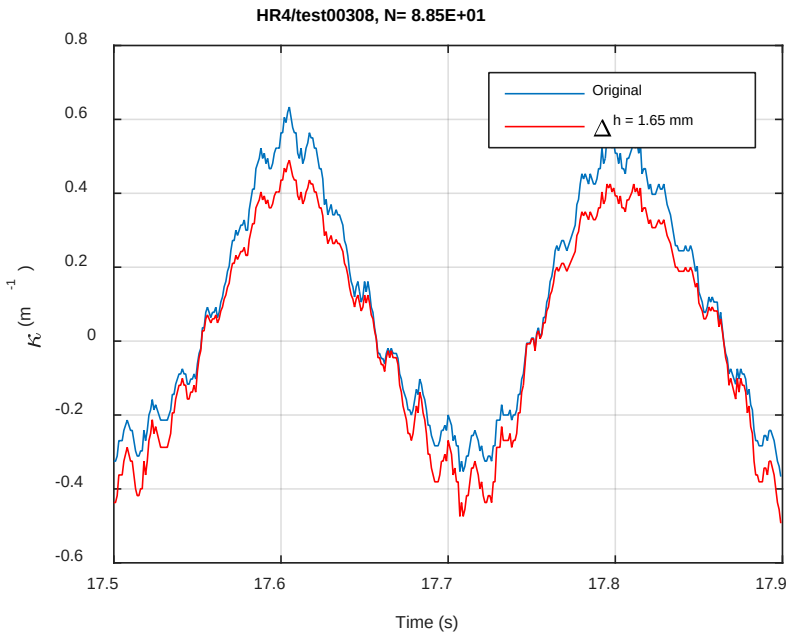
HR4/test00308, N= 8.85E+01
Original
Δh = 1.65 mm
κ (m -1)
Time (s)
0.8
0.6
0.4
0.2
0
-0.2
-0.4
-0.6
17.5
17.6
17.7
17.8
17.9

(a)

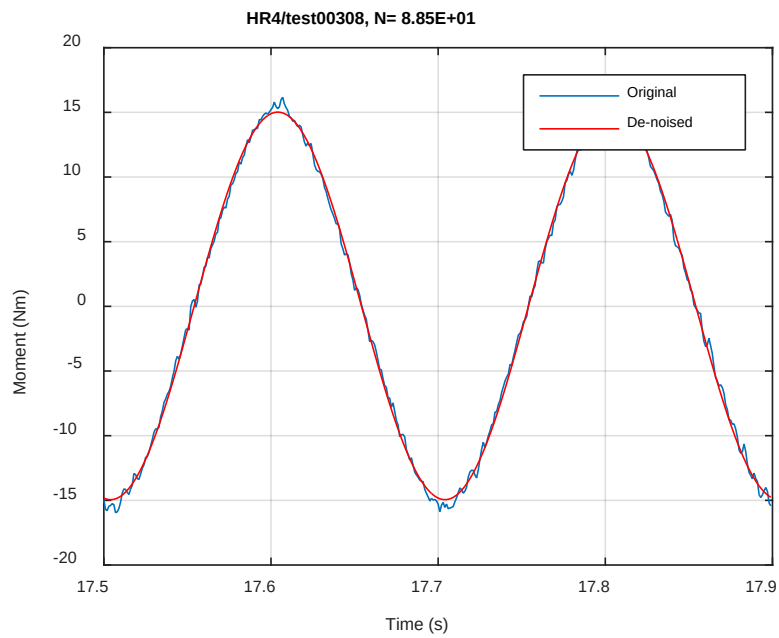
HR4/test00308, N= 8.85E+01
Original
De-noised
Moment (Nm)
Time (s)
20
15
10
5
0
-5
-10
-15
-20
17.5
17.6
17.7
17.8
17.9

(b)

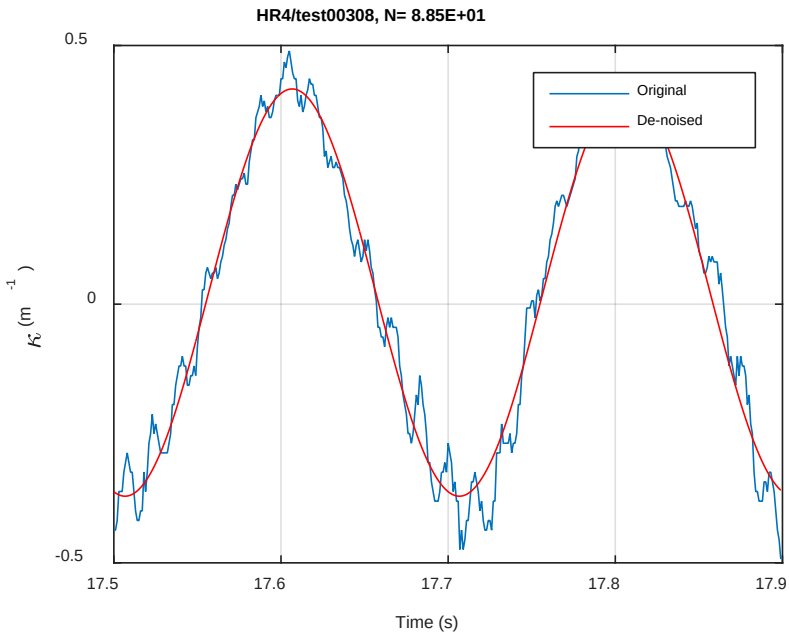

(c)

Fig. F.14 Monitoring-based responses: (a) curvature, (b) moment, (c) curvature, HR4, 16.26 Nm, Ns = 8.85E+01 cycles.

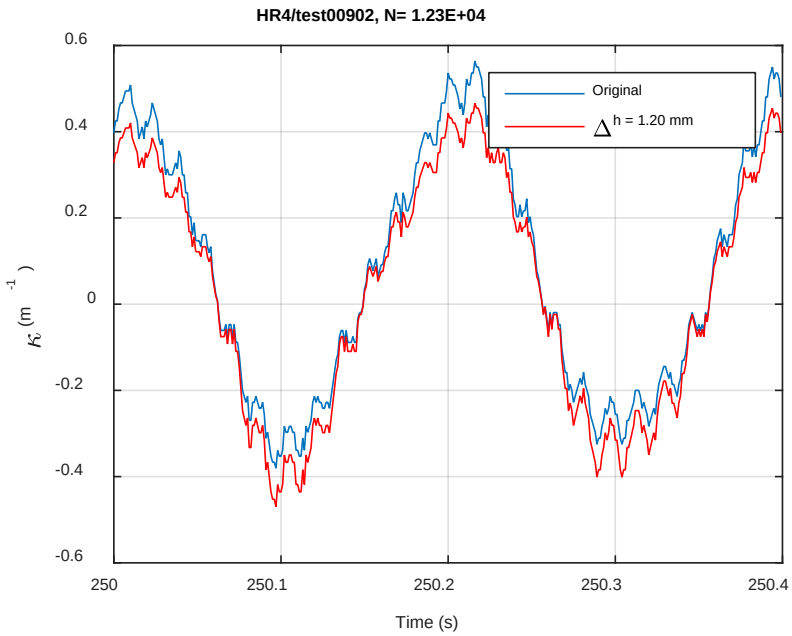
HR4/test00902, N= 1.23E+04
Original
Δh = 1.20 mm
κ (m -1)
Time (s)
0.6
0.4
0.2
0
-0.2
-0.4
-0.6
250
250.1
250.2
250.3
250.4

(a)

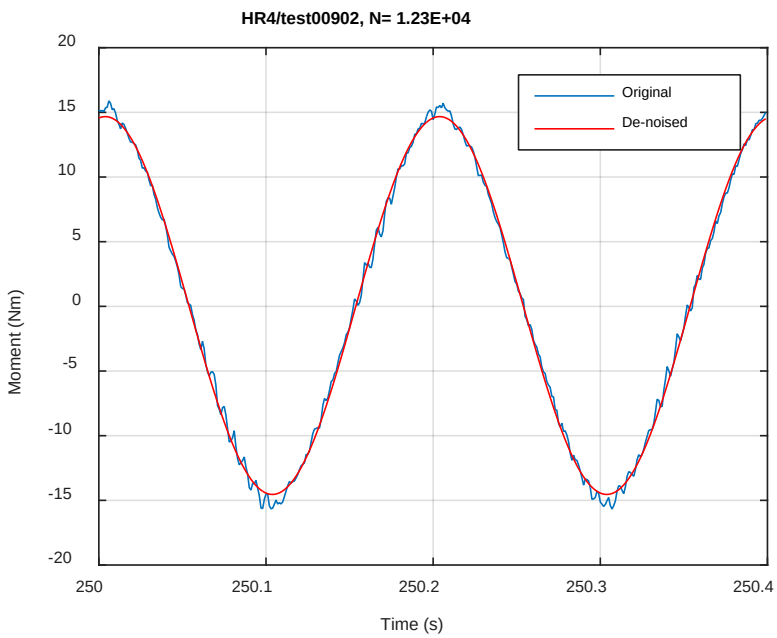
HR4/test00902, N= 1.23E+04
Original
De-noised
Moment (Nm)
Time (s)
20
15
10
5
0
-5
-10
-15
-20
250
250.1
250.2
250.3
250.4

(b)

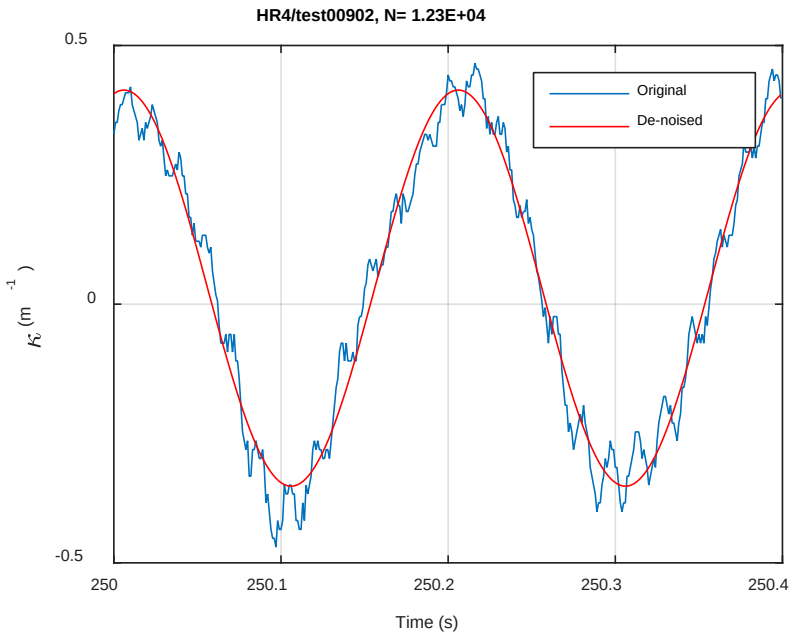

(c)

Fig. F.15 Monitoring-based responses: (a) curvature, (b) moment, (c) curvature, HR4, 16.26 Nm, Ns = 1.23E+04 cycles.

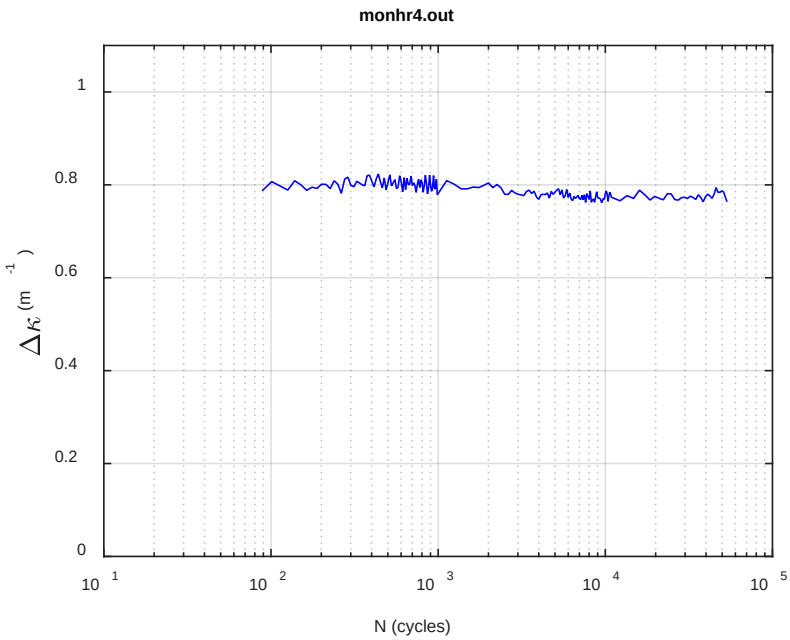
monhr4.out
1
0.8
0.6
0.4
0.2
0
Δκ (m -1)
10 1
10 2
10 3
10 4
10 5
N (cycles)

(a)

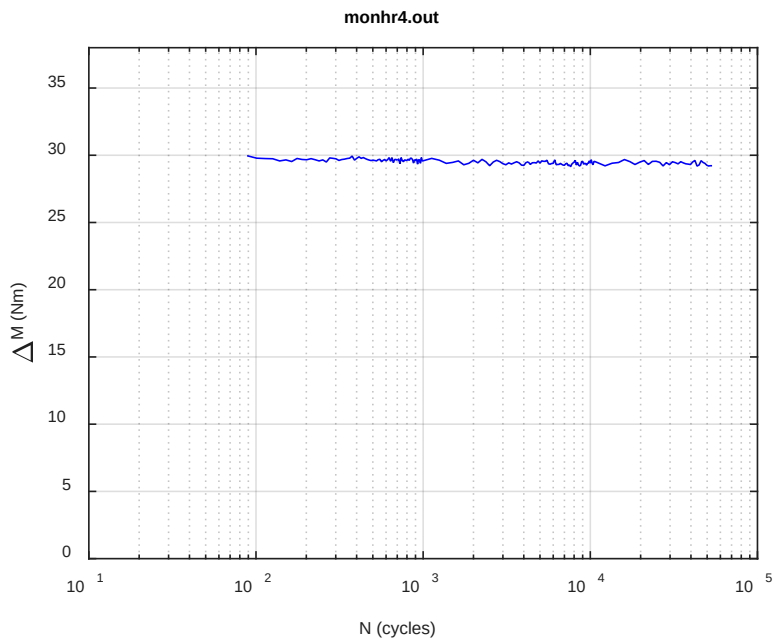
monhr4.out
35
30
25
20
15
10
5
0
Δ M (Nm)
10 1
10 2
10 3
10 4
10 5
N (cycles)

(b)

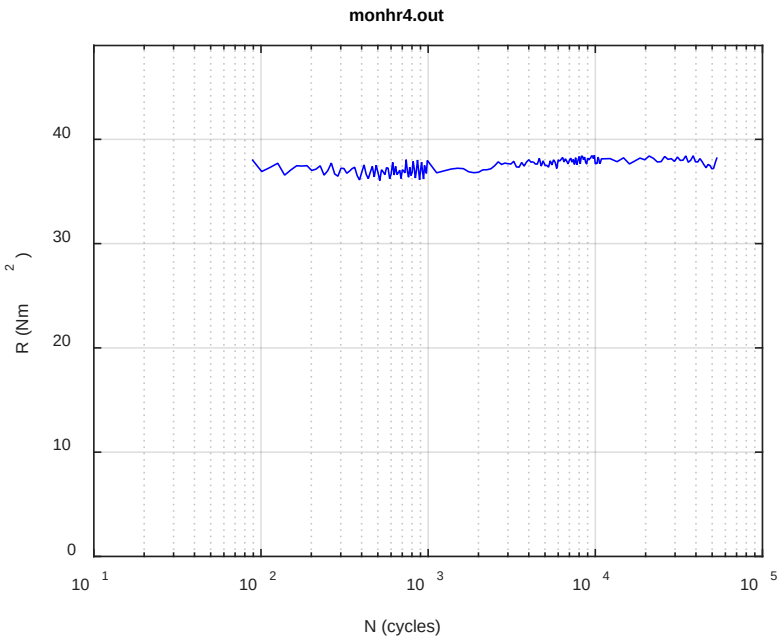
monhr4.out
40
30
20
10
0
R (Nm 2)
10 1
10 2
10 3
10 4
10 5
N (cycles)

(c)

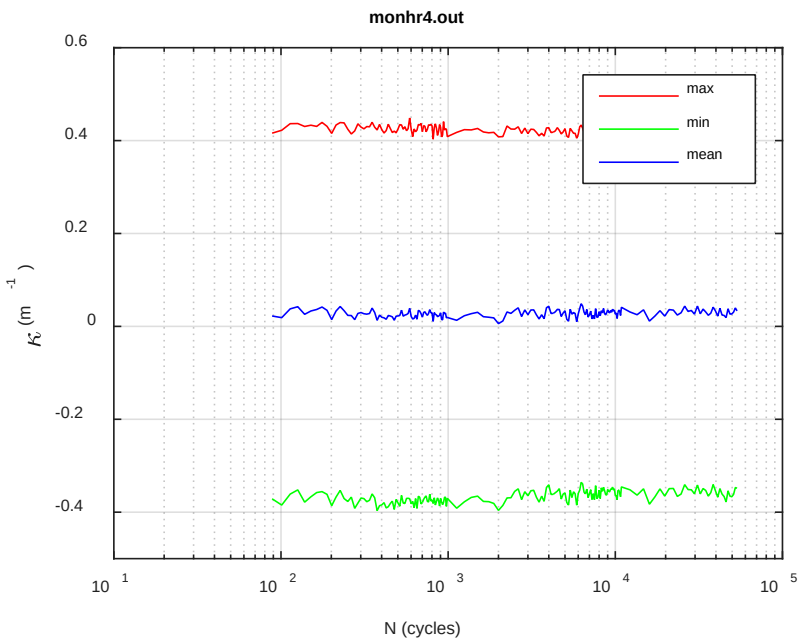
monhr4.out
0.6
0.4
0.2
0
-0.2
-0.4
κ (m -1)
max
min
mean
10 1
10 2
10 3
10 4
10 5
N (cycles)

(d)

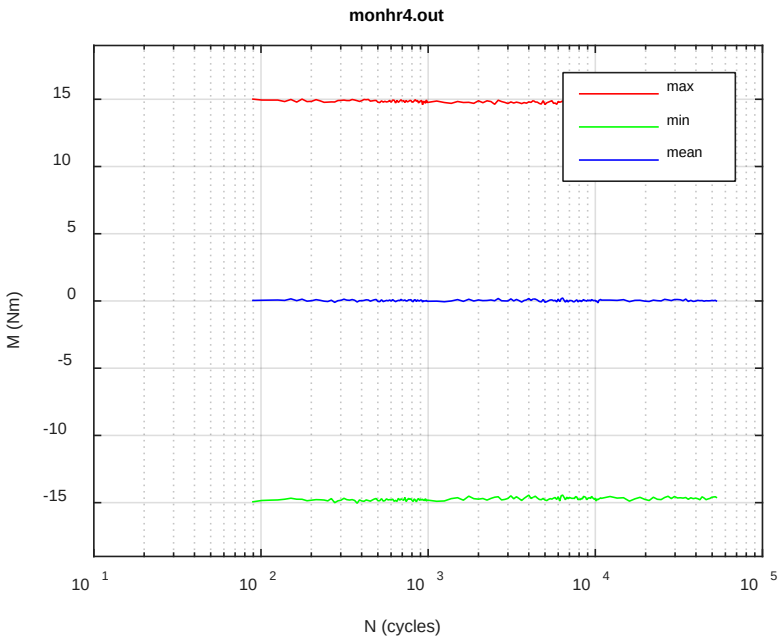

(e)

Fig. F.16 Monitoring-based responses: (a) curvature range, (b) moment range, (c) rigidity, (d) curvature peak/valley, (e) moment peak/valley, HR4, 16.26 Nm, Nf = 5.47E+04 cycles.

This page intentionally left blank.